WAVE-mediated Actin Assembly

by

Arthur Millius

DISSERTATION

Submitted in partial satisfaction of the requirements for the degree of

DOCTOR OF PHILOSOPHY

in

Cell Biology

in the

GRADUATE DIVISION

of the

for

Brian Bud Millius and Evelyn Lucille Davis

ACKNOWLEDGEMENTS

Science is fundamentally a human endeavor – our art is not drawn from depths of established method, nor on parapets of reason, nor through the twin wellsprings of time and chance, but inexorably on the shoulders of those, great and small, who guided, gave, cheered and commiserated along the way. Here I express thanks, first and foremost, to my mentor Orion Weiner for his passion, creativity and patience; for showing me the secrets of science karma; for tapas-style projects, ideas, and conversation; and for unwavering encouragement. I am especially indebted to two colleagues, Sheel Dandekar and Andrew "Iowa" Houk, whose efforts contributed to a thesis chapter herein. I would also like to thank Naoki Watanabe, Masahiro Maruoka and Hiroaki Mizuno for their hospitality in Japan – 本当にありがとうございます. I am grateful to current and past Weiner Lab members Jaime Green, Gary Huang, Sarah Wilson, Oliver Hoeller, Benjamin Rhau, Delquin Gong, Grace Peng, Anna Reade, Anna Payne-Tobin, Jared Toettcher, Julie Wu and Doug Tischer; my thesis committee Ron Vale, Henry Bourne, and Jack Taunton; CPL faculty Wendell Lim, Dyche Mullins, and Dan Fletcher; fellow UCSF colleagues Derek Wong, Scott Hansen, Gigi Knudsen and Angi Chau; and my talented Tetrad classmates for synchronized swimming mitosis, bioreg, class "research talks", and Alice in Wonderland. I want to particularly thank my undergraduate advisor Bonnie Bartel, my high school biology teacher Barry Shapiro, and my fellow SEP scientists and educators for their inspiration, imagination, and dedication to teaching. I am blessed by an incredible support network of friends from Rice, agricola, wine-tasting, futsal, squash, Japanese class and roommates – thank you for *more* than just fun and games. Lastly, I am humbled by the unconditional love and support of my family who are a constant source of strength. And to Mari, we did it!

STATEMENT REGARDING AUTHOR CONTRIBUTIONS

Chapter two is a reprint of a *Methods in Molecular Biology* chapter published in 2009 (volume 571, pp 167-177) by me and Orion Weiner. The methods were modified from Orion's original protocols and manufacturer's instructions (i.e. amaxa nucleofection) for best results in my hands with HL-60 cells. I illustrated the figures and and wrote the text with comments and suggestions from Orion.

Chapter three is a reprint of a *Current Biology* article published in 2009 (volume 19, issue 3, pp 253-259) by me, Sheel Dandekar, Andrew Houk, and Orion Weiner. Sheel, Andrew, and I made equal contributions to this paper – I performed the micropipette and drug-treatment experiments (figures 1, 2, and 4); Andrew examined "waves" in other cell types and did the uniform agonist experiments (figures 1 and 3); Sheel developed Matlab software and analyzed the data (figures 1-4). Sheel, Andrew, Orion, and I made equal contributions to writing the paper.

Chapter four is the product of my own labors with guidance from my thesis committee and technical support from various UCSF colleagues. In particular, Derek Wong helped me develop the lipid bead assays, guided me through Arp2/3 complex purification, and supplied purified NWASP. Scott Hansen helped with actin biochemistry and pyrene assays. Gigi Knudsen performed the mass spectrometry. Peter Hordijk furnished the GFP-βpix construct.

Chapter five is adapted from an article in press at the *Journal of Cell Science* by me, Naoki Watanabe and Orion Weiner. Naoki, Orion, and I conceived the experiments, which were performed by me in both Naoki and Orion's labs. Naoki supplied the delCMV actin, p40, and WAVE2 constructs. I performed the analysis and wrote the script to derive lateral diffusion coefficients from Matlab software published by the Danuser lab. I created the figures and Orion and I wrote the paper.

WAVE-mediated Actin Assembly

Arthur Millius

Abstract

This thesis presents work toward understanding the biophysical mechanisms that control polarized cell movement. Many cells move in response to external cues, and this directed movement occurs during development, axon guidance, wound healing, tumor progression, and the immune response. Cells must interpret external signals through signal transduction networks and engage actin polymerization machinery to generate mechanical force for membrane protrusion at the leading edge of the cell. Our work focuses specifically on the interface between the cell's signaling guidance system and actin nucleation machinery.

In the first project, we analyzed the protein dynamics of a major cytoskeleton regulator called the WAVE complex in a human neutrophil-like cell line in response to gradient and uniform agonist stimulations (Chapter 3). We demonstrated that biased generation and selection of WAVE-complex activity drives the development of morphological polarity and we discovered that actin polymer sculpts the localization of the WAVE-complex.

In the second project, we developed a biochemical system to study the WAVE complex, discovered a GTPase exchange factor likely involved in WAVE-complex activation, searched for other WAVE-complex binding proteins through immunoprecipitation, and examined cell behavior in response to temporal changes in agonist (Chapter 4).

In the third project, we studied the single-molecule behavior of cytoskeletal proteins in XTC cells using epifluorescence and TIRF microscopy. We showed that the WAVE complex intercalates into the actin network during retrograde grade flow. Additionally, we observed lateral diffusion of both the WAVE complex and the Arp2/3 complex and captured the transition of the Arp2/3 complex from diffusion to network incorporation.

TABLE OF CONTENTS

LIST OF FIGURES

CHAPTER ONE

Introduction

A hungry graduate student can always find free food

-Keith Mostov's 2nd law

How does a cell move from one location to another? Cells do not have a national transportation infrastructure or an automobile, or even a bicycle or a pair of running shoes. A cell has neither a pair of legs nor a brain to direct its motion, yet everyday our cells move to and fro – hunting bacteria, closing wounds, or honing to sites of inflammation. Cells accomplish this migration through an extraordinary feat of engineering – the coordinated and polarized construction and destruction of its entire structural network. Imagine sitting in a car where directed motion occurs when a NASCAR pit crew disassembles the back wheels, chassis and engine, and then reassembles everything in front of the car (so that the front wheels now become the back wheels) – repeating the process until you arrive at a desired destination. The prospect is absurd! And yet a cell does just this and can do it in under 60 seconds.

Actin-based cell motility

Cell movement is crucial in many avenues of biology from bacteria chemotaxis to eukaryotic cells undergoing gastrulation during development. Cells must be able to adjust their movement in response to external cues. Directed cell migration is exquisitely sensitive – human neutrophils can detect just a 1% gradient across their cell surface (Zigmond, 1977). However, cell motility also must be tightly controlled; loss of control can lead to metastatic cancer and tumor progression (Rafelski and Theriot, 2004).

Cell movement occurs through dynamic rearrangements of structural elements within the cell. This structure is called the actin cytoskeleton. Actin is a protein with a unique property – it self-assembles into filaments – like Lego bricks being built without a builder. And like Lego bricks, actin filaments are modified by all sorts of different proteins. There is a protein that causes a filament to branch into two filaments called the Arp2/3 complex; another protein that caps a filament to prevent further growth called capping protein; another protein that takes apart filaments called cofilin; and many more. However, indiscriminate building and disassembly of cellular structures would hardly get a cell where it needs to go. Instead, there are signaling systems that control how and where actin networks are built and destroyed.

Force-generating and guidance systems in cell motility

Cell migration is an interplay between a molecular guidance system and a force-generating system. The guidance system is a complex network of signaling proteins – receptors, kinases/phosphatases, lipid signaling molecules, Rho family GTPases and their associated regulators. These molecules act as sensing, adapting, and amplifying circuit modules. In human neutrophils bacteria shed formylated peptides that act as ligands, which stimulate a G-protein coupled receptor on the membrane surface of the neutrophil.

The receptor activates a Rho-family GTPase, a protein that switches between a GDP-bound inactive confirmation and GTP-bound active confirmation, which in turn activates lipid kinases and a protein complex called the WAVE complex (Stradal et al., 2004).

The WAVE complex: an essential intermediate that couples signaling to cytoskeletal machinery

How do signaling systems engage force-generating machinery? One class of molecules that link signals to actin polymerization are called nucleation-promoting factors, which include Wiskott Aldrich Syndrome Protein (WASP) and WASP Verprolin-related protein (WAVE). These molecules directly bind actin monomers and the Actin-related (Arp) 2/3 complex, a large seven-protein complex involved in actin filament nucleation and branching (Stradal et al., 2004). Both WAVE and WASP bind actin and Arp2/3 at a c-terminal domain in their protein called the VCA domain. While this domain is sufficient to promote Arp2/3-mediated actin assembly, full length proteins are inhibited through auto-inhibition (WASP) or binding in a regulatory complex (WAVE). Only when upstream signals are present, which include GTPases, phosphoinositides, and kinases, are WASP and WAVE activated. Native WAVE complex, for example, is only activated by a combination of the Rho family GTPase Rac and the phosphoinositide PIP3 (Lebensohn and Kirschner, 2009). WAVE-complex molecules associate in "waves" at the leading edge of a cell (Weiner et al., 2007). Deletion of the WAVE complex is required for movement and morphogenesis of cells in C. elegans (Patel et al., 2008), Drosophila (Zallen et al., 2002), and mice (Steffen et al., 2004; Rakeman and Anderson, 2006), but, surprisingly, also abrogates the activity of Rac (Weiner, Rentel, et al., 2006). These observations reveal the critical nature of the WAVE complex and related proteins as

nodes both controlling the actin cytoskeleton and feeding back on the signaling network.

Key questions

In this thesis we pursue several questions surrounding the biophysical activity of the WAVE complex. First, how does the WAVE complex contribute to the development of morphological polarity in an initially unpolarized, quiescent cell? We analyzed a fluorescently-tagged WAVE complex in response to several different types of agonist stimulations and quantified how cells responded (Millius et al., 2009). We determined that development of a polarized front can occur through one of two routes. Either cells from their earliest moments generate a polarized WAVE-complex distribution or cells respond with a global burst of WAVE-complex activity that ultimately is pared down to a polarized front. The route used depends on the level of agonist stimulation and the spatial presentation mode.

Second, how does actin assembly, a product of WAVE-complex activity, shape the distribution of the WAVE complex? We treated cells with actin-destabilizing drugs and discovered that WAVE-complex distribution is reciprocally affected by actin polymer (Millius et al., 2009). Additionally, we used single-molecule imaging to track WAVE-complex molecules after they have incorporated into the actin cytoskeleton (Millius et al., 2011, *in press*). We observed retrograde movement of WAVE-complex molecules away from the leading edge at speeds and lifetimes similar to actin retrograde flow. Inhibition of actin assembly interfered with this retrograde movement. Together, these results suggest that actin assembly is an important component of WAVE-complex recycling.

Third, how is the WAVE-complex activated? We developed a biochemical system to explore WAVE-complex activation on the surface of lipid-coated beads. We showed

binding of the GTPase Rac, a WAVE-complex activator, to these beads in a nucleotide and GEF-dependent fashion and developed a pyrene assay to explore WAVE-complex mediated actin assembly. Others showed a critical role for phosphorylation of the WAVE-complex in addition to Rac and anionic phospholipids for its full activation (Lebensohn and Kirschner, 2009), and future studies should focus on developing protocols for purified phosphorylated WAVE-complex. Finally, we also examined GFP-tagged GEFs for localization similar to the WAVE complex in neutrophil-like HL-60 cells, found a GEF β-pix, and showed that β-pix exists in a large complex of similar size to the WAVE complex. Future studies should be aimed at uncovering the components of this complex and analyzing the activity of the WAVE complex in β-pix knock-down cells.

Finally, how do nucleation factors like the Arp2/3 complex or the WAVE complex arrive at sites of nucleation? We used high-speed, single-molecule, TIRF imaging to show that both the Arp2/3 and WAVE complexes diffuse before incorporating into the actin network (Millius et al., 2011, *in press*). For the Arp2/3 complex, we captured the transition from diffusion to retrograde flow. This demonstrates that nucleation factors perform a rapid two-dimensional search along the plasma membrane for nucleation sites.

REFERENCES

Lebensohn, A. M. and Kirschner, M.W. (2009). Activation of the WAVE complex by coincident signals controls actin assembly. *Mol. Cell*, **36**, 512-524.

Millius, A., Dandekar, S. N., Houk, A. R., and Weiner, O. D. (2009). Neutrophils establish rapid and robust WAVE complex polarity in an actin-dependent fashion. *Curr Biol*, **19**, 253-9.

Millius, A., Watanabe, N., and Weiner, O.D. (2011). Diffusion, capture, and recycling of SCAR/WAVE and Arp2/3 complexes observed in cells with single-molecule imaging. *J Cell Sci, in press*

Patel, F. B., Bernadskaya, Y. Y., Chen, E., Jobanputra, A., Pooladi, Z., Freeman, K. L., Gally, C., Mohler, W. A., and Soto, M. C. (2008). The WAVE/SCAR complex promotes polarized cell movements and actin enrichment in epithelia during C. elegans embryogenesis. *Developmental biology*, **324**, 297-309.

Rafelski, S. M. and Theriot, J. A. (2004). Crawling toward a unified model of cell mobility: spatial and temporal regulation of actin dynamics. *Annual review of biochemistry*, **73**, 209-39.

Rakeman, A. S. and Anderson, K. V. (2006). Axis specification and morphogenesis in the mouse embryo require Nap1, a regulator of WAVE-mediated actin branching. *Development*, **133**, 3075-83.

Steffen, A., Rottner, K., Ehinger, J., Innocenti, M., Scita, G., Wehland, J., and

Stradal, T. E. (2004). Sra-1 and Nap1 link Rac to actin assembly driving lamellipodia formation. *Embo J*, **23**, 749-59.

Stradal, T. E. B., Rottner, Klemens, Disanza, A., Confalonieri, S., Innocenti, Metello, and Scita, Giorgio (2004). Regulation of actin dynamics by WASP and WAVE family proteins. *Trends Cell Biol*, **14**, 303-311.

Weiner, O. D., Marganski, W. A., Wu, L. F., Altschuler, S. J., and Kirschner, M.W. (2007). An actin-based wave generator organizes cell motility. *PLoS Biol*, **5**, e221.

Weiner, O. D., Rentel, M. C., Ott, A., Brown, G. E., Jedrychowski, M., Yaffe, M. B., Gygi, S. P., Cantley, L. C., Bourne, H. R., and Kirschner, M.W. (2006). Hem-1 complexes are essential for Rac activation, actin polymerization, and myosin regulation during neutrophil chemotaxis. *PLoS Biol*, **4**, e38.

Zallen, J. A., Cohen, Y., Hudson, A. M., Cooley, L., Wieschaus, E., and Schejter, E. D. (2002). SCAR is a primary regulator of Arp2/3-dependent morphological events in Drosophila. *J Cell Biol*, **156**, 689-701.

Zigmond, S. H. (1977). Ability of polymorphonuclear leukocytes to orient in gradients of chemotactic factors. *The Journal of cell biology*, **75**, 606-16.

CHAPTER TWO

Chemotaxis in neutrophil-like HL-60 cells

Six months in the lab will save a day or two in the library

-Dan Fletcher

If your logic is impeccable, but your premise if false, then invariably you're doomed to failure

-Kim Naysmith

I'm cheaper than a monkey

-Orion Weiner

Adapted from Millius and Weiner (2009), Chemotaxis in neutrophil-like HL-60 cells. In *Methods in Molecular Biology* volume 571, pp167-177. Humana Press. Tian Jin and Dale Hereld, editors.

SUMMARY

Asymmetric localization of intracellular proteins and signals directs movement during axon guidance, endothelial cell invasion, and immune cell migration. In these processes, cell movement is guided by external chemical cues in a process known as chemotaxis. In particular, leukocyte migration in the innate immune system has been studied in the human neutrophil-like cell line (HL-60). Here, we describe the maintenance and transfection of HL-60 cells and explain how to analyze their behavior with two standard chemotactic assays. Finally, we demonstrate how to fix and stain the actin cytoskeleton of polarized cells for fluorescent microscopy imaging.

1. INTRODUCTION

Directed cell migration toward chemical cues, or chemotaxis, is critical in eukaryotic cells for immune response, wound healing, axon guidance, and embryogenesis (1). An especially useful model for eukaryotic chemotaxis is the human neutrophil. Neutrophils seek infectious bacteria to engulf at wound sites as part of the innate immune system. They follow gradients of formylated peptides released by the bacteria (1). Yet, many open questions remain in neutrophil and eukaryotic cell migration. How do cells interpret shallow gradients or initially establish polarity? How is their cytoskeleton rearranged during a turn, and what limits this rearrangement to one part of the cell and not another? What signaling components and circuitry are required to accomplish theses processes?

The human promyelocytic leukemia (HL-60) cell line was developed as a simple model system to study neutrophil cell migration without the need to derive cells from primary tissue (2). The immortal cell line can be sustained for extended periods of time in culture and may be frozen for longer term storage. This is impossible with bone marrow or peripheral blood derived neutrophils. When needed, neutrophil-like cells can be derived from HL-60 cells through differentiation with DMSO (3). Differentiated HL-60 cells (dHL-60) can then be used in chemotaxis assays and to the visualize the cytoskeleton of a polarized cell (4). Amaxa nucleofection may be used in dHL60 cells to knock genes down (5-8) or transfect cells with a fluorescent tag to analyze protein localization (our unpublished results). Cell behavior can be analyzed either in response to a point source of chemoattractant (9-11), or using the EZ-TAXIS system, which allows simultaneous measurement of directionality and speed for six different assay conditions (12, 13).

2. MATERIALS

2.1. HL-60 cell culture and differentiation

1. Culture media: Roswell Park Memorial Institute (RPMI) 1640 plus L-glutamine and 25 mM HEPES (10-041-CM, Fisher Scientific) supplemented with antibiotic/antimycotic (15240, Invitrogen) and 15% heat-inactivated fetal bovine serum (FBS; 16140, Invitrogen); store at 4°C (*see* **Note 1**).
2. Dimethyl sulphoxide (DMSO), endotoxin and hybridoma tested (D2650, Sigma).

2.2 Amaxa nucleofection of HL-60 cells

1. Recovery media: monocyte media (VZB-1003, Amaxa) supplemented with 1X glutamine (25030, Invitrogen) and 20% FBS.
2. 100 μl of transfection solution containing supplement (VCA-1003, Amaxa) mixed with 2 μg DNA per reaction (*see* **Note 2**).

2.3 Plating cells for microscopy

1. Fibronectin from bovine plasma (F4759, Sigma); store lyophilized protein at -20°C.
2. Ca^{2+}/Mg^{2+} free phosphate buffered saline (PBS): prepare 1X stock with 137 m*M* NaCl, 2.7 m*M* KCl, 10 m*M* Na_2HPO_4, 1.8 m*M* KH_2PO_4 or purchase (10010, Invitrogen).
3. Gold seal cover glass 20x40 mm No. 1.5 (3405, Fisher Scientific).
4. Lab-Tek 8 well permanox chamber slide (177445, Nunc).

5. Chemoattractant: formylated Methione-Leucine-Phenylalanine (fMLP; F3506, Sigma) store at 10 mM in DMSO at -20°C. Prepare working stocks at 100 μM in RMPI and store at 4°C up to 1 month (*see* **Note 3**).

2.4 Micropipette assay

1. Glass capillary with filament (TW100-4, World Precision Instruments) (*see* **Note 4**).
2. Alexa Fluor 594 hydrazide (A-10438, Invitrogen) 1 mg sodium salt dissolved in 132 μl DMSO to give a 10 mM working stock; store at 4°C and protect from light.
3. Chemoattractant solution: prepare 200 nM fMLP and 10 μM Alexa594 in RPMI culture media; protect from light.

2.5 EZ-TAXIScan Assay

1. RPMI culture media.
2. Chemoattractant solution: 200 nM fMLP in RMPI culture media.

2.6 Staining the actin cytoskeleton

1. Intracellular buffer: prepare 10X stock with 1.4 M KCl, 10 mM $MgCl_2$, 20 mM EGTA, 200 mM Hepes pH 7.5. Prepare 2X working solution by dilution of two parts with eight parts water; store at 4°C. Add 0.4% low endotoxin albumin from human serum (A-5843, Sigma) fresh and let sit at room temperature for 30 min before mixing (*see* **Note 5**).

2. 2X Fixation buffer: 2X intracellular buffer plus 640 mM sucrose and 7.4% formaldehyde (F-1268, Sigma); store at 4°C (*see* **Note 6**).

3. Stain buffer: intracellular buffer plus 0.2% triton and 2 μl/ml rhodamine phalloidin (R415, Invitrogen) (*see* **Note 7**).

3. METHODS

3.1 Maintenance of HL-60 cell culture line

1. Unless imaging, all cell work is performed under a biological safety cabinet (SG303, The Baker Company).

2. HL-60 cells are passaged when the cells reach a density between 1-2 million cells/ml in 25 cm^2 cell culture flasks with 0.2 μm vent cap (430639, Corning). Split cells to 0.15 million cells/ml in a total volume of 10 ml prewarmed culture media. Cells will need to be passaged again after 2-3 days (**Fig. 1**). Maintain cells at 37°C and 5% CO_2 in standard tissue culture incubator (Forma Scientific) (*see* **Note 8**).

3. Differentiate cells in culture media plus 1.3% DMSO (130 μl DMSO in 10 ml media + cells). Because DMSO is more viscous and denser that culture media, premix media with DMSO before adding cells. Cells stop proliferating upon differentiation and typically achieve a density of 1-2 million cells/ml at 7 days post-differentiation (**Fig. 1**). Cells are most active 5-6 days post-differentiation, but can still respond even after 8 days (*see* **Note 9**).

4. To freeze cells, pellet cells by spinning at 100xg for 10 min. Aspirate media and resuspend in chilled culture media plus 10% DMSO at 10 million cells/ml. Aliquot 1.8 ml each into cryovials (5001-0020, Nalgene), place in cryofreezing container with isopropanol (5100-0001, Nalgene) at -80°C for 2 days, and then transfer to liquid nitrogen storage (*see* **Note 10**).

5. Thaw cells by quickly warming a cryovial at 37°C just until last bit of ice has melted. Dilute thawed cells in 10 ml of prewarmed culture media and spin at 100xg for 10 min. Remove supernatant, resuspend pellet in 20 ml culture media,

and recover in a 75 cm^2 culture flask (430641, Corning).

3.2 Transient transfection of DNA into HL-60 cells

1. Prepare ~2 ml of recovery media per transfection in a 6 well plate (3335, Corning) and let equilibrate at 5% CO_2 and 37°C for 15 minutes or more. Add 500 μl of equilibrated recovery media to an eppendorf tube (50-400-411, Fisher Scientific) per transfection (*see* **Note 11**).
2. Spin 5 million cells in a 10 ml falcon tube (05-539-1, Fisher Scientific) at 100xg for 10 min. Use a separate falcon tube for each transfection.
3. After spin, remove all media with aspirator and gently resuspend cells in 100 μl transfection solution with a L-1000 pipette (Rainin) (*see* **Note 12**).
4. As quickly as possible, transfer transfection solution to nucleofection cuvette (VCA-1003, Amaxa). Electroporate in single chamber nucleofector (Amaxa) on program Y-001.
5. Immediately remove cuvette, use plastic pipette (VCA-1003, Amaxa) to obtain 500 μl recovery media from eppendorf tube, flush chamber, and replace media containing cells in eppendorf tube.
6. Incubate for 30 min in eppendorf tube at 37°C (*see* **Note 13**).
7. Transfer 500 μl recovery media and cells with L-1000 pipette to 1.5 ml recovery media in a 6 well plate. Expression in viable cells occurs in ~2 hours with best behavior <8 hours after transfection (**Fig. 2**).

3.3 Preparing for live cell microscopy

1. Dissolve 1 ml of sterile water in 1 mg fibronectin and let sit at room temperature for 1 hour. Avoid shaking or physically mixing because this may denature the fibronectin.

2. Add 4 ml of Ca^{2+}/Mg^{2+} free PBS to fibronectin solution to obtain 200 μg/ml solution (**Fig. 3A**): store fibronectin solution at 4°C for up to 2 weeks.

3. Remove exterior gaskets from permanox chamber slide and the interior gasket with a razor blade. Discard 8 well plastic walls to expose underlying epoxy mold. With razor, cut single well epoxy chambers and adhere to glass coverslips (*see* **Note 14**).

4. Add 125 μl fibronectin solution to epoxy chamber on coverslip. Incubate at room temperature for 1 hour.

5. Aspirate fibronectin solution and rinse once in RPMI culture media. Add 250 μl RPMI culture media until ready to plate cells. Fibronectin coated slides may be stored up to 2 days at 4°C (**Fig. 3B**).

6. For cell plating, remove culture media on slide and replace with 250 μl differentiated cells (in RPMI culture media) or transfected cells (in monocyte media). Incubate at 37°C for 5-15 min (*see* **Note 15**).

7. Aspirate cells at the corner of the epoxy chamber (avoid touching the coverslip), rinse in RPMI, and replace with 125 μl RPMI. Cells are most migratory at 37°C, but also function at room temperature.

8. During image acquisition, 125 μl 200 nM fMLP may be added to coverslip (final concentration is 100 nM) to show random migration in response to uniform chemoattractant.

3.4 Micropipette-stimulated cell migration

1. Pull glass filaments on Sutter Model P-87 (Program: heat = 750, pull = 0, velocity = 20, time = 250, pressure = 100, loops 2 or 3 times) to achieve ~2-3 μm needle diameter.

2. Backfill needles with chemoattractant solution and connect to a needle holder (MINJ4, Tritech). Flick to remove air bubbles at the tip. Needle holder is held by a micromanipulator (MM-89, Narishige) and agonist flow controlled by adjusting balance pressure between 0-3 psi on an IM-300 injection system (Narishige) (*see* **Note 16**).

3. Place cells seeded on a coverslip on microscope and find focus of cells in brightfield.

4. Orient needle in light path and switch to the back focal plane of the objective (usually labeled "B" for Bertrand lens). Find the needle and lower it until just above the cells, then switch back to the normal focal plane for viewing.

5. Image dye in fluorescence or Total Internal Reflection Fluorescence (Nikon Eclipse TE2000-E inverted microscope with a 60x, PlanApo TIRF, 1.49 NA objective) microscopy using appropriate filter sets (Chroma) with ~20 ms exposures and near maximal multiplication on an EM-CCD camera (Cascade II 512, Photometrics) (*see* **Note 17**). An example of a cell migrating toward a micropipette filled with chemoattractant is shown in **Fig. 4**.

3.5 Ascertaining directionality and velocity of migrating cells with the "EZ-TAXIS" assay system

1. Place "40 Glass" (41 Glass is used in conjunction with a #1.5 coverslip) in holder

base. Fill with 3 ml of culture media, place small "o" ring beneath wafer housing, and add wafer housing into holder base. Place large "o" ring on top of wafer housing. Gently close inner lever.

2. Place EZ-TAXIScan chip gently into wafer housing with forceps. Chip should fit snuggly on top of glass and between wafer holder (*see* **Note 18**). Place rubber gasket (to protect chip) beneath the wafer clamp and place wafer clamp on wafer housing. Gently close outer lever.

3. Place assembled device on top of preheated EZ-TAXIS microscope (**Fig. 5, A and B**).

4. Using syringe guide, add 1 μl of cells to lower chamber using microsyringe (MS-E10MIC, Exmire). Use a plastic pipette to draw cells into imaging surface.

5. Add 1 μl of 100 nM – 1 μM chemoattractant to upper chamber. Begin image acquisition immediately (**Fig. 5C**).

3.6 Staining the actin cytoskeleton

1. Stimulate adherent cells with micropipette or uniform chemoattractant. Alternatively, you can stimulate cells in solution.

2. Add 2X fixation buffer to cells. (Thus, if you had 125 μl cells in RMPI media, you would add 125 μl fixation buffer to give a final concentration of 320 mM sucrose and 3.7% formaldehyde.) Fix for 20 min at 4°C (*see* **Note 19**).

3. Aspirate supernatant (adherent cells) or spin down cells at 400xg for 1 min and then aspirate supernatant (suspended cells).

4. Permeabilize cells with 125 μl stain buffer and protect from light for 20 minutes

(**Fig. 6**).

5. Remove supernatant, replace with intracellular buffer, and image (*see* **Note 20**).

4. NOTES

1. HL-60 cells acidify their media quite rapidly, so HEPES is essential to counterbalance the pH.
2. Poor expression occurs in retroviral LTR-containing vectors.
3. If an exact concentration of fMLP is required, make stocks fresh weekly because formyl peptide will slowly oxide in aqueous solutions over time.
4. Capillaries with filaments are easier to load than capillaries without filaments.
5. HL-60 cells may be spuriously stimulated with albumin containing endotoxins. Additionally, it is important to add the albumin fresh because it oxidizes in aqueous solution to products that may also activate HL-60 cells.
6. Sucrose is important to maintain osmolarity.
7. Unlike Alexa Fluor 594, rhodamine phalloidin increases its fluorescence upon binding to actin filaments. This makes it preferable to Alexa Fluor 594. However, for imaging in the green channel, we would use Alexa Fluor 488 or similar fluorophore over the rapidly bleaching FITC.
8. Keep a basin of water on the bottom shelf of the incubator to maintain humidity.
9. Cells may also be differentiated with retinoic acid (14).
10. As an alternative to nalgene freezing chambers, two styrofoam 15 ml falcon tube holders may be sandwiched around tubes to provide insulation during slow freezing process.
11. Our protocol differs significantly from the standard Kit V protocol from amaxa, because we have optimized for cells to retain chemotactic function (not necessarily highest transfection efficiency).

12. It is important to remove every drop of media from falcon tube because FBS will interfere with transfection. Large tip pipettes minimize shearing of cells and increases the number of healthy cells post-transfection.

13. Cells will adhere to each other and form a thin, white film during the 30 min incubation in eppendorf tube. This step increases recovery efficiency. Additionally, cells are fragile after transfection and they behavior poorly if centrifuged.

14. An 8 well chamber will yield four molds. Only bottom surface (side touching permanox chamber slide) of epoxy mold is sticky. Additionally, Lab-Tek 8 well cover glass #1.5 chamber slide (155409, Nunc) may be used for epifluorescence and brightfield microscopy. However, the epoxy that hold the chamber walls to the coverslip is autofluorescent and thus less suitable for TIRF.

15. Cells may be plated in culture media containing chemoattractant for a higher proportion of adherent cells.

16. Load needles without gloves. It is difficult to handle capillaries with gloves on. Also, even if no bubbles are visible by eye, flick the needle vigorously to remove microscopic bubbles. Do not try to force air bubbles through the tip by increasing air pressure. Invariably, the bubbles will become stuck and the needle rendered useless.

17. For quantification of gradient, TIRF imaging is superior to epifluorescence microscopy because TIRF reveals the agonist concentrations in the same plane as the cell. The signal obtained from epifluorescence is a combination of the agonist the cell experiences plus out of focus blur from fluorescent dye above the cell. Confocal imaging can also be used to quantitate the gradient.

18. Chips come in four different sizes (4 μm, 5 μm, 6 μm, and 8 μm) depending on the gap space between the chip and glass. We have used the 4-6 μm chips with success.

19. Formaldehyde can partially permeabilize cells, allowing water influx due to high internal protein concentration.

20. Can repeat wash if background too high. If pressed for time, can immediately image after adding stain buffer. However, this will give high background staining. You can also mount cells in Vectashield (H-1000, Vector Laboratories) for decreased spherical aberrations and photobleaching.

ACKNOWLEDGEMENTS

We would like to thank the NIH R01GM084040 and a National Defense Science and Engineering Graduate Fellowship to A. Millius.

REFERENCES

1. Ridley, A. J., Schwartz, M. A., Burridge, K., Firtel, R. A., Ginsberg, M. H., Borisy, G., Parsons, J. T., and Horwitz, A. R. (2003) *Science* **302,** 1704-9.

2. Collins, S. J., Gallo, R. C., and Gallagher, R. E. (1977) *Nature* **270,** 347-9.

3. Collins, S. J., Ruscetti, F. W., Gallagher, R. E., and Gallo, R. C. (1978) *Proc Natl Acad Sci U S A* **75,** 2458-62.

4. Rao, K. M., Currie, M. S., Ruff, J. C., and Cohen, H. J. (1988) *Cancer Res* **48,** 6721-6.

5. Carter, B. Z., Milella, M., Tsao, T., McQueen, T., Schober, W. D., Hu, W., Dean, N. M., Steelman, L., McCubrey, J. A., and Andreeff, M. (2003) *Leukemia* **17,** 2081-9.

6. Nakata, Y., Tomkowicz, B., Gewirtz, A. M., and Ptasznik, A. (2006) *Blood* **107,** 4234-9.

7. de la Fuente, J., Manzano-Roman, R., Blouin, E. F., Naranjo, V., and Kocan, K. M. (2007) *BMC Infect Dis* **7,** 110.

8. Gattenloehner, S., Chuvpilo, S., Langebrake, C., Reinhardt, D., Muller-Hermelink, H. K., Serfling, E., Vincent, A., and Marx, A. (2007) *Blood* **110,** 2027-33.

9. Weiner, O. D., Servant, G., Welch, M. D., Mitchison, T. J., Sedat, J. W., and Bourne, H. R. (1999) *Nat Cell Biol* **1,** 75-81.

10. Servant, G., Weiner, O. D., Herzmark, P., Balla, T., Sedat, J. W., and Bourne, H. R. (2000) *Science* **287,** 1037-40.

11. Wang, F., Herzmark, P., Weiner, O. D., Srinivasan, S., Servant, G., and Bourne, H. R. (2002) *Nat Cell Biol* **4,** 513-8.

12. Ferguson, G. J., Milne, L., Kulkarni, S., Sasaki, T., Walker, S., Andrews, S.,

Crabbe, T., Finan, P., Jones, G., Jackson, S., Camps, M., Rommel, C., Wymann, M., Hirsch, E., Hawkins, P., and Stephens, L. (2007) *Nat Cell Biol* **9,** 86-91.

13. Nishio, M., Watanabe, K., Sasaki, J., Taya, C., Takasuga, S., Iizuka, R., Balla, T., Yamazaki, M., Watanabe, H., Itoh, R., Kuroda, S., Horie, Y., Forster, I., Mak, T. W., Yonekawa, H., Penninger, J. M., Kanaho, Y., Suzuki, A., and Sasaki, T. (2007) *Nat Cell Biol* **9,** 36-44.

14. Breitman, T. R., Selonick, S. E., and Collins, S. J. (1980) *Proc Natl Acad Sci U S A* **77,** 2936-40.

Figure 1

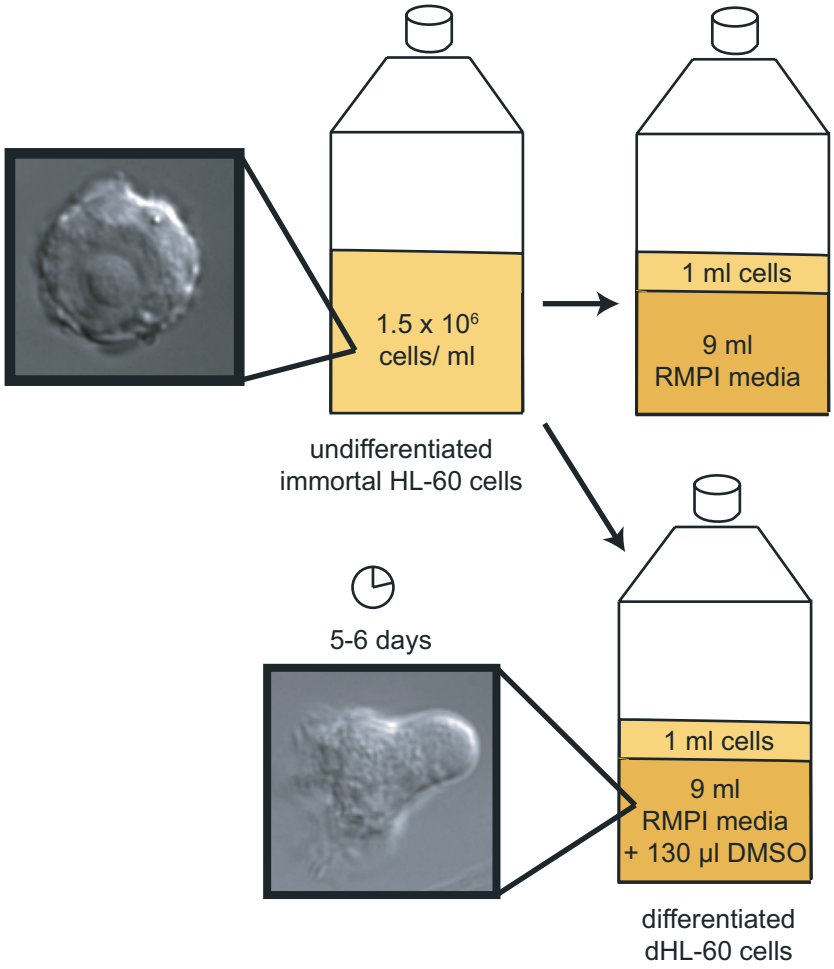

Fig. 1. Passaging and differentiating HL-60 cells. When cells reach a density between 1-2 million cells/ml, split to 0.15 million cells/ml in a total volume of 10 ml prewarmed culture media. Differentiate cells in culture media plus 1.3% DMSO; cells take ~5 days to become migratory.

Figure 2

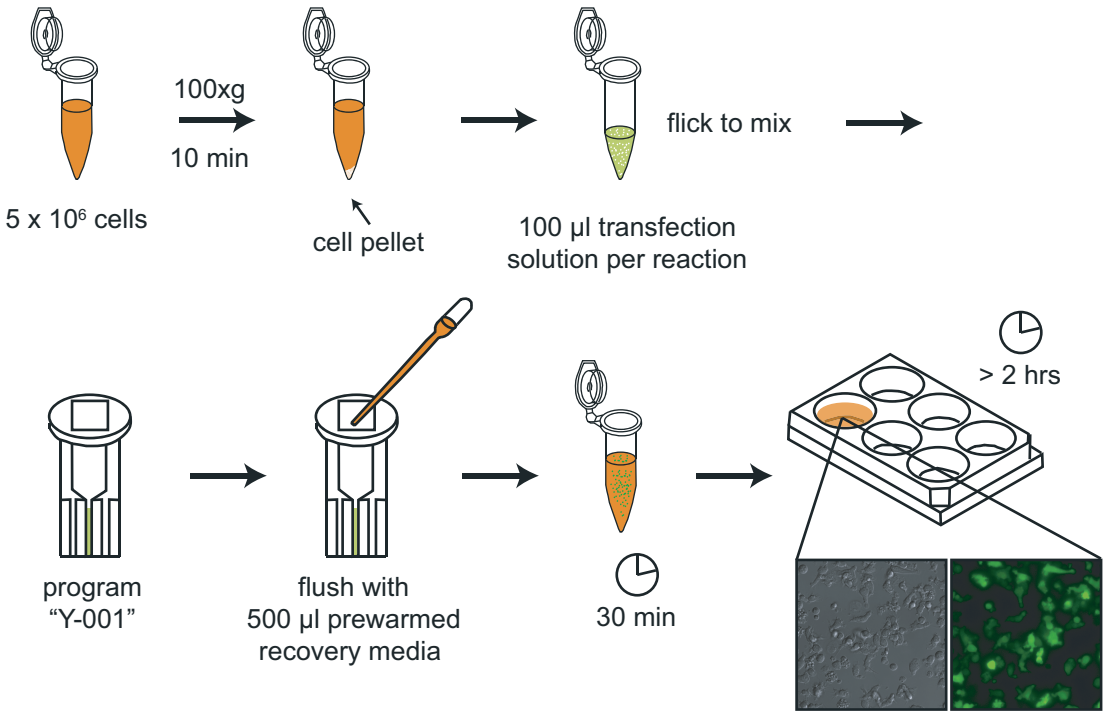

Fig. 2. Transient transfection of HL-60 cells with amaxa nucleofection. Spin ~5 million cells at 100xg. Aspirate supernatant and resuspend pellet in 100 μl transfection solution per reaction and nucleofect with amaxa program “Y-001”. Flush with prewarmed recovery media and incubate in an eppendorf tube for 30 min. Transfer to a 6-well dish with 1.5 ml of recovery media; expression occurs after 2 hours. Shown is an example of HL-60 cells 5 hours after transfection with GFP visualized with DIC and fluorescence microscopy.

Figure 3

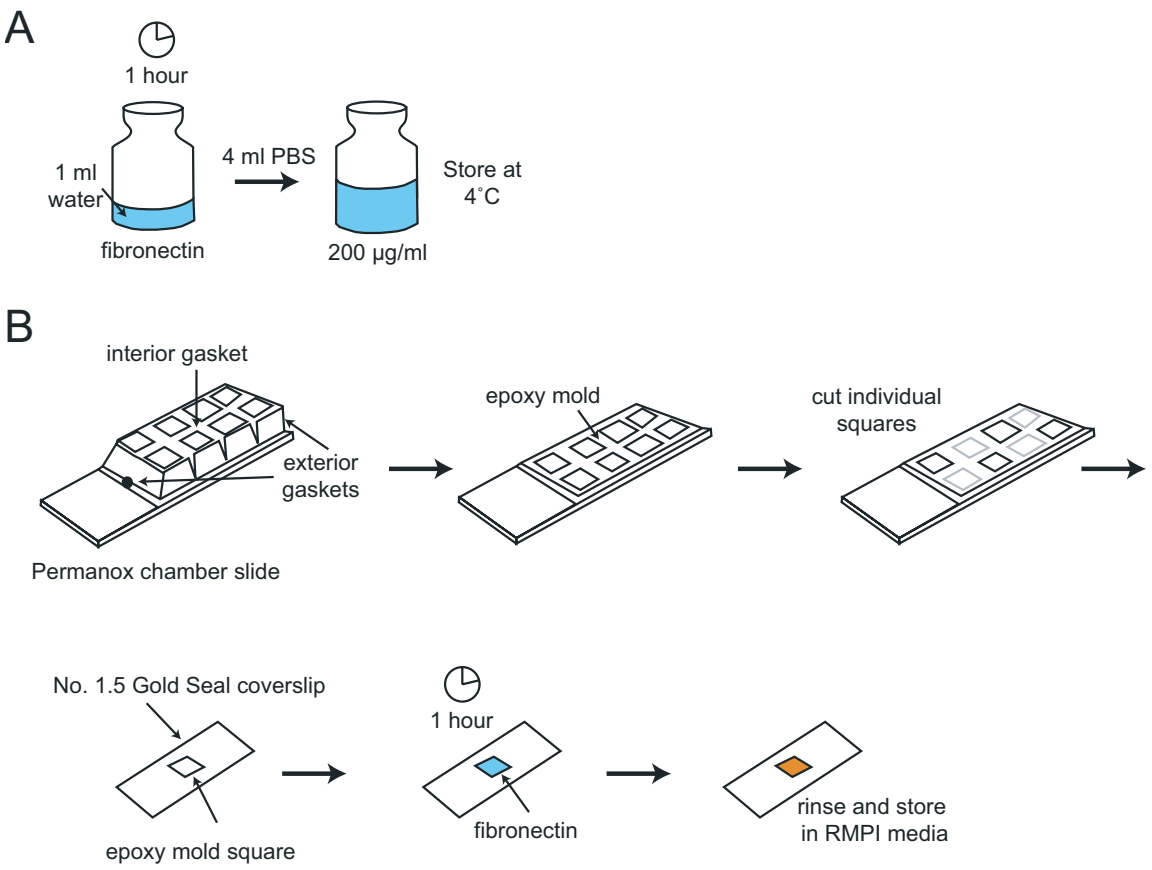

Fig. 3. Preparing a coverslip for live cell microscopy. (A) Dissolve 1 mg of bovine fibronectin in sterile water. After 1 hour, add 4 ml of PBS and store 200 μg/ml fibronectin solution at 4°C. (B) Remove gaskets from plastic permanox 8 well chamber. Cut epoxy mold squares and stick to No. 1.5 gold seal cover glass. Add 125 μl of fibronectin, let sit for 1 hour, rinse once with RPMI culture media, and store in RPMI media until ready to image.

Figure 4

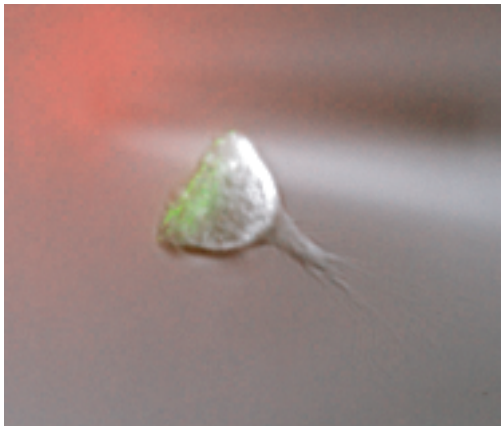

Fig. 4. An example of an HL-60 cell crawling toward a micropipette visualized with DIC and TIRF microscopy. Asterisk indicates micropipette tip.

Figure 5

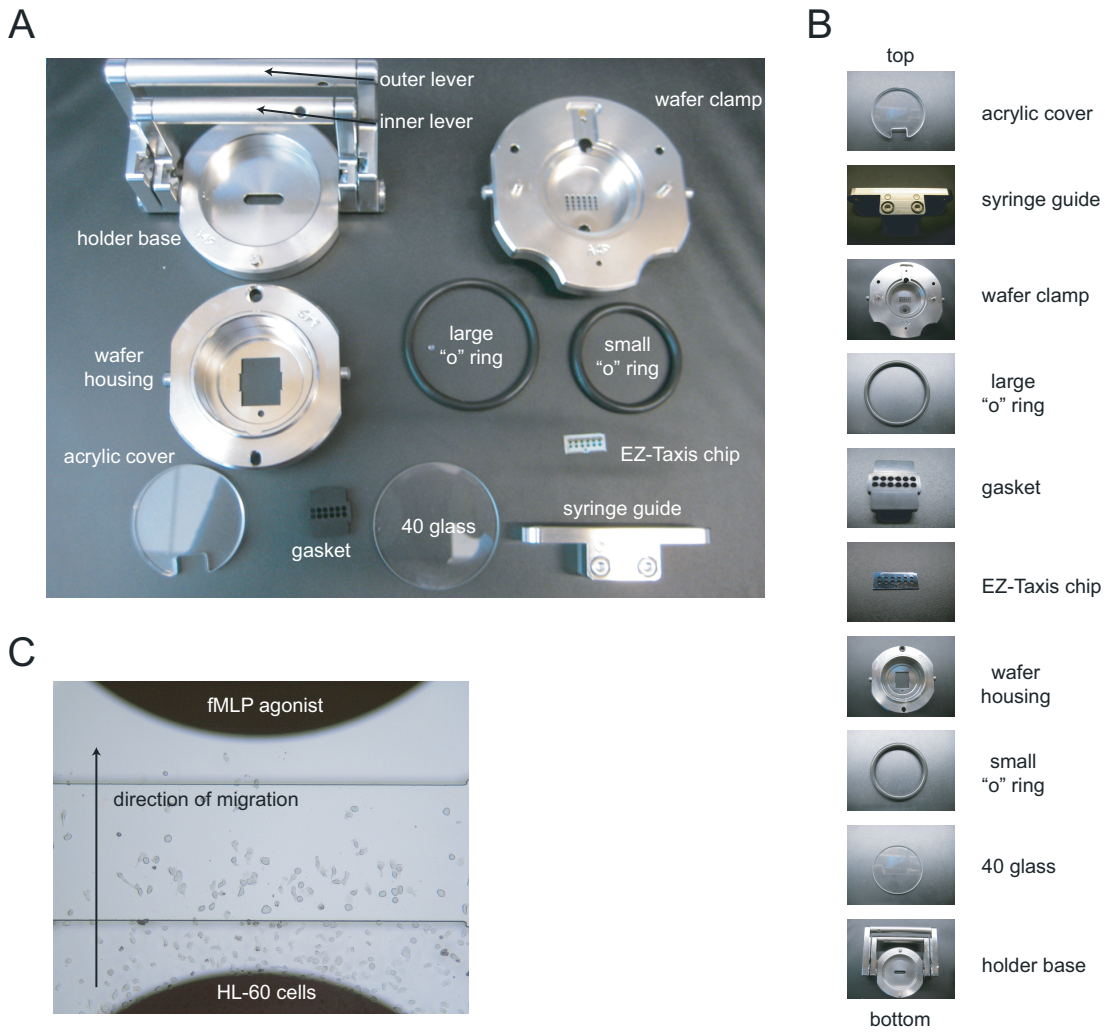

Fig. 5. The components of the EZ-TAXIS system are shown in (a) with the individual components in their order of assembly from top to bottom shown in (b). (C) An example of HL-60 cells migrating toward chemoattractant in the EZ-TAXIS assay visualized with brightfield microscopy.

Figure 6

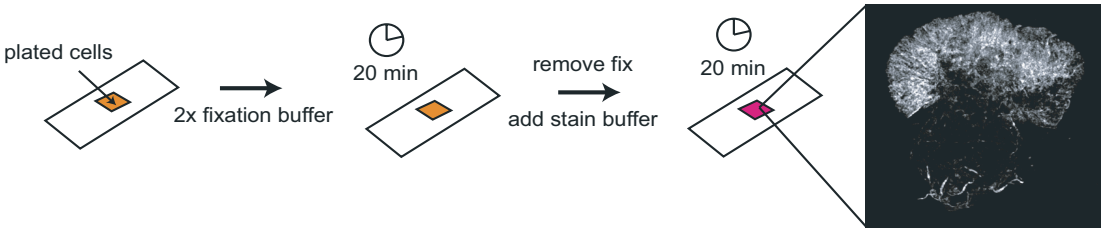

Fig. 6. Staining the actin cytoskeleton. Add 2x fixation buffer to plated cells and fix for 20 min at 4°C. Remove fixation buffer and replace with stain buffer for 20 min; protect from light. Shown is an example of an HL-60 cell stained with rhodamine phalloidin visualized with structured illumination microscopy.

CHAPTER THREE

Neutrophils establish rapid and robust WAVE complex polarity in an actin-dependent fashion

I was seduced by the dark side, and did a postdoc in eukaryotes

-Hazel Barton

Science is like a hoagie: sometimes nasty, sometimes tasty

-Uri Alon

Nature usually uses both/and rather than either/or for any god-damned thing

-Henry Bourne

Adapted from Millius A., Dandekar S.N., Houk A.R., and Weiner O.D. (2009), Neutrophils establish rapid and robust WAVE complex polarity in an actin-dependent fashion. In *Current Biology* volume 19, issue 3, pp 253-259.

SUMMARY

Asymmetric intracellular signals enable cells to migrate in response to external cues. The multiprotein WAVE (SCAR/WASF) complex activates the actin-nucleating Arp2/3 complex [1-4] and localizes to propagating "waves", which direct actin assembly during neutrophil migration [5, 6]. Here, we observe similar WAVE complex dynamics in other mammalian cells and analyze WAVE complex dynamics during the establishment of neutrophil polarity. Earlier models proposed that either spatially-biased generation [7] or selection of protrusions [8] enables chemotaxis. These models require existing morphological polarity to control protrusions. Similar spatially-biased generation and selection of WAVE complex recruitment occur in morphologically unpolarized neutrophils during the development of their first protrusions. Additionally, several mechanisms limit WAVE complex recruitment during polarization and movement: intrinsic cues restrict WAVE complex distribution during the establishment of polarity, and asymmetric intracellular signals constrain WAVE complex distribution in morphologically polarized cells. External gradients can overcome both intrinsic biases and control WAVE complex localization. After latrunculin-mediated inhibition of actin polymerization, addition and removal of agonist gradients globally recruits and releases the WAVE complex from the membrane. Under these conditions the WAVE complex no longer polarizes, despite the presence of strong external gradients. Thus, actin polymer and the WAVE complex reciprocally interact during polarization.

RESULTS AND DISCUSSION

For neutrophils, the WAVE complex is required for motility and polarity, exhibits propagating waves generated through rapid sequential rounds of recruitment and release of the complex from the plasma membrane, and requires actin polymer for its recycling from the plasma membrane [6]. Several pieces of evidence suggest that similar WAVE complex dynamics organize protrusion in other metazoan cells: the WAVE complex is required for the movement and morphogenesis of cells in *C. elegans* [9], *Drosophila* [10, 11], and mice [3, 12]; the WAVE complex localizes to the tips of protruding lamellipodia in B16F10 murine melanoma cells [13] (Fig. 1A, Movie S1); and this leading edge localization represents rapidly cycling WAVE complex (half life 8.6 s for WAVE in murine melanoma cells compared to 6.4 s for the Hem-1 component of the neutrophil WAVE complex [6, 14]). To determine whether actin assembly is required for WAVE complex recycling in cells other than neutrophils, we depolymerized the actin cytoskeleton in B16F10 cells expressing a fluorescently tagged subunit of the WAVE complex (Abi1). Actin disassembly resulted in cessation of WAVE complex movement and significant WAVE complex enrichment (2.4 +/- 0.3 fold, $P < .005$) near the plasma membrane (Fig. 1B, Movie S2), suggesting that actin is also required for WAVE complex recycling in these cells. Collectively, these data suggest that the WAVE complex exhibits similar properties in diverse mammalian cells and is likely a general regulator of cell migration throughout metazoans.

WAVE complex dynamics exhibit several features that make them ideal for a quantitative readout of polarity in neutrophils over other internal signals such as the phospholipid PIP_3 [15-17] or cell morphology [7, 8, 18]. PIP_3 now appears to be dispensable for chemotaxis in neutrophils [19] and *Dictyostelium* [20]. Morphology

results from the integration of many signals. Compared to previous morphological studies [7, 8], our use of TIRF imaging only visualizes the footprint of the cell and is likely to emphasize stabilized protrusions versus protrusions that are unlinked to the surface.

To compare WAVE complex dynamics and cell morphology as readouts for polarity, cells were analyzed following exposure to chemoattractant gradients (Fig. 1C and 1D; Movie S3). We developed automated image analysis software (Fig. S1) to quantify the input/output relation between agonist perturbations and WAVE complex response for a large number of cells. When a micropipette containing agonist was moved to a new location, WAVE complex recruitment changed more dramatically in the following 10 s than did cell morphology (Fig 1C., compare 84 s to 94 s). For quiescent cells exposed to gradients of chemoattractant, significant WAVE complex asymmetry was observed in the absence of obvious morphological polarity (Fig 2B, 14 s time point). These cells were examined to determine how morphological protrusions and WAVE complex behavior relate to the external gradient. Both were highly accurate in predicting the ultimate gradient direction. However, protrusions oscillated significantly around the true gradient direction (SD = 24%), whereas changes in WAVE complex behavior were more precisely aligned with the gradient (SD = 12%). These data suggest that under our stimulation conditions, changes in WAVE complex dynamics represent a more quantitative and robust readout of polarity than cell morphology.

The establishment of WAVE complex asymmetry was determined by analyzing the signaling response of an initially quiescent cell to chemoattractant (Fig. 2A). Quiescent cells were exposed to a range of agonist increases and split into two equal size populations based on the size of the mean estimated increase in fractional receptor occupancy (see methods; 0.63 was the median increase). Among our micropipette

experiments, the average receptor occupancy change correlated better with cell response than did the slope of the gradient (data not shown). Cells exposed to increases in estimated mean receptor occupancy from 0 to < 0.63 responded to the new gradient with focused generation of WAVE complex recruitment (Fig 2B and 2D; Movie S4). For mean receptor occupancy increases greater than 0.63, most cells produced a relatively uniform distribution of WAVE complex recruitment that collapsed into a focused distribution on the up-gradient surface (Fig. 2C and 2D; Movie S5). In both cases, WAVE complex asymmetry ultimately aligns with the external agonist gradient.

Previous analyses of uniformly stimulated neutrophils showed initially uniform signaling responses before cells became polarized [6, 17]. It is unknown whether cells can also produce initially asymmetric signaling in response to uniform stimulation. To test this possibility, the responses of quiescent cells (when cells lost all WAVE complex dynamics and any obvious morphological front and back) were observed. A mean receptor occupancy increase from 0 to 0.1 caused the cells to produce focused WAVE complex recruitment (Fig. 3A and 3C; Movie S6). In contrast, a mean receptor occupancy increase from 0 to 0.7 caused cells to produce a spatially uniform distribution of WAVE complex recruitment that ultimately collapsed into a focused distribution (Fig. 3B and 3C; Movie S7). The first detectable response in either case occurred approximately 12-18 s after stimulation. These data suggest that immediate signaling asymmetries are generated in response to small agonist steps. Previous studies examining the establishment of PIP_3 asymmetry [17] and WAVE asymmetry [6] used larger increases in receptor occupancy, conditions that prevent the initially focused recruitment of WAVE complex in response to uniform chemoattractant (Fig. 3B and 3C).

There are several potential mechanisms that could constrain WAVE complex dynamics

to a limited region of the cell surface. For instance, upstream molecular asymmetries could act to restrict WAVE complex recruitment to a limited region of the cell surface during the establishment of polarity. An example of this type of internal directional bias is centrosome position, which influences the initial axis of morphological polarity in response to uniform chemoattractant [21]. This sort of intrinsic bias could be responsible for the immediate WAVE complex polarity in response to small steps in uniform chemoattractant (Fig 3A). A second source of internal directional bias could operate during migration. Moving cells have polarized morphologies and intracellular signals, which act as a directional bias to restrict protrusions near the existing leading edge [18, 22]. This type of internal directional bias spatially restricts WAVE complex responses for intermediate increases in mean receptor occupancy (Fig. 3D; Movie S8) in a manner similar to the role of an intrinsic bias during the establishment of polarity. However, larger steps of uniform agonist elicited uniform WAVE complex recruitment (Fig. 3E and 3F; Movie S9), indicating that this bias can be overcome.

During chemotaxis, both an external bias from the agonist gradient and the cell's intrinsic biases could influence the establishment of WAVE complex asymmetries. In other cell types, such as *Dictyostelium*, only agonist gradients and not uniform chemoattractant produce signaling polarity [15]. Under these conditions, it is difficult to separate the effects of intrinsic biases from the external gradient. In contrast, neutrophils exhibit signaling polarity in uniform chemoattractant as well as gradients [17], enabling us to determine the role of internal directional bias independent of gradient sensing.

External gradients limit the spatial extent of WAVE complex recruitment for initially quiescent cells (Fig. 2B). Here, external gradients set the final direction of WAVE complex polarity and overwhelm any internal signaling biases within the cell. This occurs for mean receptor occupancy increases less than 0.63. In contrast, under a

condition where only internal signaling biases operate, a similar step size (an increase of 0.34), elicited uniform WAVE complex recruitment in polarized cells (Fig. 3E). These data indicate that gradient sensing can overwhelm intrinsic biases and can constrain cell responses over a larger range of agonist increases than intrinsic biases.

Some cues such as PIP_3 can polarize in the absence of actin rearrangements [15, 17, 23, 24], but it is unclear whether WAVE complex asymmetry can also be uncoupled from downstream actin-dependent morphological rearrangements. Neutrophils were treated with latrunculin to inhibit actin polymerization. Even in the absence of external agonist, latrunculin transiently increased the concentration of WAVE complex at the membrane (Fig. 4A, 40 s). Under these conditions the WAVE complex still responds to stimulation, although WAVE complex puncta are observed instead of propagating waves. Sudden addition of an agonist gradient increased WAVE complex recruitment (Fig. 4A, 160 and 300 s), whereas removal of agonist caused WAVE complex release from the membrane (Fig. 4A, 200 and 360 s). In latrunculin-treated cells exposed to gradients of chemoattractant, the localization of WAVE complex was relatively uniform (Fig. 4B, 170 and 330 s; Movie S10). Untreated cells typically produced focused WAVE complex recruitment in response to small increases in agonist gradients (Fig. 2B). In contrast, latrunculin-treated cells that experienced a similar increase in receptor occupancy exhibited a significantly wider WAVE complex distribution (Fig. 4C). Therefore, actin polymer, which is generated downstream of the WAVE complex, also appears to be required for the initial generation of WAVE complex asymmetry in neutrophils. Additionally, for control cells exposed to large increases in agonist gradients, the WAVE complex was initially relatively uniform but resolved into a more focused distribution over time. In contrast, this selection mechanism was not apparent over the timescale analyzed in latrunculin-treated cells (Fig. 4D). Furthermore, previous studies implicate

actin polymer as a factor that stabilizes signaling components at the membrane [25, 26], whereas our data suggest that actin polymerization can also remove signaling proteins from the membrane.

Biochemical fractionation was used to measure WAVE complex enrichment near the plasma membrane as a complement to our TIRF studies. A significant two-fold enrichment of the WAVE complex was observed in the plasma membrane fraction following stimulation and actin depolymerization, indicating that at least some of the TIRF-visible pool of the WAVE complex represents plasma-membrane association (Fig. S3).

CONCLUSIONS

Two models cover how cells reorient polarity during directional migration, and aspects of each apply to how cells initially establish polarity. One model showed that *Dicytostelium* respond by selectively retaining the pseudopod that experiences the highest agonist concentration, rather than biasing pseudopod generation [8]. In our system, the unit of selection is not a pseudopod, but rather smaller organizing units consisting of WAVE complex recruitment events. In contrast, the local generation model for chemotaxis proposes that the chemotactic behavior of the cell is the sum of local, independent protrusion events all over the surface of the pseudopod [7]. Once a cell is polarized, the probability of a protrusion event occurring in a particular location on the pseudopod depends on the relative local concentration of agonist. Extending this generation-based model to unpolarized cells can explain how a cell can initially bias WAVE complex asymmetry when receptor occupancy is low (~0.1), a phenomenon inexplicable by a selection-based model. However, the generation-based model fails to explain how cells could generate WAVE complex recruitment everywhere and selectively retain WAVE complex recruitment up-gradient; so each model succeeds where the other fails.

We propose a model where local generation events are linked to cellular adaptation machinery. For small increases in agonist, a generation-based mechanism leads to immediately focused polarity. For larger increases in agonist, the generation machinery is saturated, resulting in a uniform WAVE complex distribution. In this case, global adaptation allows the cell to selectively retain WAVE complex recruitment to achieve WAVE asymmetry in a direction set by intrinsic biases or the external gradient. Our model enables the cell to balance rapid polarization (initial signal generation to the up-gradient side) with a more robust polarization (a slower gradual selection of uniform

signal distribution, which can occur over a wider range of stimulation conditions). Importantly, the dominant mechanism of polarization depends on the amount of stimulation.

Intriguingly, actin polymerization is essential for WAVE complex polarization during chemotaxis. There are many examples of loss-of-function perturbations of chemotactic signaling that block intracellular signaling responses including PIP_3 generation, Ras and Rac activation, actin polymerization, and morphological changes in response to external chemoattractant [5, 26-32]. The WAVE complex is the first example of an intracellular signal that depends on actin polymer for its polarization but not for its global responsiveness to stimulation.

ACKNOWLEDGEMENTS

We thank John Sedat for image denoising collaboration, the Nikon Imaging Center at UCSF for Matlab analysis software, Scott Foster for leukocyte preparation, and Henry Bourne, Oliver Hoeller, Steve Altschuler, Lani Wu, Max Krummel, Benjamin Rhau, Mark Von Zastrow, Alexander Watters, Sarah Wilson, Bryant Chhun, Delquin Gong, and Julie Wu for helpful comments on the manuscript.

This work was supported by NIH R01 (GM084040), the UCSF/UCB Cell Propulsion lab (an NIH Nanomedicine Development Center), was supported by the UCSF/UCB Cell Propulsion Lab - a National Institutes of Health Nanomedicine Development Center, a Searle Scholars Award, GM084040an American Heart Association National Scientist Development Grant, a National Defense Science and Engineering Graduate Fellowship to A. Millius, an American Heart Association Graduate Fellowship to A. Houk, and an Achievement Awards for College Scientists (ARCS) Scholarship to S. Dandekar.

REFERENCES

1. Machesky, L.M., and Insall, R.H. (1998). Scar1 and the related Wiskott-Aldrich syndrome protein, WASP, regulate the actin cytoskeleton through the Arp2/3 complex. Curr Biol *8*, 1347-1356.

2. Kunda, P., Craig, G., Dominguez, V., and Baum, B. (2003). Abi, Sra1, and Kette control the stability and localization of SCAR/WAVE to regulate the formation of actin-based protrusions. Curr Biol *13*, 1867-1875.

3. Steffen, A., Rottner, K., Ehinger, J., Innocenti, M., Scita, G., Wehland, J., and Stradal, T.E. (2004). Sra-1 and Nap1 link Rac to actin assembly driving lamellipodia formation. The EMBO journal *23*, 749-759.

4. Stradal, T.E., and Scita, G. (2006). Protein complexes regulating Arp2/3-mediated actin assembly. Current opinion in cell biology *18*, 4-10.

5. Weiner, O.D., Rentel, M.C., Ott, A., Brown, G.E., Jedrychowski, M., Yaffe, M.B., Gygi, S.P., Cantley, L.C., Bourne, H.R., and Kirschner, M.W. (2006). Hem-1 complexes are essential for Rac activation, actin polymerization, and myosin regulation during neutrophil chemotaxis. PLoS Biol *4*, e38.

6. Weiner, O.D., Marganski, W.A., Wu, L.F., Altschuler, S.J., and Kirschner, M.W. (2007). An Actin-Based Wave Generator Organizes Cell Motility. PLoS Biol *5*, e221.

7. Arrieumerlou, C., and Meyer, T. (2005). A local coupling model and compass parameter for eukaryotic chemotaxis. Developmental cell *8*, 215-227.

8. Andrew, N., and Insall, R.H. (2007). Chemotaxis in shallow gradients is mediated independently of PtdIns 3-kinase by biased choices between random protrusions. Nature cell biology *9*, 193-200.

9. Patel, F.B., Bernadskaya, Y.Y., Chen, E., Jobanputra, A., Pooladi, Z., Freeman, K.L.,

Gally, C., Mohler, W.A., and Soto, M.C. (2008). The WAVE/SCAR complex promotes polarized cell movements and actin enrichment in epithelia during C. elegans embryogenesis. Dev Biol.

10. Zallen, J.A., Cohen, Y., Hudson, A.M., Cooley, L., Wieschaus, E., and Schejter, E.D. (2002). SCAR is a primary regulator of Arp2/3-dependent morphological events in Drosophila. The Journal of cell biology *156*, 689-701.

11. Rogers, S.L., Wiedemann, U., Stuurman, N., and Vale, R.D. (2003). Molecular requirements for actin-based lamella formation in Drosophila S2 cells. The Journal of cell biology *162*, 1079-1088.

12. Rakeman, A.S., and Anderson, K.V. (2006). Axis specification and morphogenesis in the mouse embryo require Nap1, a regulator of WAVE-mediated actin branching. Development (Cambridge, England) *133*, 3075-3083.

13. Hahne, P., Sechi, A., Benesch, S., and Small, J.V. (2001). Scar/WAVE is localized at the tips of protruding lamellipodia in living cells. FEBS Lett *492*, 215-220.

14. Lai, F.P., Szczodrak, M., Block, J., Faix, J., Breitsprecher, D., Mannherz, H.G., Stradal, T.E., Dunn, G.A., Small, J.V., and Rottner, K. (2008). Arp2/3 complex interactions and actin network turnover in lamellipodia. The EMBO journal *27*, 982-992.

15. Parent, C.A., Blacklock, B.J., Froehlich, W.M., Murphy, D.B., and Devreotes, P.N. (1998). G protein signaling events are activated at the leading edge of chemotactic cells. Cell *95*, 81-91.

16. Meili, R., Ellsworth, C., Lee, S., Reddy, T.B., Ma, H., and Firtel, R.A. (1999). Chemoattractant-mediated transient activation and membrane localization of Akt/PKB is required for efficient chemotaxis to cAMP in Dictyostelium. The EMBO journal *18*, 2092-2105.

17. Servant, G., Weiner, O.D., Herzmark, P., Balla, T., Sedat, J.W., and Bourne, H.R. (2000). Polarization of chemoattractant receptor signaling during neutrophil chemotaxis. Science *287*, 1037-1040.

18. Zigmond, S.H., Levitsky, H.I., and Kreel, B.J. (1981). Cell polarity: an examination of its behavioral expression and its consequences for polymorphonuclear leukocyte chemotaxis. The Journal of cell biology *89*, 585-592.

19. Ferguson, G.J., Milne, L., Kulkarni, S., Sasaki, T., Walker, S., Andrews, S., Crabbe, T., Finan, P., Jones, G., Jackson, S., et al. (2007). PI(3)Kgamma has an important context-dependent role in neutrophil chemokinesis. Nature cell biology *9*, 86-91.

20. Hoeller, O., and Kay, R.R. (2007). Chemotaxis in the absence of PIP3 gradients. Curr Biol *17*, 813-817.

21. Xu, J., Van Keymeulen, A., Wakida, N.M., Carlton, P., Berns, M.W., and Bourne, H.R. (2007). Polarity reveals intrinsic cell chirality. Proc Natl Acad Sci U S A *104*, 9296-9300.

22. Xu, J., Wang, F., Van Keymeulen, A., Herzmark, P., Straight, A., Kelly, K., Takuwa, Y., Sugimoto, N., Mitchison, T., and Bourne, H.R. (2003). Divergent signals and cytoskeletal assemblies regulate self-organizing polarity in neutrophils. Cell *114*, 201-214.

23. Janetopoulos, C., Ma, L., Devreotes, P.N., and Iglesias, P.A. (2004). Chemoattractant-induced phosphatidylinositol 3,4,5-trisphosphate accumulation is spatially amplified and adapts, independent of the actin cytoskeleton. Proc Natl Acad Sci U S A *101*, 8951-8956.

24. Xu, X., Meier-Schellersheim, M., Yan, J., and Jin, T. (2007). Locally controlled inhibitory mechanisms are involved in eukaryotic GPCR-mediated chemosensing. The Journal of cell biology *178*, 141-153.

25. Devreotes, P., and Janetopoulos, C. (2003). Eukaryotic chemotaxis: distinctions between directional sensing and polarization. The Journal of biological chemistry *278*, 20445-20448.

26. Sasaki, A.T., Chun, C., Takeda, K., and Firtel, R.A. (2004). Localized Ras signaling at the leading edge regulates PI3K, cell polarity, and directional cell movement. The Journal of cell biology *167*, 505-518.

27. Shefcyk, J., Yassin, R., Volpi, M., Molski, T.F., Naccache, P.H., Munoz, J.J., Becker, E.L., Feinstein, M.B., and Sha'afi, R.I. (1985). Pertussis but not cholera toxin inhibits the stimulated increase in actin association with the cytoskeleton in rabbit neutrophils: role of the "G proteins" in stimulus-response coupling. Biochem Biophys Res Commun *126*, 1174-1181.

28. Wu, L., Valkema, R., Van Haastert, P.J., and Devreotes, P.N. (1995). The G protein beta subunit is essential for multiple responses to chemoattractants in Dictyostelium. The Journal of cell biology *129*, 1667-1675.

29. Kumagai, A., Hadwiger, J.A., Pupillo, M., and Firtel, R.A. (1991). Molecular genetic analysis of two G alpha protein subunits in Dictyostelium. The Journal of biological chemistry *266*, 1220-1228.

30. Sun, C.X., Downey, G.P., Zhu, F., Koh, A.L., Thang, H., and Glogauer, M. (2004). Rac1 is the small GTPase responsible for regulating the neutrophil chemotaxis compass. Blood *104*, 3758-3765.

31. Chen, L., Iijima, M., Tang, M., Landree, M.A., Huang, Y.E., Xiong, Y., Iglesias, P.A., and Devreotes, P.N. (2007). PLA2 and PI3K/PTEN pathways act in parallel to mediate chemotaxis. Developmental cell *12*, 603-614.

32. Veltman, D.M., Keizer-Gunnik, I., and Van Haastert, P.J. (2008). Four key signaling

pathways mediating chemotaxis in Dictyostelium discoideum. The Journal of cell biology *180*, 747-753.

Figure 1

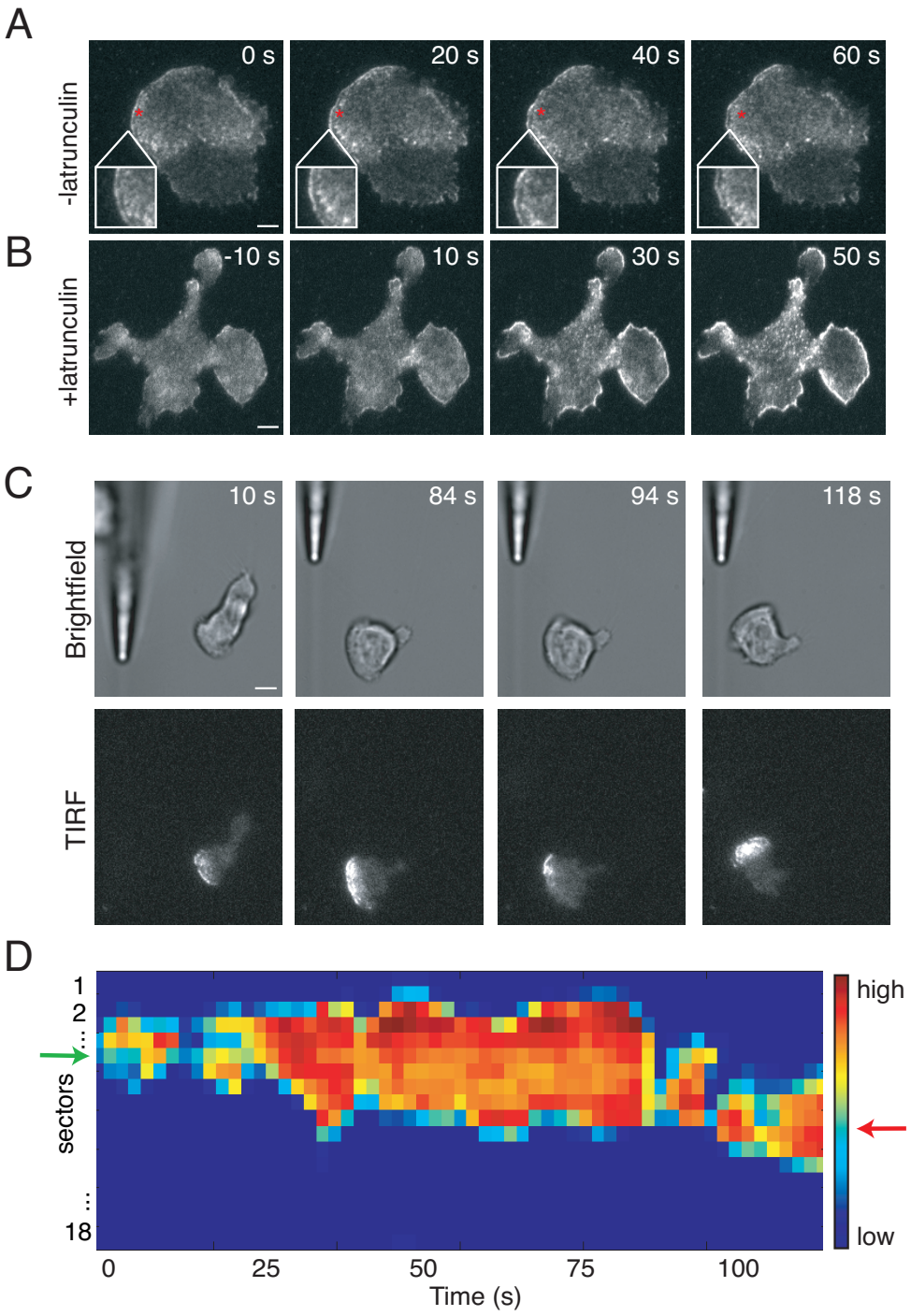
A
-latrunculin
0 s
20 s
40 s
60 s
B
+latrunculin
-10 s
10 s
30 s
50 s
C
Brightfield
TIRF
10 s
84 s
94 s
118 s
D
sectors
1
2
...
18
high
low
0
25
50
75
100
Time (s)

Figure 1. Propagating waves of the WAVE complex are mechanistically conserved in other mammalian cells and represent a dynamic quantitative polarity readout in neutrophils (A) Representative TIRF time-lapse sequences for a B16F10 fibroblast cell migrating on fibronectin expressing Abi1 (a component of the WAVE complex) tagged with YFP. Similar to HL-60 cells, propagating waves of the WAVE complex are observed at the leading edge (Movie S1). (B) Representative Abi1-YFP TIRF time-lapse sequences for a migrating B16F10 fibroblast exposed to 10 μM latrunculin at 0 s. Similar to HL-60 cells, B16F10 cells exhibit an enrichment of WAVE complex near the membrane following latrunculin treatment, suggesting a role for actin polymer in WAVE complex recycling (Movie S2). (C) Representative brightfield and Hem1-YFP TIRF time-lapse sequences for a HL-60 cell executing a turn in response to a change in the direction of the agonist gradient (Movie S3). (D) Corresponding heatmap shows wave response. Green arrow indicates initial up-gradient direction; red arrow indicates final up-gradient direction. Bars, 5 μm.

Figure 2

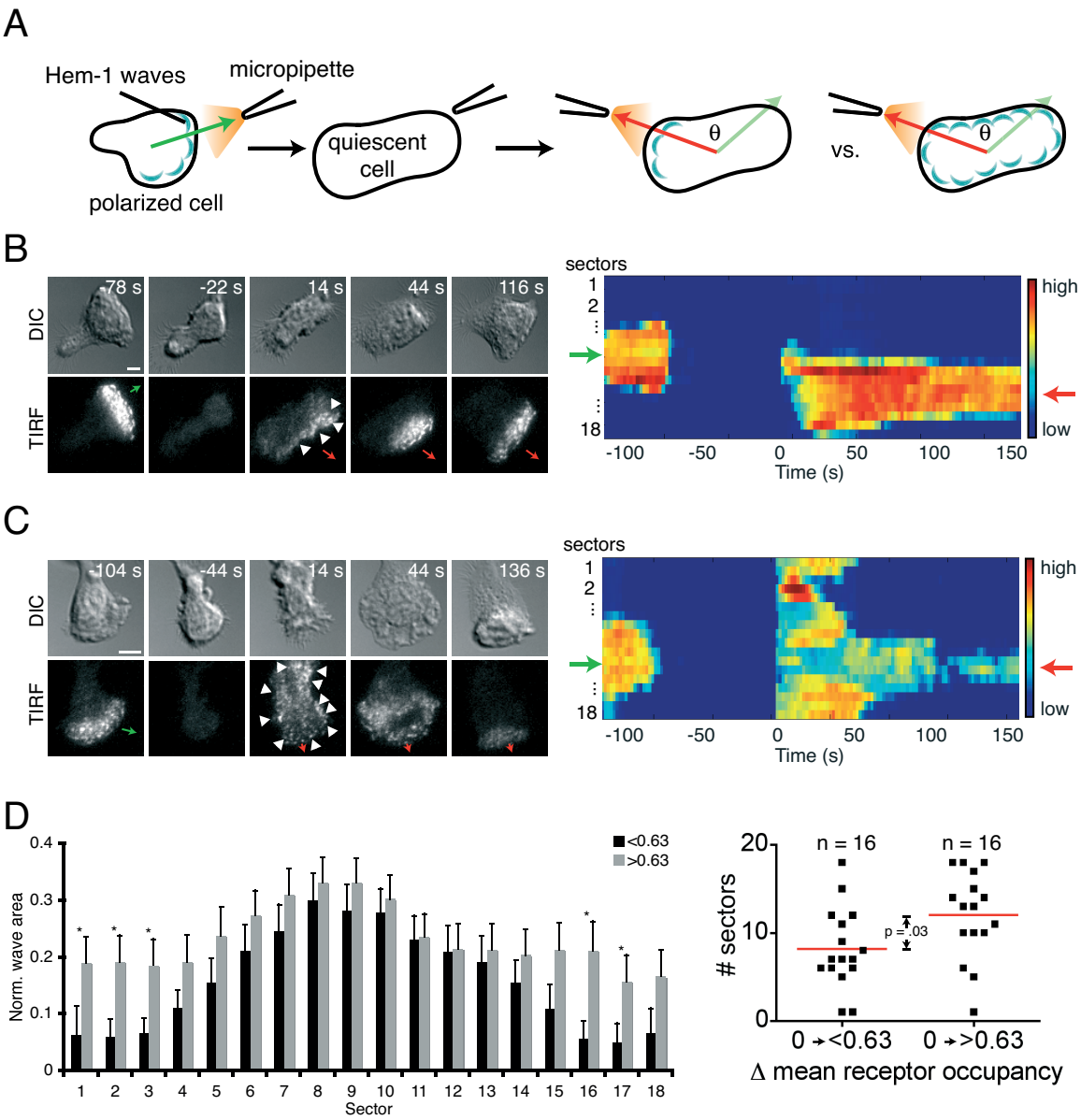
A
Hem-1 waves
micropipette
polarized cell
quiescent cell
θ
vs.
B
DIC
TIRF
-78 s
-22 s
14 s
44 s
116 s
sectors
high
low
Time (s)
C
-104 s
-44 s
14 s
44 s
136 s
D
<0.63
>0.63
Norm. wave area
Sector
n = 16
n = 16
p = .03
# sectors
0→<0.63
0→>0.63
Δ mean receptor occupancy

Figure 2. Cells establish Hem-1 wave asymmetry through either focused generation or uniform generation followed by selection. (A) Illustration of experimental setup. An agonist gradient was applied to a cell and then removed. This process was necessary to ensure quiescence because cells adhered to a coverslip often exhibited polarity and motility even in the absence of chemoattractant. Cells were classified as quiescent when they lost all wave dynamics and any obvious morphological front and back. The micropipette was repositioned at a different angle and the gradient reapplied at t = 0 s. Therefore, all cells start with a mean receptor occupancy of 0 for this figure. The angle difference and interval between agonist applications did not affect WAVE complex distribution, nor did the cell retain memory of the original micropipette position after the micropipette was turned back on (Fig. S2). (B and C) Representative DIC and Hem-1-YFP TIRF time-lapse sequences and corresponding heatmaps show that cells exhibit a focused (B, Movie S4) or uniform (C, Movie S5) distribution of waves. Note that wave asymmetry is apparent in the absence of any obvious morphological differences (arrowheads). Green arrows indicate initial up-gradient direction; red arrows indicate final up-gradient direction. Bars, 5 μm. (D) Bar graph (left) of a 20 s average of wave response immediately after gradient reapplication. Black bars show response for cells with mean receptor occupancy (post-stimulation) of <0.63. Gray bars indicate cells with mean receptor occupancy (post-stimulation) of >0.63. Error bars are s.e.m. Asterisks indicate statistically significant differences between means of each sector ($p < 0.05$, Student's t-test). Dot plot (right) shows a statistically significant difference ($p = .03$, Student's t-test) between the mean width (red line) of the distributions as defined in Fig. S1.

Figure 3

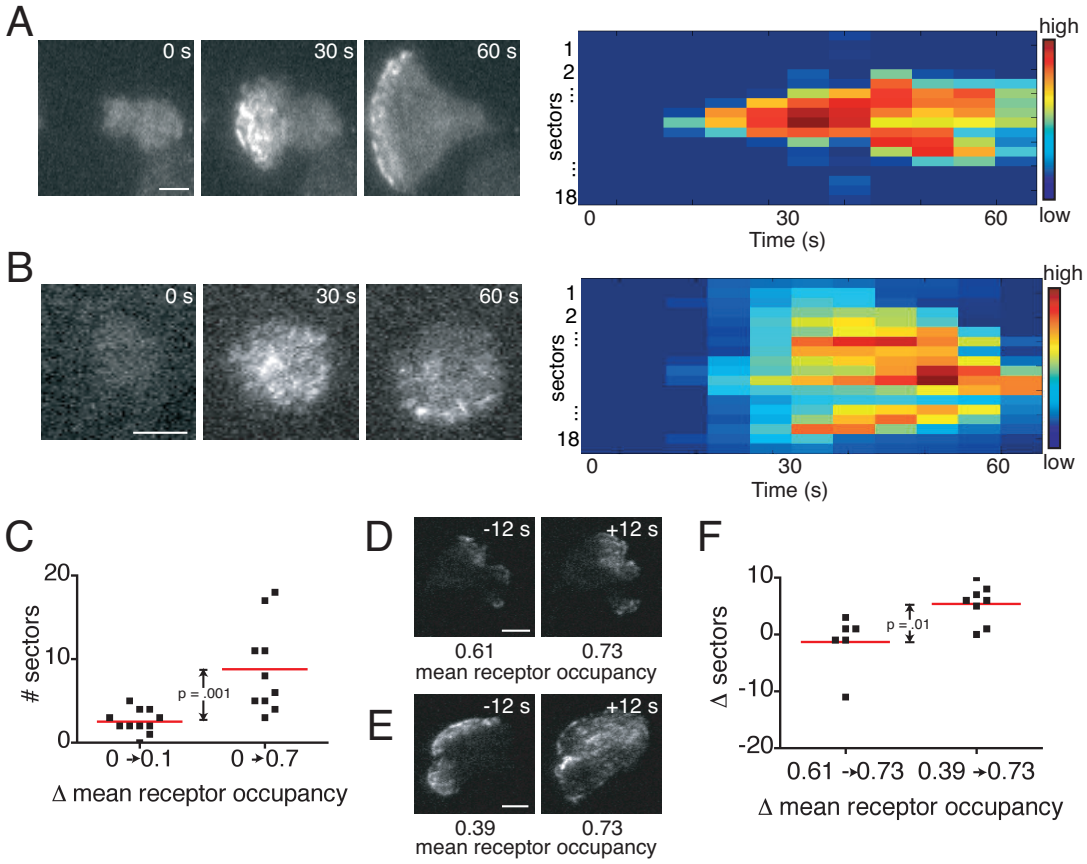
A
0 s
30 s
60 s
high
low
sectors
1
2
18
0
30
60
Time (s)
B
0 s
30 s
60 s
high
low
sectors
1
2
18
0
30
60
Time (s)
C
sectors
20
10
0
p = .001
0 →0.1
0 →0.7
Δ mean receptor occupancy
D
-12 s
+12 s
0.61
0.73
mean receptor occupancy
E
-12 s
+12 s
0.39
0.73
mean receptor occupancy
F
Δ sectors
10
0
-10
-20
p = .01
0.61 →0.73
0.39 →0.73
Δ mean receptor occupancy

Figure 3. Directional bias limits wave generation in response to small increases in mean receptor occupancy. (A and B) Initially quiescent cells were subjected to spatially uniform mean receptor occupancy increases from 0 to 0.1 (at t = 0 s), which produced focused waves (A, Movie S6), or 0 to 0.7 (at t = 0 s), which produced a spatially uniform distribution of Hem-1 waves that ultimately collapsed into a focused distribution (B, Movie S7). Bars, 5 μm. (C) Dot plot shows a statistically significant difference (p = . 001, Student's t-test) between the mean width (red line) of the distributions. (D and E) Representative time-lapse images of cells with prepolarized WAVE complex distributions responding to spatially uniform increases in mean receptor occupancy from (D) 0.61 to 0.73 (n = 6, Movie S8) or (E) 0.39 to 0.73 (n = 8, Movie S9). (F) Dot plot shows a statistically significant difference (p = 0.002, Student's t-test) between the changes in wave width for small versus large increases in mean receptor occupancy (note that mean receptor occupancies are statistically different even after removing the outlier for the 0.61 to 0.73 increase). These data suggest that intrinsic directional bias can maintain the asymmetric distribution of Scar/WAVE over a limited range of agonist concentrations in both quiescent and prepolarized cells.

Figure 4

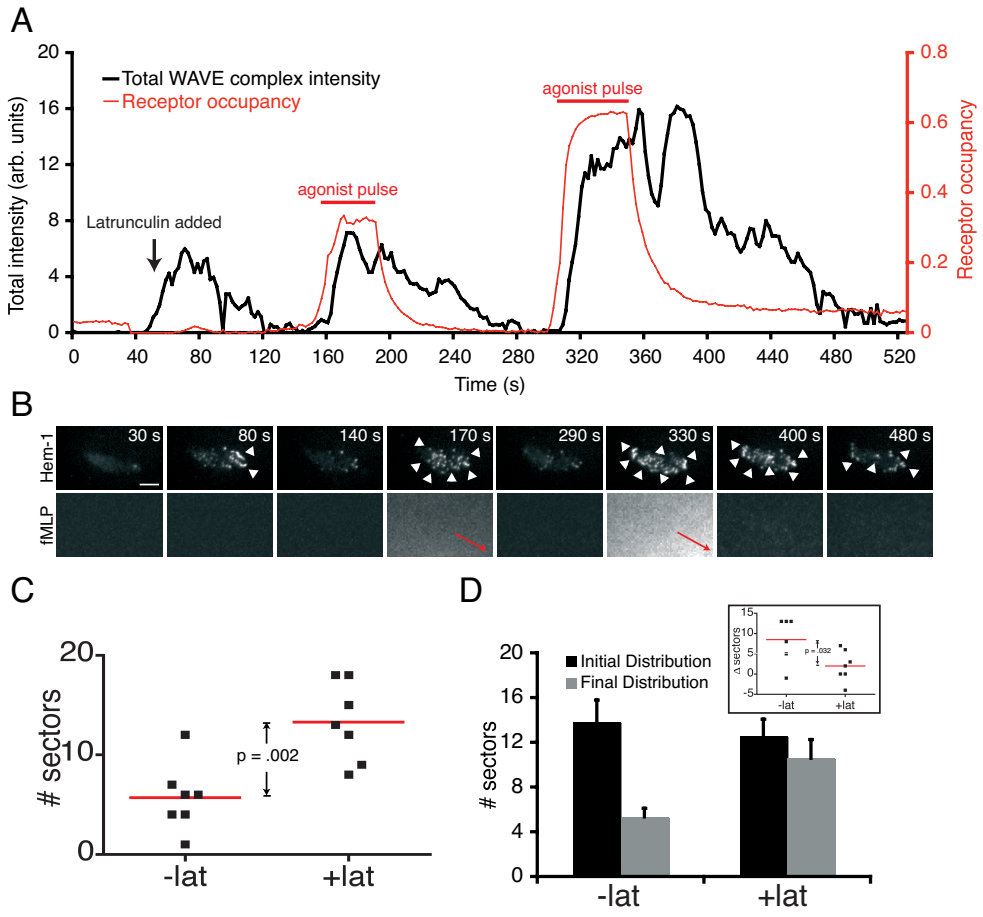
A
Total WAVE complex intensity
Receptor occupancy
Total intensity (arb. units)
Receptor occupancy
Latrunculin added
agonist pulse
agonist pulse
Time (s)
B
Hem-1
fMLP
30 s
80 s
140 s
170 s
290 s
330 s
400 s
480 s
C
# sectors
p = .002
-lat
+lat
D
Initial Distribution
Final Distribution
sectors
-lat
+lat

Figure 4. Actin polymer is required for establishment of Hem-1 wave asymmetry (A) Transient fMLP pulses (red trace) induce transient Hem-1-YFP (black trace) accumulation at the membrane. An initially migrating cell was subjected to 20 μM latrunculin treatment to depolymerize the actin cytoskeleton (40 s). This induced Hem-1-YFP recruitment even in the absence of external stimuli. Subsequent fMLP pulses from a micropipette (160 and 300 s) induced further recruitment. When the agonist was removed, Hem-1-YFP quickly disappeared from the membrane. (B) Selected TIRF and DIC images (Movie S10) from the traces shown in (A). Red arrows indicate direction of gradient pulses. Arrowheads indicate areas of significant Hem-1-YFP accumulation at the membrane. Note the broad distribution following each agonist pulse. Bar, 5 μm. (C) Dot plot of a 20 s average of wave response immediately after an agonist pulse for cells untreated (-lat) and treated with 20 μM latrunculin (+lat). There is a statistically significant difference between the mean width (red lines) of the two populations ($p = .002$, Student's t-test). (D) Untreated cells that showed an initially broad wave distribution after an agonist pulse were compared to latrunculin-treated cells. The wave distribution in untreated cells converged into a focused distribution, whereas the wave distribution in latrunculin-treated cells did not converge. Error bars are s.e.m. Inset shows statistical significance between the difference in mean sectors (red lines) of the two populations ($p = .002$, Student's t-test).

SUPPLEMENTAL EXPERIMENTAL PROCEDURES

Cell culture

The HL-60 cell line stably expressing Hem-1-YFP was generated, cultured, and differentiated as described previously [1]. Cells were plated on #1.5 coverslips (Lab-Tek) precoated with 0.2 mg/ml bovine fibronectin (Sigma) and stimulated in RPMI plus L-glutamine, 10% FBS, and 25 mM HEPES (10-041-CM, Fisher) with indicated concentrations of formyl-met-leu-phe (fMLP, Sigma) mixed with Alexa594 hydrazide (Invitrogen).

Image acquisition

Images were taken at 37°C on a Nikon Eclipse TE2000-E inverted microscope with a 60x PlanApo TIRF 1.49 NA objective and an electron microscopy charge-coupled device (EM-CCD) camera (Cascade II 512, Photometrics; http://www.photomet.com). Sample drift was minimized using an autofocus system (Perfect Focus, Nikon). 514 nm and 561 nm lasers (20 mW ion and solid-state lasers, Melles Griot) were used for excitation of Hem-1-YFP and Alexa594 hydrazide, respectively. Nikon Elements software version 3.0 was used for image acquisition; levels of still images were adjusted linearly in Photoshop to enhance contrast.

Micropipette experiments

Typical imaging conditions used 600 ms YFP-TIRF, 20 ms 594-TIRF, and 5 ms DIC exposures every 2 s with near maximal multiplication on the EMCCD to minimize phototoxicity and photobleaching. Glass filaments (TW100F-4, World Precision Instruments) were pulled on Sutter Model P-87 (program: heat = 750, pull = 0, velocity =

20, time = 250, pressure = 100, loops 2 or 3 times) to achieve ~2-3 μm needle tip diameter. Needles were backfilled with 5 μl 200 nM fMLP containing 10 μM Alexa594 and held by a micromanipulator (MM-89, Narishige). Agonist flow rate was controlled by adjusting balance pressure between 0-3 psi on an IM-300 injection system (Narishige) connected to a needle holder (MINJ4, Tritech).

Uniform experiments

Typical imaging conditions used ND2 neutral density filter, 100 ms YFP-TIRF, 20 ms 594-TIRF and 5 ms DIC exposures every 6 s with maximal multiplication on the EMCCD to minimize phototoxicity and photobleaching. Cells were plated in 0.1 mL media. The coverslips were then placed on the microscope and time-lapse movies were started. Increases or decreases in chemoattractant were monitored by mixing Alexa594 into the fMLP stocks. For Fig. 3, cells were pre-stimulated with 20 nM fMLP for 3 minutes; the fMLP was completely removed and replaced with 0.1 mL media before the start of the movie. This was done to increase the number of quiescent cells prior to stimulation with chemoattractant.

Biochemical fractionation

One liter of 7 day differentiated HL-60 cells (or fresh pig leukocytes [2]) were spun at 1500 x g for 15 min, resuspended in ~4 mL mHBSS containing 3 mM DFP, and incubated for 15 min at room temperature. Cells were spun again for at 90 x g for 10 min and resuspended in warm cavitation buffer or cavitation buffer containing 1 μM fMLP, 10 mM Latrunculin B, and 100 μM GTPγS. Cells were pressurized for 5 min at 37°C for 5 min, lysed into 2 mM EGTA, spun at 1500 x g for 10 min at 4°C, layered on a

15%/38%/60% sucrose gradient, and spun at 100,000 x g for 1 hour. The 15%/38% interface was collected, TCA precipitated, and subsequently used for a Western blot for Hem-1 and NaK ATPase (a membrane loading control).

WAVE complex visualization within B16F10 cells

B16F10 cells were cultured on 10 cm dishes in MEM Eagle with Earle's BSS, 10% FBS, non-essential amino acids and antibiotic/antimycotic. The cells were transfected with Abi1-YFP (Lipofectamine2000) 48 hours before the experiment. For WAVE-complex visualization during spreading (Fig. 1A), Abi1-YFP transfected cells were trypsinized, replated on fibronectin-coated coverslips, and Abi1-YFP was visualized immediately after replating. This allowed us to visualize waves as cells initially spread along the coverslip. For latrunculin experiments, Abi1-YFP transfected cells were trypsinized and replated on fibronectin-coated coverslips 24 hours before the experiment. AlF was added (30 mM NaF, 50 mM $AlCl_3$) to stimulate spreading approximately 10 min before Latrunculin B addition (10 mM). In both sets of experiments, the cells were plated on LabTek 8 well #1.5 coverglass chambers pre-coated with 0.05 mg/mL bovine fibronectin (Sigma).

Image denoising

The Hem1-YFP channel of the acquired image series was cropped in space so that only one cell was in the image. The resulting time series was denoised in collaboration with John Sedat, using software developed by Jerome Boulanger, as described in (Fig. S1), [3]. Default parameters were chosen for a two-dimensional time series, except for the patch size, which was 7x7. The effect of the denoising was to remove speckle noise

from the background while minimizing feature loss from the waves, which enabled semi-automatic segmentation of the cell and wave regions. In the fMLP channel for both the uniform and micropipette experiments, the true intensities should be smoothly varying. To get rid of hot pixels (extremely bright or dark relative to surroundings), the fMLP channel was smoothed following image reconstruction examples [4].

Image segmentation

The cell region (region of the cell in contact with the coverslip) and wave region (regions of high Hem-1 density within the cell region) were defined using the denoised image. Two user-defined intensity thresholds were chosen using ImageJ, where the region of the image above the low threshold was the cell region (distinguishable above background because of cytosolic Hem-1) and the region of the image above the high threshold was the wave region (Fig. S1). For Fig. 4 (latrunculin-treated cells), the cytosolic pool of Hem-1 was greatly depleted, making it difficult to segment the cell region automatically. For these experiments, the cell region was a user-defined circle. This method of segmentation consistently underreported the width of the WAVE distribution when compared to the intensity thresholding method using control cells (data not shown).

Image analysis

We wrote analysis software in MATLAB 7.4 with Image Processing Toolbox and the help of the Nikon Imaging Center at UCSF. For the micropipette experiments, the position of the micropipette was calculated as the centroid of the region with intensity greater than 0.9*(max pixel intensity of smoothened fMLP channel). A total of 18 sectors

covering 20 degrees each were drawn using the centroid of the cell region as the center, and the up-gradient direction falling between the middle two sectors. Sectors with normalized fractional wave area greater than 0.1 were defined as sectors containing waves (Fig. S1).

Concentration and receptor occupancy calculations

For uniform chemoattractant experiments, chemoattractant concentration was known, and receptor occupancy was calculated in the same manner as the gradient experiments. For the gradient experiments, concentration was calculated by mixing known concentrations of Alexa594 with fMLP and drawing a standard curve under defined imaging conditions. Two curves were created and the average slope used to calculate concentration. Fractional receptor occupancy was calculated for a K_d of 9.5 nM for binding of fMLP to its receptor [5] using the equation $receptor\_occupancy = [fMLP]/(K_d + [fMLP])$**.** Background was subtracted from the fMLP channel in the following manner. For experiments in which some images in the time series were taken with no chemoattractant (Fig. 2), the median fMLP intensity during periods without chemoattractant was subtracted from all measurements, and all resulting negative values set to 0. For experiments in which all images had some chemoattractant, a constant value (2500 CCD counts) estimated from the median fMLP intensity values reported from the images without chemoattractant was instead subtracted, and all resulting negative values set to 0. To calculate the concentration following a change in fMLP, the median sector fMLP intensity for frames in the 20 s prior to and following the change were calculated, and the minimum and maximum for each, respectively, was used.

Statistical methods

Unpaired, two-tailed Student's t-test was used to compare mean widths for wave distributions in Fig. 2-4. These data met the criteria for normalcy by the Lilliefors test and the Jarque-Bera test.

SUPPLEMENTAL REFERENCES

1. Weiner, O.D., Marganski, W.A., Wu, L.F., Altschuler, S.J., and Kirschner, M.W. (2007). An Actin-Based Wave Generator Organizes Cell Motility. PLoS Biol *5*, e221.

2. Weiner, O.D., Rentel, M.C., Ott, A., Brown, G.E., Jedrychowski, M., Yaffe, M.B., Gygi, S.P., Cantley, L.C., Bourne, H.R., and Kirschner, M.W. (2006). Hem-1 complexes are essential for Rac activation, actin polymerization, and myosin regulation during neutrophil chemotaxis. PLoS Biol *4*, e38.

3. Kervrann, C., and Boulanger, J. (2006). Optimal spatial adaptation for patch-based image denoising. IEEE Trans Image Process *15*, 2866-2878.

4. Gonzalez, R., Woods, R., Eddins, S. (2004). Digital Image Processing Using Matlab, (Upper Saddle River, NJ: Pearson Prentice Hall).

5. Coats, W.D., Jr., and Navarro, J. (1990). Functional reconstitution of fMet-Leu-Phe receptor in Xenopus laevis oocytes. The Journal of biological chemistry *265*, 5964-5966.

Supplemental Figure 1

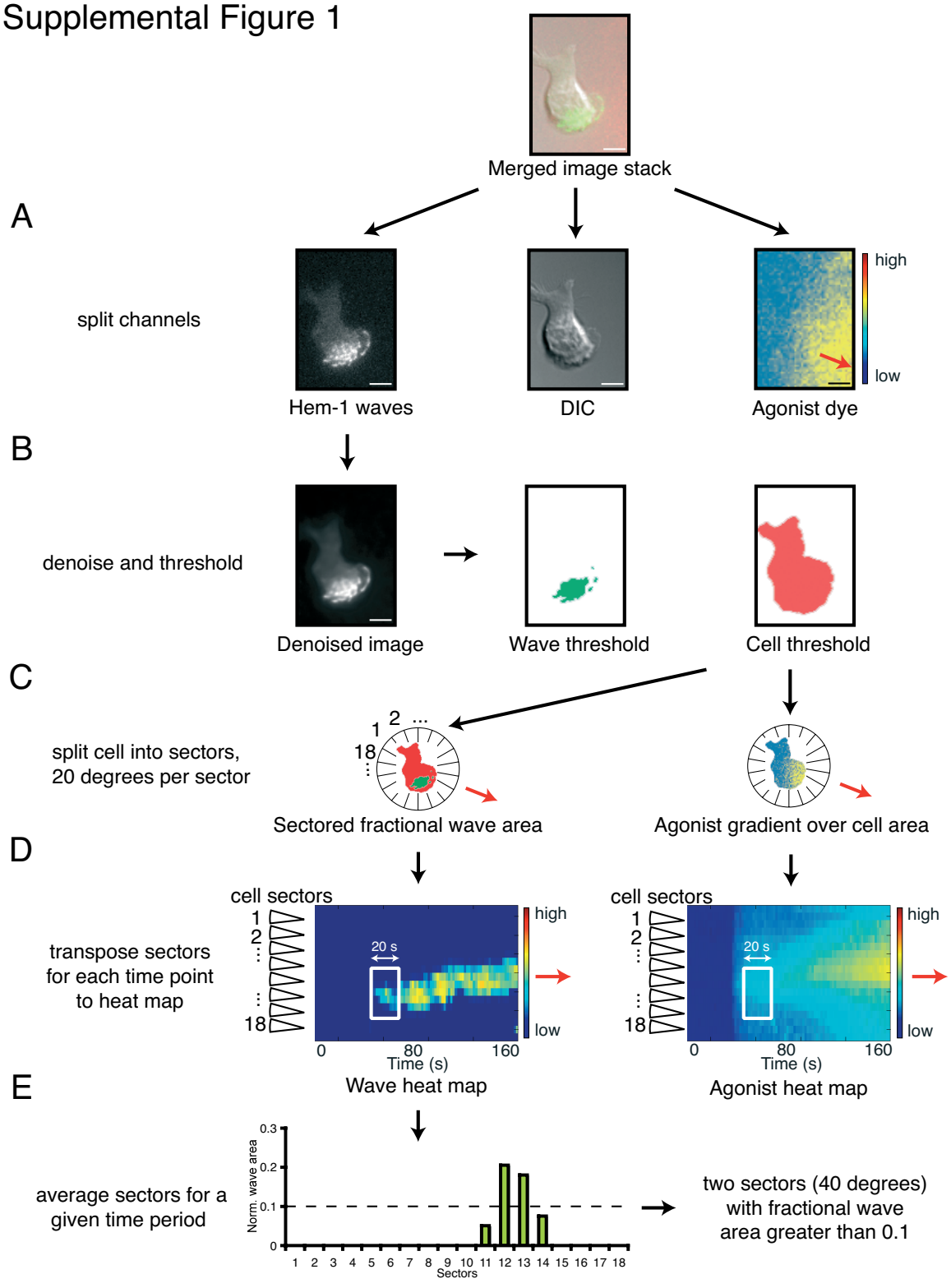

Figure S1. Illustration of image acquisition, processing, and analysis used in this paper. (A) A three channel merged image stack (top) is split into Hem-1-YFP distribution in TIRF (left), cell morphology in DIC (center), and fMLP distribution (visualized by the fluorescent dye Alexa594, which has a similar diffusion constant to fMLP) in TIRF (pseudocolored, right). Red arrow indicates up-gradient direction. Bars, 5 μm. (B) The Hem-1 channel is denoised and segmented into a wave region, which contains high Hem-1 concentration on the membrane, and a cell region, which additionally contains cytosolic Hem-1. (C) For each frame the cell is divided up into 18 equiangular sectors with the up-gradient direction (denoted by red arrow) between sectors 9 and 10. For each sector the ratio of wave area to cell area (left) and the average agonist concentration (right) are calculated. This agonist concentration is converted into a crude estimation of mean receptor occupancy using the reported Kd of the formyl peptide receptor {Coats, 1990 #27}. (D) The data from (C) is pictorially represented over the course of the movie as a heatmap. Each column is one time point, and the rows correspond to each sector's position, with high values shown in red and low values shown in blue. (E) The average of the wave response over 20 s following an agonist change (white box shown in D) is plotted on a bar graph, and the number of sectors with fractional wave area > 0.1 defines the width of the wave region.

Supplemental Figure 2

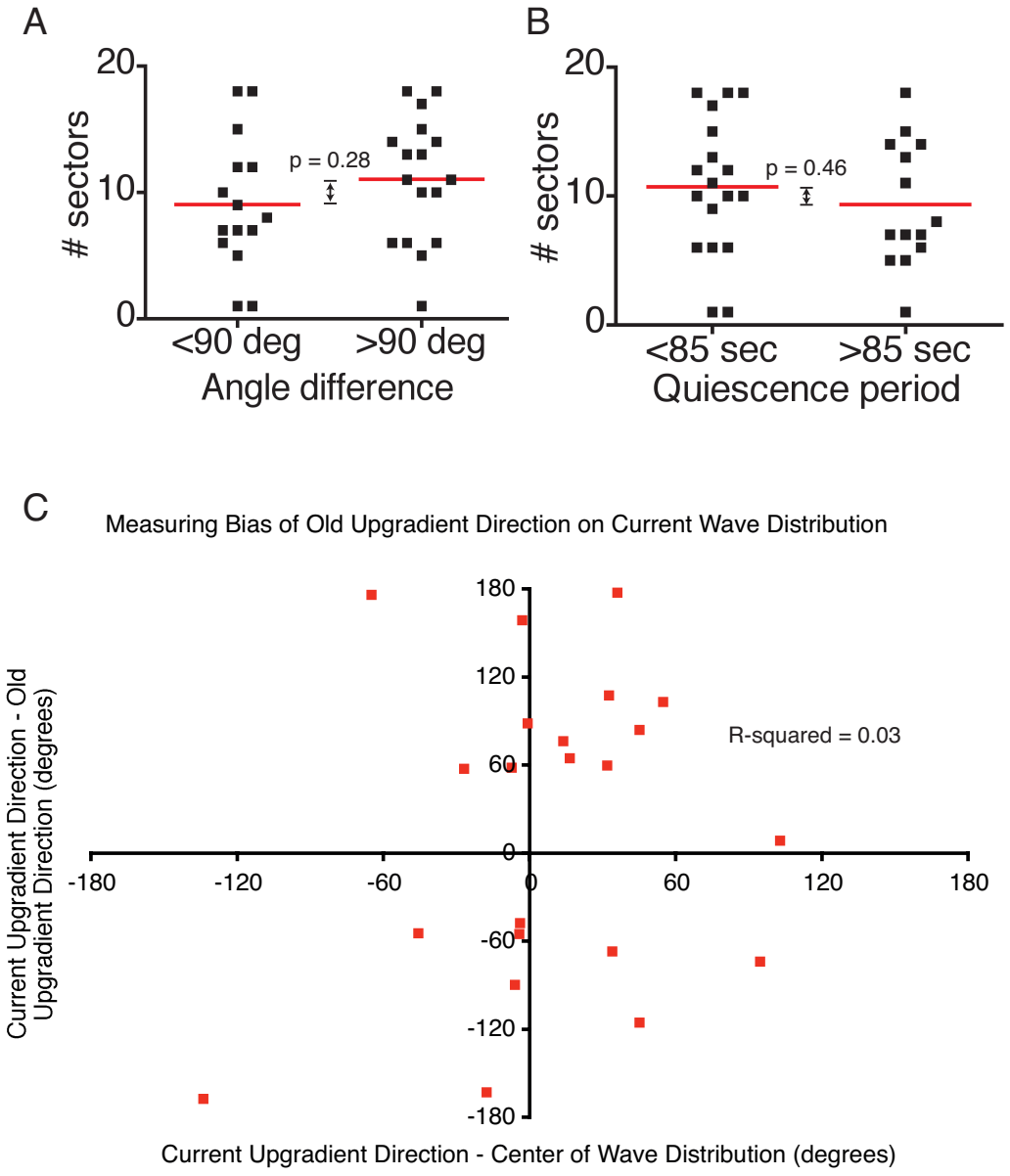

Figure S2. Angle difference and quiescence period do not affect wave distribution, nor are cells skewed toward original micropipette location. (A) Movies from Fig. 2 were sorted according to angle differences between old and new micropipette positions. Dot plot shows no statistical significance ($p = 0.28$, Student's t-test) between mean sector widths (red line). (B) Movies from Fig. 2 were sorted according to the duration between agonist applications (quiescence period). The average quiescence period was 85 s. Dot plot shows no statistical significance ($p = 0.46$, Student's t-test) between mean sector widths (red line). (C) There was no correlation between the old micropipette location on the center of the wave distribution relative and the new micropipette location (R-squared = 0.03).

Supplemental Figure 3

A

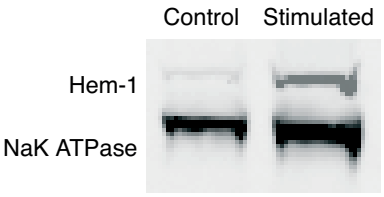

B

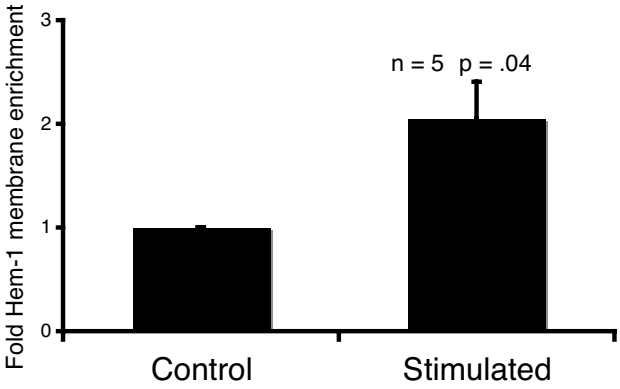

Figure S3. The WAVE complex biochemically fractionates to the plasma membrane upon fMLP stimulation and latrunculin treatment. The WAVE complex normally rapidly fluxes in and out of the TIRF field (with a half-life of 6.4 s), but stably associates in the TIRF field following actin depolymerization by latrunculin treatment {Weiner, 2007 #1}. Cavitation and discontinuous sucrose gradients were used to purify the plasma membrane of unstimulated cells versus stimulated latrunculin-treated cells. (A) Western blot shows Hem-1 and NaK ATPase (a membrane loading control) plasma membrane fractions for both untreated and stimulated (+fMLP, +latB, +GTPγS) cells. (B) Quantification shows a significant ~2-fold enrichment of the WAVE complex at the plasma membrane after stimulation compared to controls cells ($p = 0.04$, one-sample student's t-test) for 5 independent experiments.

SUPPLEMENTAL MOVIE LEGENDS

Movie S1. WAVE complex dynamics occur in B16F10 murine melanoma cells. A B16F10 fibroblast cell expressing Abi1-YFP was imaged at 37°C by TIRF while migrating on fibronectin. Playback speed is 10 frames per s. Corresponds to Fig. 1A.

Movie S2. WAVE complex dynamics arrest in latrunculin-treated B16F10 murine melanoma cells. A B16F10 fibroblast cell expressing Abi1-YFP was imaged at 37°C by TIRF while migrating on fibronectin and exposed to 10 μM latrunculin. Playback speed is 10 frames per s. Corresponds to Fig. 1B.

Movie S3. Hem-1 wave dynamics in response to a moving point source of chemoattractant. An HL-60 cell expressing Hem-1-YFP was imaged at 37°C by TIRF and brightfield microscopy once every 2 s (overlay, left; TIRF, right). Note that Hem-1-YFP waves are a more sensitive readout of polarity during a turn than morphology. Playback speed is 10 frames per s. Corresponds to Fig. 1C.

Movie S4. HL-60 cells spatially bias wave generation in response to small increases in chemoattractant gradients. An initially unpolarized HL-60 cell expressing Hem-1-YFP was suddenly exposed to an fMLP gradient at t = 0 s and imaged at 37°C (Hem-1-YFP TIRF alone, left; overlay, right) by TIRF (green) and DIC microscopy with 2 s frame intervals. Alexa594 dye corresponding to agonist from the micropipette was imaged in TIRF (red). Playback speed is 10 frames per s. Corresponds to Fig. 2B.

Movie S5. HL-60 cells exhibit spatially unbiased wave generation followed by

selection to establish wave asymmetry in response to large increases in chemoattractant gradients. An initially unpolarized HL-60 cell expressing Hem-1-YFP was suddenly exposed to an fMLP gradient at t = 0 s and imaged at 37°C (Hem-1-YFP TIRF alone, left; overlay, right) by TIRF (green) and DIC microscopy with 2 s frame intervals. Alexa594 dye corresponding to agonist from the micropipette was imaged in TIRF (red). Playback speed is 10 frames per s. Corresponds to Fig. 2C.

Movie S6. HL-60 cells spatially bias wave generation in response to small increases in uniform chemoattractant. An initially quiescent HL-60 cell expressing Hem-1-YFP was exposed to a sudden uniform increase in receptor occupancy from 0 to 0.1 at t = 0 s and imaged at 37°C by TIRF and DIC microscopy with 6 s frame intervals. Playback speed is 10 frames per s. Corresponds to Fig. 3A.

Movie S7. HL-60 cells exhibit spatially unbiased wave generation followed by selection to establish wave asymmetry in response to large increases in uniform chemoattractant. An initially unpolarized HL-60 cell expressing Hem-1-YFP was exposed to a sudden uniform increase in mean receptor occupancy from 0 to 0.7 at t = 0 s and imaged at 37°C by TIRF and DIC microscopy with 6 s frame intervals. Playback speed is 10 frames per s. Corresponds to Fig. 3B.

Movie S8. For cells with a prepolarized distribution of the WAVE complex, small increases in uniform agonist do not alter wave distribution. An HL-60 cell expressing Hem-1-YFP was exposed to an increase in mean receptor occupancy from 0.61 to 0.73 delivered at t = 0 s and imaged at 37°C by TIRF microscopy with 6 s frame

intervals. Playback speed is 10 frames per s. Corresponds to Fig. 3D.

Movie S9. For cells with a prepolarized distribution of the WAVE complex, intermediate increases in uniform agonist produces unbiased wave generation. An HL-60 cell expressing Hem-1-YFP was exposed to an increase in mean receptor occupancy from 0.39 to 0.73 delivered at t = 0 s and imaged at 37°C by TIRF microscopy with 6 s frame intervals. Playback speed is 10 frames per s. Corresponds to Fig. 3E.

Movie S10. Actin polymer is required for establishment of Hem-1 wave asymmetry. An initially unpolarized HL-60 cell expressing Hem-1-YFP was treated with 20 mM latrunculin at t = 40 s, followed by pulses of fMLP from a micropipette at t = 160 and 300 s. Cells were imaged at 37°C by TIRF (green) and DIC microscopy with 2 s frame intervals. Alexa594 dye corresponding to agonist from the micropipette was imaged in TIRF (red). Playback speed is 10 frames per s. Corresponds to Fig. 4B.

CHAPTER FOUR

The Cloud

We're going to discover something when we're in the cloud

-Uri Alon

It's hard to find a black cat in a dark room, especially if there is no cat

-Orion Weiner (and others)

If you don't come out with a certain degree of failure, then you're a failure

-Julie Theriot

SUMMARY

This chapter recounts my efforts to 1) reconstitute WAVE-mediated actin assembly using biochemical components and lipid-coated beads, 2) discover WAVE-complex-associated proteins through immunoprecipitation and mass spectrometry, 3) analyze Rac GTPase exchange factors (GEFs) involved in WAVE-complex activation and actin polymerization, and 4) examine the difference between gradient and uniform agonist increases and decreases. None of the experiments and results were published, but the work herein constitutes a large fraction of my time spent at UCSF. Uri Alon would say that I was lost in a "cloud" because I spent much of my time wandering through multiple projects without focus or direction. However, I learned several new experimental techniques – how to purify proteins, cell transfection, assay development, immunoprecipitation, and mass spectrometry – and how to focus my efforts to defined goals and project outcomes, which ultimately led to a successful story in the following chapter.

INTRODUCTION

Chemotaxis, or directed cell migration toward chemical cues, is critical for immune response, wound healing, axon guidance, and embryogenesis. In particular, neutrophils respond to chemical cues from bacteria through a G-protein coupled receptor that triggers a signal transduction cascade ending in actin polymerization and cell protrusion (Figure 1). The multiprotein WAVE complex enables cell migration via the actin-nucleating Arp2/3 complex and is essential for regulating morphogenesis and movement (Stradal et al., 2004). The Hem-1 component of the WAVE complex is required for actin polymerization, Rac activation, and polarization in neutrophils (Weiner et al., 2006). Previously, we found that the leading edge of a neutrophil-like HL-60 cell is composed of numerous, propagating waves of Hem-1 recruitment and release at the membrane (Weiner et al., 2007). Actin helps to sculpt the spatial distribution of the WAVE complex in cells (Millius et al., 2009), but it is still not clear how the complex is regulated and activated. This fact is apparent by examining the location of WAVE-complex activators and effectors using TIRF microscopy; although, their distributions occur near the leading edge of the cell, they do not overlap. We took two approaches to discover new WAVE-complex regulators: 1) analyze candidate proteins with TIRF microscopy to find similar distributions as the WAVE complex and 2) immunoprecipitate interacting proteins with a WAVE-complex antibody. Furthermore, we developed in vitro systems to study how these purified proteins affect and activate WAVE-complex activity.

RESULTS AND DISCUSSION

We developed and modified protocols to purify actin, verprolin/cofilin/acidic (VCA) peptide from NWASP, Rac/GDI complex, Arp2/3 complex, the Rac-binding domain of p21-activating kinase (PBD), the DHPH domain of the Rac GEF Trio, and the WAVE complex (see chemotaxis.tiddlyspot.com for methods). We took a two-pronged approach to reconstituting WAVE-mediated actin assembly – using reaction mixtures that could initiate actin assembly independent of signaling inputs (i.e. independent of Rac, phospholipids, etc.) and using reaction mixtures that could signal properly (i.e. Rac-GTP recruitment to lipids) in the absence of the WAVE complex. In theory, we would get whole system to eventually work by progressing from both ends until we met somewhere in middle. We made significant progress on both ends and figures 2-4 are the culmination of those labors.

PBD binds RacGTP-bound, lipid-coated glass beads in a nucleotide-dependent manner

We developed a fluorescence readout for Rac binding to a lipid-coated bead in its "charged" GTP-bound state. We purified PBD with a single cysteine on the N-terminus and used maleimide chemistry to label the protein with either Alexa488 or Alexa594 dye. We coated glass beads with a mixture of PE/PS/PIP2/cholesterol lipids and doped in a small amount of labeled lipid to mark the bead (Figure 2A). We incubated Rac/GDI and labeled PBD in the presence of a charging reagent (either Trio DHPH or EDTA) and observed recruitment of PBD to lipid beads in a Rac-dependent manner (Figure 2B). We varied the amount of Rac and observed an increase in the PBD fluorescence signal (Figure 2C). Additionally, our reaction depended on the type of nucleotide used to charge the Rac. With exogenous GDP or no nucleotide, GDI can extract Rac from lipid surfaces.

However, once Rac is loaded with GTP or GTPγS, it rapidly bound to our lipid-coated beads (Figure 2D). We wondered if nucleation-promoting factors such as NWASP or the WAVE complex could also be recruited to these Rac-GTP bound, lipid-coated beads. We labeled purified NWASP and WAVE complex and could see recruitment to a lipid-coated bead in a Rac-dependent manner (Figure 3). A similar *in vitro* system was used to dissect NWASP activation and actin assembly with intersectin-activated Cdc42 (Co et al., 2007).

ProteinC-purified WAVE-complex is inactive in a pyrene assay unless heat-denatured

Next, we investigated the fidelity of our actin assembly components – actin, Arp2/3 and the WAVE complex – using pyrene assays and bead assays. We cross-linked VCA peptide, a potent activator of the Arp2/3 complex, to a poly-styrene bead. After addition of Arp2/3, we saw a noticeable increase in the amount of actin surrounding the bead as visualized by rhodamine phalloidin staining (Figure 4A). Phalloidin specifically binds filamentous actin. Without actin, no fluorescence was observed. In a pyrene assay, which measures the kinetics of actin assembly, we saw a rapid increase in polymerization after mixing VCA, Arp2/3, and actin (Figure 4B). Together, these data suggest that our purified actin and Arp2/3 are competent to mediate actin assembly.

We tested a variety of strategies to purify the WAVE complex and settled on one that uses proteinC as an affinity tag (Derivery et al., 2009). Here, an antibody binds the Abi subunit of the WAVE complex in the presence of calcium. Addition of EGTA, a calcium chelator, is sufficient to elute the complex from the antibody-bound beads. We typically recovered 0.5 – 2 mg/ml of protein in ~1ml. Addition of the WAVE complex to Arp2/3 and actin in pyrene assays does not increase the amount of actin assembly (Figure 4B). This is expected because in its folded, native state the active VCA portion of WAVE2 should be covered by other proteins. When we heat-denatured the complex to expose the

VCA domain, actin assembly occurred almost as well as naked VCA peptide (Figure 4B). However, addition of Rac and lipids with beads or in solution at several concentrations failed to activate our purified complex (data not shown). Because our purification did not take considerable care with phosphatase inhibitors, our complex may have been less susceptible to activation by Rac and anionic phospholipids (Lebensohn and Kirschner, 2009). Future studies should focus on obtaining large quantities of phosphorylated WAVE complex.

A long-standing goal of the Weiner lab is to understand the biochemical mechanisms of polarity. Dissecting the biochemical aspect of the WAVE-complex "wave"generator is a step toward understanding chemotaxis. We planned to move the lipid-coated bead assay to lipid-coated surfaces. There, we could examine the spatial patterns generated by actin-based WAVE generator in a manner similar how to the Min oscillator was examined on lipid bilayers (Loose et al., 2008). Towards that end, we created fluid lipid bilayers in conjunction with Dave Richmond in Dan Fletcher's lab and examined single molecules of fluorescently labeled PBD bound to Rac molecules (Figure 4C). In these assays and the ones described above, it remains a possibility that some missing component is required for WAVE-complex activation or pattern formation (Figure 4D). Therefore, we developed two projects to find WAVE-complex associated effectors.

Actin, cofilin, and l-plastin bind membrane-associated WAVE-complex

Previously, components that bound the WAVE-complex in the cytosol after immunoprecipitation were identified by mass spectrometry (Weiner et al., 2006). However, the WAVE complex activates the Arp2/3 complex and actin assembly on the membrane because the WAVE complex is activated by anionic phospholipids and lipid-bound RacGTP. Therefore, we tried a similar immunoprecipitation and mass spectrometry strategy with plasma membrane as a starting material. First, we tested

whether WAVE-complex bound to Hem-1 antibody can bind RacQ61L, a GTP-locked version of Rac (Figure 5A). We found that we could not immunoprecipitate Rac from pig leukocyte lysate, but could immunoprecipitate Rac we added exogenously to the assay. However, addition of RacQ61L weakened the binding site on the WAVE complex for the Hem-1 antibody (Figure 5B). This suggests that Rac and the Hem-1 antibody compete for binding. This is worrisome because interesting effector proteins may also be occluded by the Hem-1 antibody during the immunoprecipitation. Nevertheless, we isolated cytosol, membrane, and granule compartments from HL-60 cells stimulated by fMLP and cytosol from pig lysate stimulated with fMLP and GTPγS or latrunculin (Figure 5C). We noticed several bands that were present in some fractions but not others and decided to pursue these with mass spectrometry (Figure 5D). We isolated several components of the WAVE complex, which suggests that our immunoprecipitation is functional. Several proteins including cofilin, actin, and l-plastin were observed in our immunoprecipitation and mass spectrometry experiment that were not observed when the same immunoprecipitation was performed on cytosol (Weiner et al., 2006). Future studies should focus on finding immunoprecipitation conditions that enable Rac to maintain its interaction with the WAVE complex. Under those conditions, the chance of finding the relevant RacGEF is higher.

β-PIX localization resembles the WAVE complex in HL-60 cells and forms a complex larger in size than the WAVE complex

We hypothesized that a RacGEF scaffolds active RacGTP next to the WAVE complex for WAVE-complex activation. We predicted that this candidate GEF would resemble the localization of active Rac (fluorescent PBD) and the WAVE complex (Hem-1 YFP). We searched the literature for GEFs involved in cell migration and actin assembly, obtained fluorescently tagged constructs for a few candidates, transiently nucleofected them into HL-60 cells, and observed their behavior during cell migration. Only one GEF β-PIX

had similar dynamics to Hem-1 YFP (Figure 6A). We obtained antibodies against β-PIX, performed a continuous sucrose gradient on pig leukocyte lysate, and show that β-PIX forms a complex that is at least as large as the WAVE complex (Figure 6B). Our initial attempts to knock-down this protein with RNAi were unsuccessful (data not shown), but it will be interesting to observe the dynamics of Hem-1-YFP in the absence of β-PIX. If β-PIX contributes to WAVE-complex localization and activation, then Hem-1 waves may be perturbed in β-PIX knockdown cells.

The spatial presentation of chemoattractant determines sensitivity to temporal changes in receptor occupancy

In Figure 7, we show that gradient sensing dominates wave dynamics in response to temporal shifts in mean receptor occupancy. We first allowed cells to migrate randomly or persistently towards a micropipette and then acutely increased (Figure 7A, black arrow) the level of chemoattractant. The direction of the gradient did not change during the micropipette experiments, but every region of the cell surface received a sudden increase in mean receptor occupancy to approximately the same level of receptor occupancy. A given increase in mean receptor occupancy caused less expansion when presented in a gradient compared to uniform chemoattractant (Figure 7A). This highlights the ability of the gradient sensing program to restrict wave distribution in response to moderate changes in receptor occupancy.

We performed a similar type of experiment for cells experiencing a sudden decrease in mean receptor occupancy. Three behaviors were observed in response to a decrease: cells either remained unaffected, simply extinguished Hem-1 waves, or briefly extinguished Hem-1 waves but regenerated them (Figure 7). In the final case, the cell likely adapts to the new level of stimulus and then repolarizes. We classified cells according to these three behaviors in uniform and graded drops in agonist and found that cells migrating in gradients are more capable of regenerating waves after decreases in agonist than are cells

in uniform chemoattractant (Figure 7C).

For decreases in uniform chemoattractant, every point on the cell surface is dropped below the average receptor occupancy felt by the cell. Under these conditions, all waves die, and we postulate that there is no persistent external cue to guide immediate regeneration of polarity. When cells in a gradient of chemoattractant experience a decrease, the waves initially disappear but quickly recover. Because of the gradient, there are points on the cell surface above the post-adaptation average concentration felt by the cell, enabling these regions to generate waves. The ability of gradient sensing to dominate cell response is consistent with a LEGI model of adaptation.

CONCLUSION

The generation of cell polarity is one of the most dramatic and crucial events in neutrophil chemotaxis. The actin cytoskeleton must relay dynamic changes in receptor activity to morphological protrusion and adhesion. The WAVE complex plays a key role in regulating these cytoskeletal rearrangements. In this work, we developed methods to examine the activities of purified cytoskeletal components on lipid surfaces (Figure 2-4), examined WAVE-complex interacting proteins at the membrane (Figure 5), visualized a candidate GEF with TIRF microscopy and discovered it was part of a large complex (Figure 6), and analyzed WAVE-complex dynamics in response to temporal changes in agonist (Figure 7).

Were I to continue in graduate school for a few more years, which of these projects would I continue to pursue? First, I would focus on the contribution of β-PIX to WAVE-mediated actin assembly by developing a method to RNAi genes in HL-60 cells. Then, I could take advantage of the activity readouts already developed by the lab to examine the consequence of reduced β-PIX expression on Rac, PIP3, and WAVE-complex activities. I would attempt different immunoprecipitations with the Hem-1 antibody looking for conditions that caused binding to β-PIX. These immunoprecipitations could be coupled to mass spectrometry to find other interesting effector proteins. For the biochemistry project I would develop alternative means to purify the WAVE-complex, which special attention paid to the phosphorylation state of the complex (Lebensohn and Kirschner, 2009). Purification methods could include recombinant protein from Sf9 cells and a larger scale purification from HEK293 cells expressing Abi-proteinC. Before purifying the Arp2/3 complex and actin, I would work with the Mullins and Taunton labs to examine WAVE-complex activity in pyrene assays. After establishing a reproducible method to activate the complex, I would then focus on generating reagents for lipid bead assays. Only then would replication of WAVE-complex "wave" be possible.

REFERENCES

Co, C., Wong, D. T., Gierke, S., Chang, V., and Taunton, J. (2007). Mechanism of actin network attachment to moving membranes: barbed end capture by N-WASP WH2 domains. *Cell*, **128**, 901-913.

Derivery, E., Lombard, B., Loew, D., and Gautreau, A. (2009). The Wave complex is intrinsically inactive. *Cell Motil. Cytoskeleton*, **66**, 777-790.

Lebensohn, A. M. and Kirschner, Marc W (2009). Activation of the WAVE complex by coincident signals controls actin assembly. *Mol. Cell*, **36**, 512-524.

Loose, M., Fischer-Friedrich, E., Ries, J., Kruse, K., and Schwille, P. (2008). Spatial Regulators for Bacterial Cell Division Self-Organize into Surface Waves in Vitro. *Science*, **320**, 789 -792.

Millius, A., Dandekar, S. N., Houk, A. R., and Weiner, O.D. (2009). Neutrophils establish rapid and robust WAVE complex polarity in an actin-dependent fashion. *Curr Biol*, **19**, 253-9.

Stradal, T. E. B., Rottner, K., Disanza, A., Confalonieri, S., Innocenti, M., and Scita, G. (2004). Regulation of actin dynamics by WASP and WAVE family proteins. *Trends Cell Biol*, **14**, 303-311.

Weiner, O.D., Marganski, W. A., Wu, L. F., Altschuler, S. J., and Kirschner, M.W. (2007). An actin-based wave generator organizes cell motility. *PLoS Biol*, **5**, e221.

Weiner, O.D., Rentel, M.C., Ott, A., Brown, G.E., Jedrychowski, M., Yaffe, M.B., Gygi, S.P., Cantley, L.C., Bourne, H.R., and Kirschner, M.W. (2006). Hem-1 complexes are essential for Rac activation, actin polymerization, and myosin regulation during neutrophil chemotaxis. *PLoS Biol*, **4**, e38.

Weiner, Orion D, Rentel, Maike C, Ott, Alex, Brown, Glenn E, Jedrychowski, Mark, Yaffe, Michael B, Gygi, Steven P, Cantley, Lewis C, Bourne, Henry R, and Kirschner, Marc W (2006). Hem-1 complexes are essential for Rac activation, actin polymerization, and myosin regulation during neutrophil chemotaxis. *PLoS Biol*, **4**, e38.

Figure 1

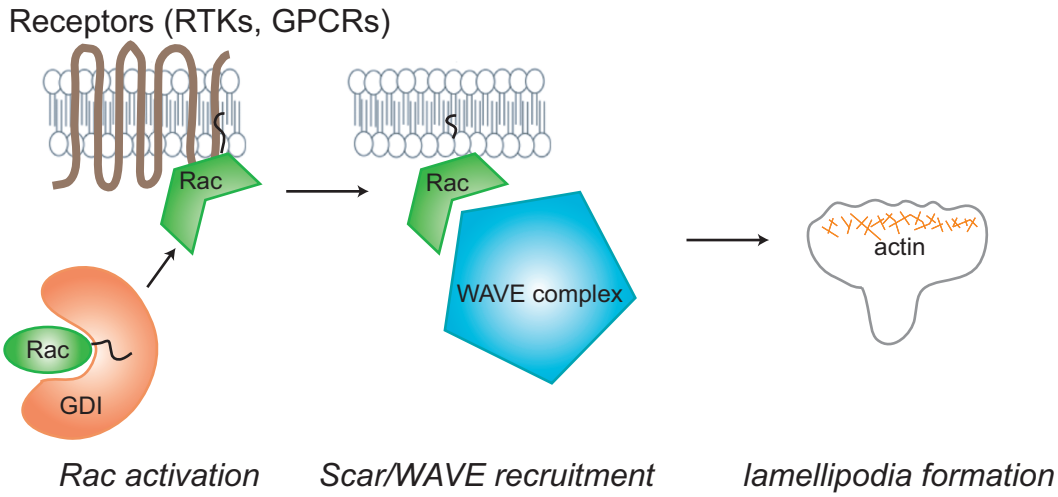

Figure 1. Diagram depicts the major proteins in neutrophil chemotaxis. The formyl-peptide receptor is activated by formylated bacteria proteins. This triggers a signal transduction cascade that includes activation of the small GTPase Rac. RacGTP and anionic phospholipids recruit the WAVE complex to the membrane where is activates the Arp2/3 complex and actin assembly. Actin nucleation at the leading edge causes lamellipodial protrusion and cell migration. From this simple circuit architecture, it is unclear how propagating waves of Hem-1 activity would result.

Figure2

A

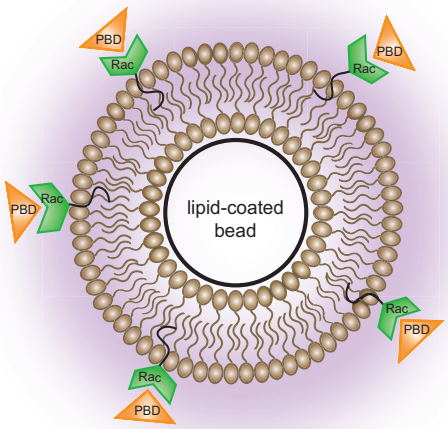

1 uM Rac/GDI

3.4 uM 20% 594 PBD

125 uM total lipids, 6.25 uM PIP2

.05% bead solids

100 uM nucleotide

1X KMEH

B

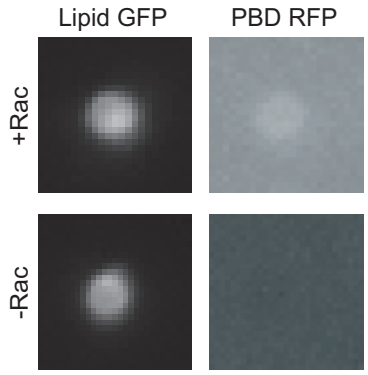

C

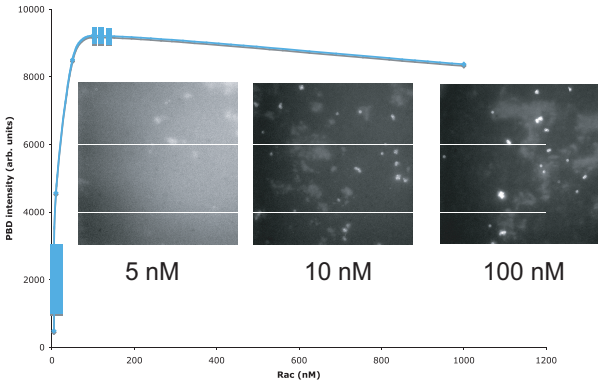

D

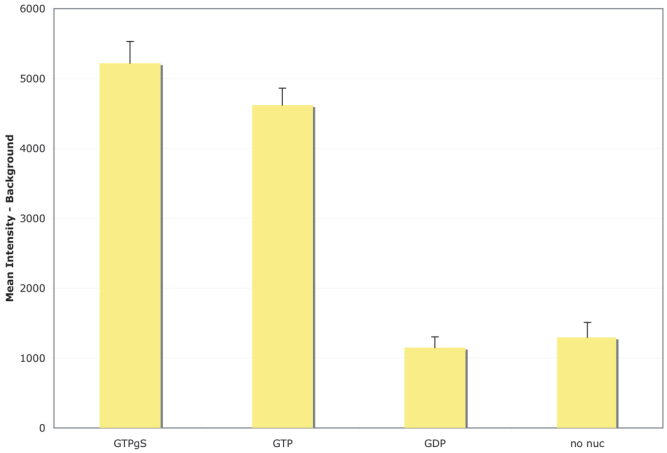

Figure 2. (A) Diagram of experimental set-up: fluorescent PBD (a readout for Rac-GTP) interacts with Rac on the surface of a lipid-coated bead. **(B)** Fluorescently labeled PBD was added to a solution containing fluorescently labeled lipid-coated beads in the presence (top) or absence (bottom) of Rac. Labeled PBD binds the bead with Rac. **(C)** Different concentrations of Rac was added to the reaction mixture. Rac binds the lipid-coated beads with a Kd a little less than 100 nM. Representative images below curve. **(D)** Rac binds lipid coated beads in the presence of GTP and GTPγS, but fails to bind with GDP or no nucleotide.

Figure 3

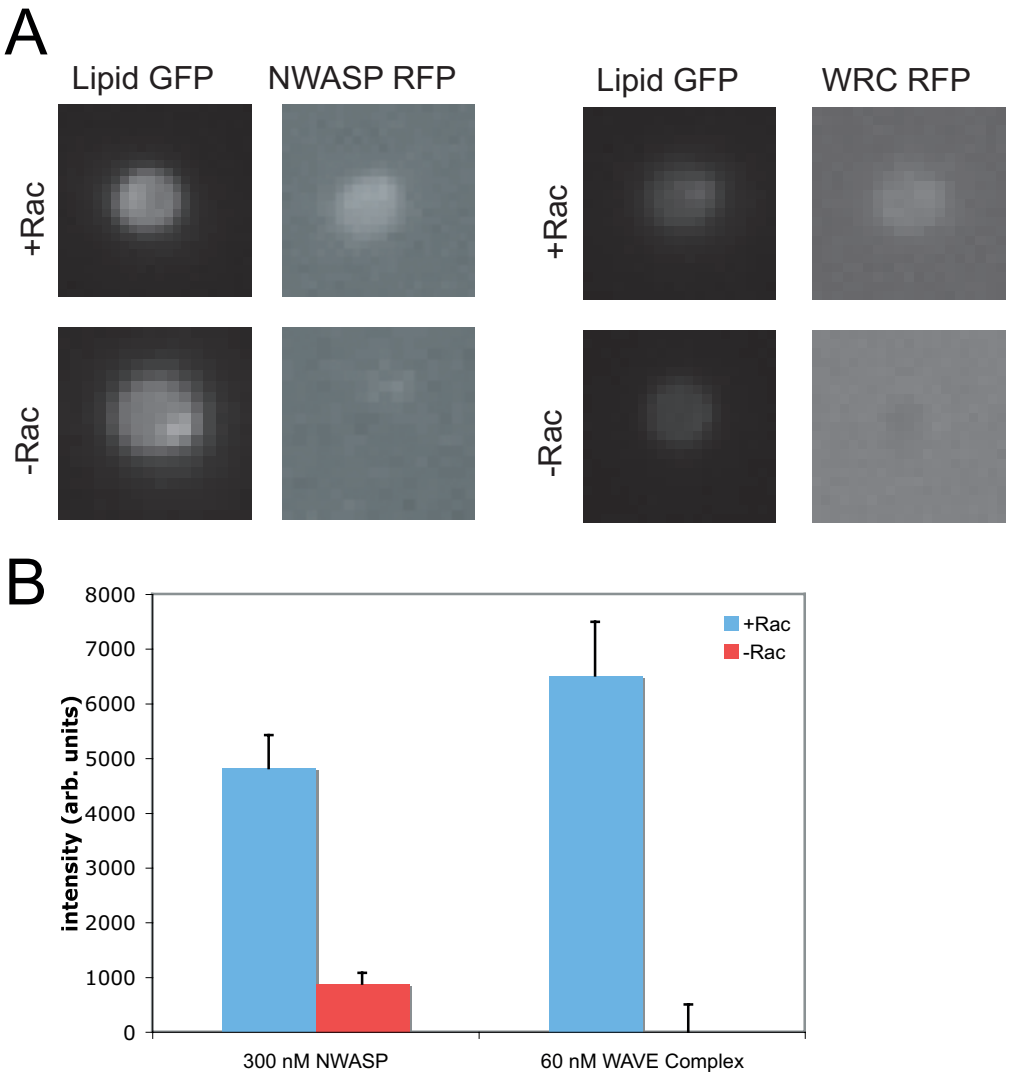

Figure 3. (A) Fluorescent NWASP and WAVE complexes also bind the surface of a lipid-coated bead in the presence of Rac (top) but not in the absence of Rac (bottom). **(B)** Quantification of NWASP and WAVE complexes binding to lipid-coated beads.

Figure 4

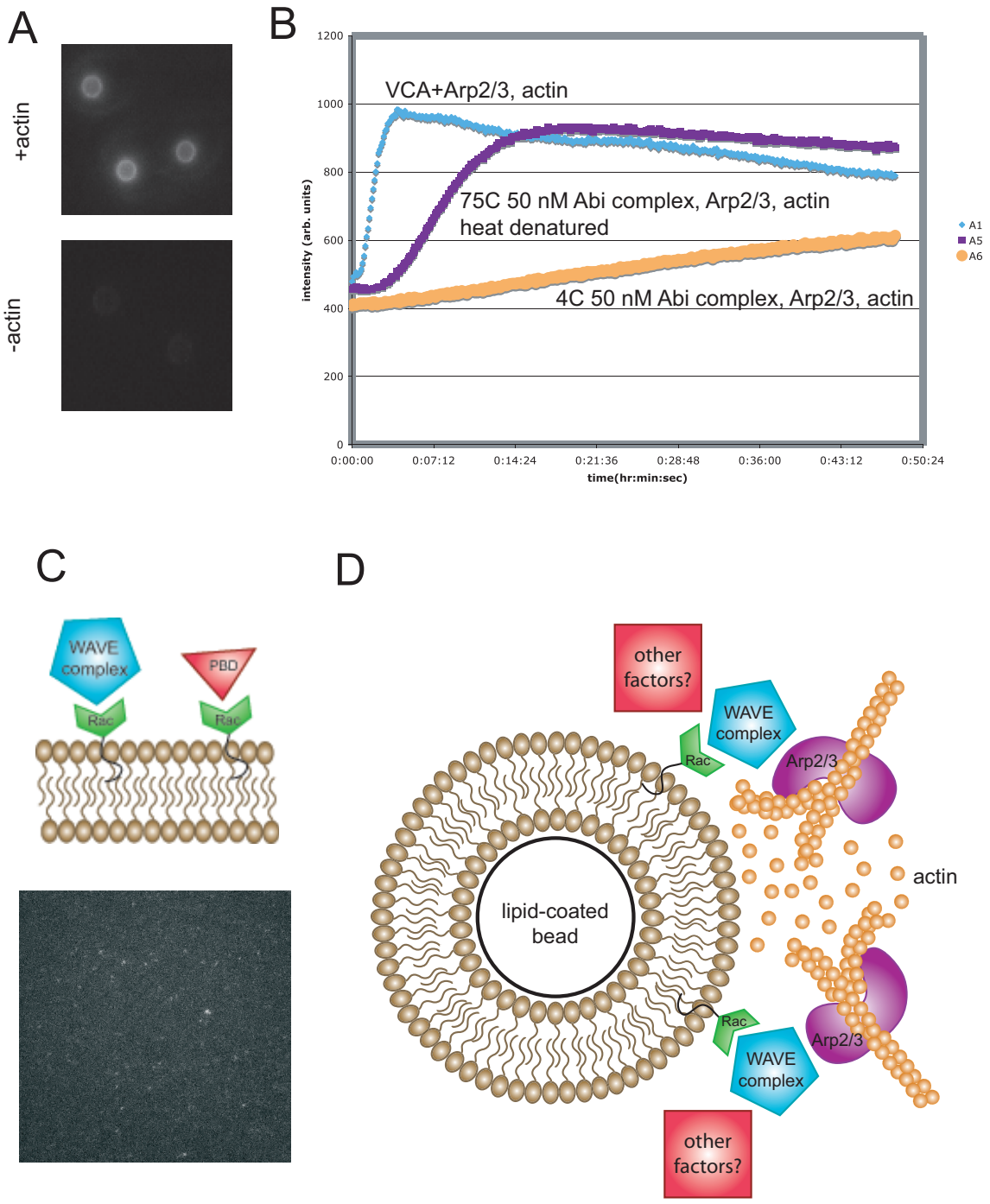
A
+actin
-actin
B
VCA+Arp2/3, actin
75C 50 nM Abi complex, Arp2/3, actin
heat denatured
4C 50 nM Abi complex, Arp2/3, actin
intensity (arb. units)
time(hr:min:sec)
A1
A5
A6
C
WAVE complex
PBD
Rac
Rac
D
other factors?
WAVE complex
Rac
Arp2/3
actin
lipid-coated bead
Rac
Arp2/3
WAVE complex
other factors?

Figure 4. (A) The VCA portion of NWASP was crosslinked to beads. VCA peptide is sufficient to stimulate Arp2/3-mediated actin assembly. Rhodamine phalloidin, a drug that selectively targets f-actin, was used to visualize the assembled actin network on the beads. **(B)** Pyrene assay with purified Arp2/3, actin, and pyrene-labeled actin. Using VCA peptide as a control input strongly activates Arp2/3 and stimulates actin assembly (blue). Purified protein C Abi complex from HEK293 cells shows no activity (orange). However, after heat denaturation the VCA portion of WAVE in the Abi complex becomes exposed and is able to activate Arp2/3 and actin assembly. **(C)** Diagram of the WAVE complex or PBD binding to a fluid lipid bilayer on a coverslip (top); visualization of single molecules of fluorescent PBD (bottom) on a fluid lipid bilayer. **(D)** Diagram of how the WAVE complex might polymerize actin from a lipid coated bead (right). Rac and an anionic phospholipid PIP3 collaborate to activate the WAVE complex. Other factors (red box) may modulate this activity.

Figure 5

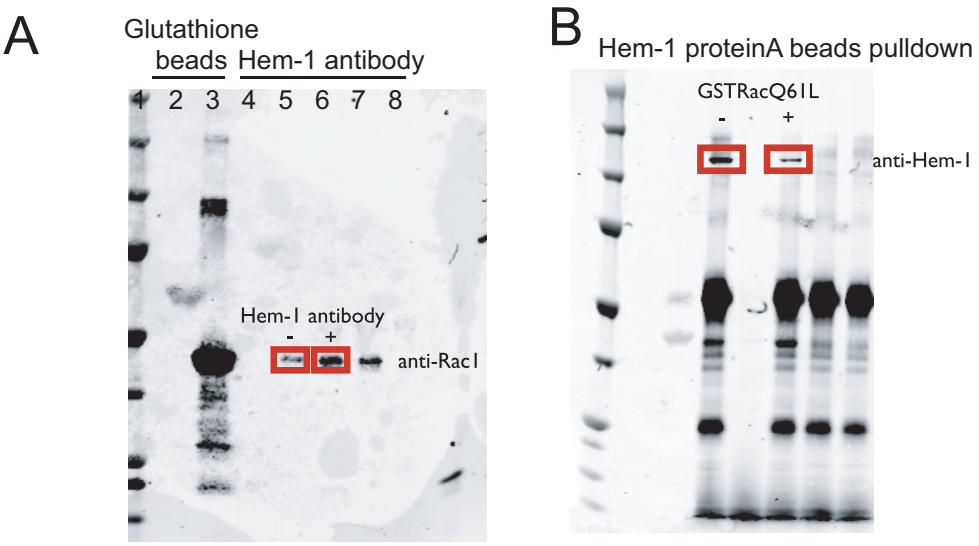

1 = MW
2 = GST bead pull down 200 µl lysate eluate
3 = GST bead pull down 200 µl lysate + ~10 µl RacQ61L eluate
4 = 200 µl lysate + Hem-1 antibody eluate
5 = 200 µl lysate + ~10 µl RacQ61L – Hem-1 antibody eluate
6 = 200 µl lysate + ~10 µl RacQ61L + Hem-1 antibody eluate
7 = RacQ61L + Hem-1 antibody eluate
8 = Hem-1 antibody eluate

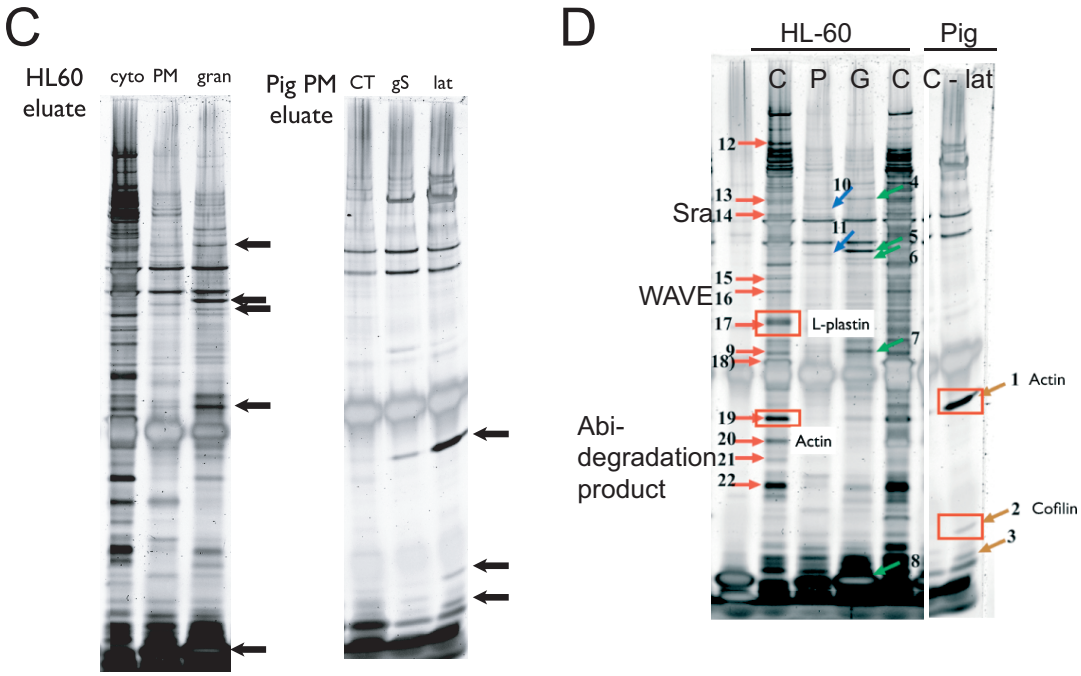

Figure 5. **(A)** Glutathione and protein A beads pulldown with immunoblot against Rac. In lanes 2 and 3, glutathione beads were incubated with pig lysate in the absence (lane 2) or presence (lane 3) of GSTRacQ61L. In lanes 4 – 8, proteinA beads were used with Hem-1 antibody for pull-downs. Hem-1 antibody does not pulldown any Rac from pig lysate alone (lane 4). With no Hem-1 antibody attached to proteinA beads, a small amount of Rac is pulled down (lane 5). Rac pulldown signal increases when Hem-1 antibody is attached to proteinA beads (lane 6). Hem-1 antibody attached to proteinA beads can bind and pulldown Rac in the absence of exogenous pig lysate (lane 7). No Rac is observed in the input pig lysate (lane 8). **(B)** ProteinA beads attached to Hem-1 antibody were used for pulldowns. Hem-1 antibody was subsequently used for immunoblot. There is more Hem-1 pulled down in the absence of exogenously added GSTRacQ61L (left red box) than in the presence of GSTRacQ61L (right red box). This may indicate that Rac binding to WAVE complex may partially occlude Hem-1 antibody binding site. **(C)** HL-60 cells were stimulated with fMLP and fractionated by a discontinuous sucrose gradient for cytosol, plasma membrane and granule fractions (left). Pig cells were stimulated with fMLP plus either GTPγS or latrunculin (right). Lysate was immunoprecipitated with a Hem-1 antibody, eluted with peptide, loaded on a protein gel and imaged with a silver stain. **(D)** Cells from (C) were subject to mass spectrometry in collaboration with Gigi Knudsen. HL-60 cytosol (C, red arrows), HL-60 plasma membrane (P, blue arrows), HL-60 granules (G, green arrows), and pig granules (G, orange arrows). Arrows are bands analyzed by mass spectrometry with interesting hits indicated.

Figure 6

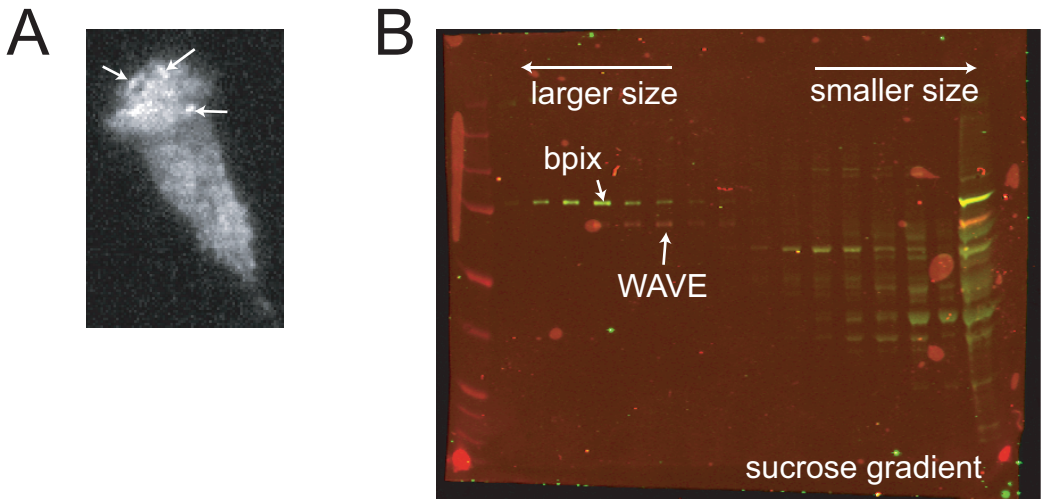

Figure 6. (A) β-PIX-GFP (a Rac GEF) was transiently transfected into HL-60 cells using the amaxa nucleofector system and imaged using TIRF microscopy. β-PIX has a similar localization as the WAVE complex. Arrows denote WAVE-like "waves". **(B)** Pig lysate was subjected to a continuous sucrose gradient, which separates proteins and protein complexes based on a combination their molecular weight and geometry. Individual fractions were collected that correspond to different size species and run on a SDS-PAGE gel. After western blot anti-β-PIX and anti-WAVE2 antibodies were used for an immunoblot. From this data it appears that β-PIX is in a protein complex at least as large as the WAVE complex.

Figure 7

A

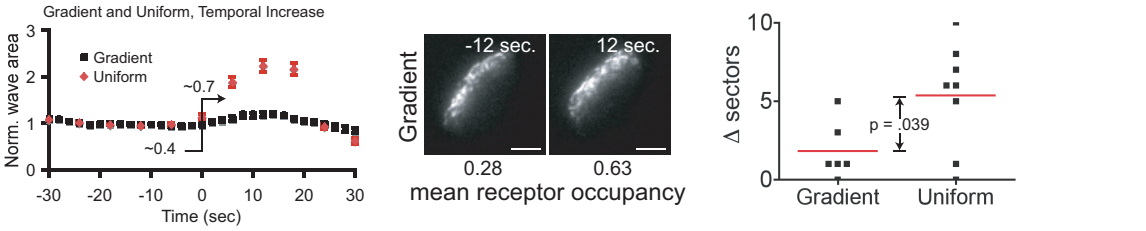
Gradient and Uniform, Temporal Increase
Norm. wave area
Gradient
Uniform
~0.7
~0.4
Time (sec)
Gradient
-12 sec.
12 sec.
0.28
0.63
mean receptor occupancy
Δ sectors
p = .039
Gradient
Uniform

B

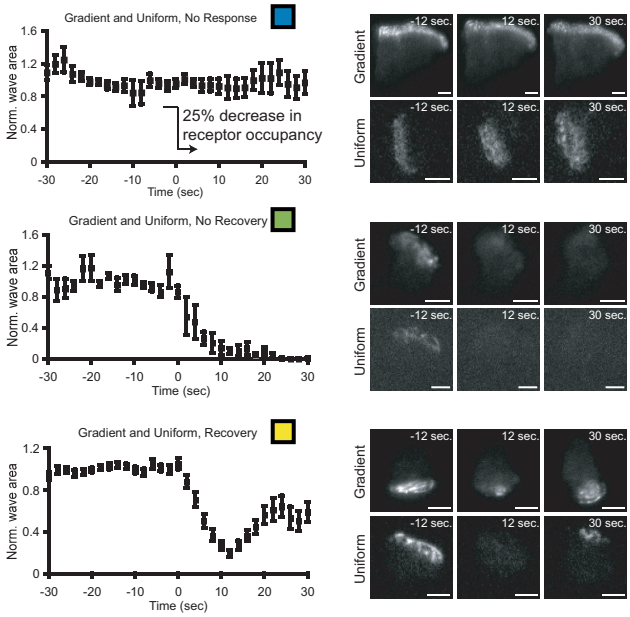
Gradient and Uniform, No Response
25% decrease in
receptor occupancy
Gradient and Uniform, No Recovery
Gradient and Uniform, Recovery
Norm. wave area
Time (sec)
Gradient
Uniform
-12 sec.
12 sec.
30 sec.

C

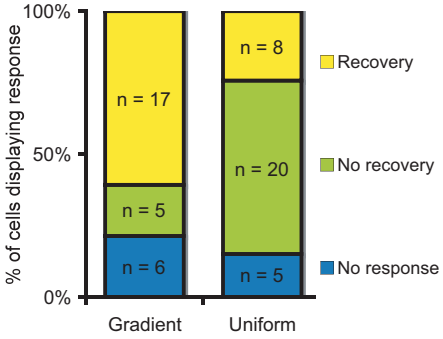
% of cells displaying response
100%
50%
0%
n = 17
n = 5
n = 6
n = 8
n = 20
n = 5
Recovery
No recovery
No response
Gradient
Uniform

Figure 7. **(A)** Cell were subjected to temporal increases in fMLP agonist that corresponded to a 0.39 to 0.73 (red diamonds, uniform) or 0.28±0.10 to 0.63±0.08 (black squares, gradient) increase in mean receptor occupancy (left). Representative time-lapse Hem-1-YFP TIRF images of a cell responding to a temporal increase in mean receptor occupancy for graded agonist (middle). Notice no expansion in WAVE area after increasing agonist. Quantification of the change in wave distribution after temporal agonist increase (right) is significantly different between gradient (n = 6) and uniform (n = 8) presentation (p = 0.039, Student's t-test). Bars, 5 μm. **(B)** Representative time-lapse Hem-1-YFP TIRF images of cells responding to temporal decreases in mean receptor occupancy for graded and uniform agonist (right) and the corresponding population averaged normalized wave distributions (left). Average wave response for cells in gradient and uniform chemoattractant were plotted according to three categories: waves unaffected by temporal decrease (top), waves extinguished by temporal decrease (middle), and waves that were extinguished but rapidly recovered (bottom). Temporal drops corresponded to a 25% decrease in mean receptor occupancy. **(C)** For both graded and uniform agonist, each cell was scored as having no response (blue bar), no recovery (green bar), or response with recovery (yellow bar). Cells in graded agonist were more likely to recovery (n = 17) than cells in uniform agonist (n = 8), which indicates that spatial presentation of the agonist affects the resulting wave distributions.

CHAPTER FIVE

Diffusion, capture, and recycling of SCAR/WAVE and Arp2/3 complexes observed in cells with single-molecule imaging

Fight that voice, especially if you're a woman, that tells you that you're not good enough. Only the dead and fools are without fear, but don't ever let fear make decisions for you.

-Gary Pesko

The young scientists aren't cheeky enough, they don't question authority

-Sydney Brenner

I learned a lot about a bunch of different things in grad school, and one of them was humility

-Philip Sabes

Adapted from Millius A., Watanabe N., and Weiner O.D. (2011 *in press*), Diffusion, capture, and recycling of SCAR/WAVE and Arp2/3 complexes observed in cells with single-molecule imaging. In *Journal of Cell Science*.

SUMMARY

The SCAR/WAVE complex drives lamellipodium formation by enhancing actin nucleation by the Arp2/3 complex. Phosphoinositides and Rac activate the SCAR/WAVE complex, but how SCAR/WAVE and Arp2/3 complexes converge at sites of nucleation is unknown. We analyzed the single-molecule dynamics of WAVE2 and p40 (subunits of the SCAR/WAVE and Arp2/3 complexes, respectively) in XTC cells. We observed lateral diffusion of both proteins and captured the transition of p40 from diffusion to network incorporation. These results suggest that a diffusive 2D search facilitates binding of the Arp2/3 complex to actin filaments necessary for nucleation. After nucleation, the Arp2/3 complex integrates into the actin network and undergoes retrograde flow, which is reflected by its broad distribution throughout the lamellipodium. In contrast, the SCAR/WAVE complex is more restricted to the cell periphery, but with single-molecule imaging we also observed WAVE2 molecules undergoing retrograde motion. WAVE2 and p40 have nearly identical speeds, lifetimes, and sites of network incorporation. Inhibition of actin retrograde flow does not prevent WAVE2 association and disassociation with the membrane but does inhibit WAVE2 removal from the cortex. Our results suggest that membrane binding and diffusion expedites the recruitment of nucleation factors to a nucleation site independent of actin assembly, but after network incorporation ongoing actin polymerization facilitates SCAR/WAVE and Arp2/3 complex recycling.

INTRODUCTION

Cells use actin nucleators such as the Arp2/3 complex to control the spatial and temporal dynamics of actin assembly. Activation of the Arp2/3 complex requires its association with actin filaments as well as nucleation-promoting factors such as the SCAR/WAVE complex (Mullins et al., 1998; Machesky and Insall, 1998; Machesky et al., 1999; Rohatgi et al., 1999). Similarly, the SCAR/WAVE complex requires multiple upstream activators such as plasma membrane-associated phosphoinositides and Rac (Miki et al., 1998; Steffen et al., 2004; Oikawa et al., 2004; Lebensohn and Kirschner, 2009; Chen et al., 2010). Proteins in the SCAR/WAVE family are essential for actin polymerization and movement in many different cell contexts (Bear et al., 1998; Miki et al., 1998; Zallen et al., 2002; Yan et al., 2003; Rogers et al., 2003; Weiner et al., 2006; Ibarra et al., 2006; Patel et al., 2008).

The Arp2/3 complex and other actin regulators associate with the actin network, which is pushed away from the leading edge of a cell in a process called retrograde flow. Retrograde flow was first visualized with techniques like FRAP and photoactivation (Wang, 1985; Theriot and Mitchison, 1991, 1992; Lin and Forscher, 1995; Cramer and Mitchison, 1997). Because data from these techniques can hide local differences in actin assembly, researchers have more recently used additional methods such as single-molecule and speckle microscopy to analyze the fine-grained spatial and temporal dynamics of actin rearrangements (Watanabe and Mitchison, 2002; Ponti et al., 2004). Single-molecule imaging has also been used to study actin-associated proteins like the Arp2/3 complex and capping protein, which have different lifetimes in the actin network (Ponti et al., 2005; Miyoshi et al., 2006; Iwasa and Mullins, 2007). However, single-molecule imaging has not been applied to nucleation-promoting factors such as the SCAR/WAVE complex, and it is unknown whether the SCAR/WAVE complex

incorporates into the actin network.

Imaging in other non-single-molecule modes shows that the SCAR/WAVE complex is recruited to the edge of the lamellipodium in fibroblasts (Stradal et al., 2001; Lai et al., 2008) and propagates in "waves" of actin assembly at the leading edge of neutrophils and Dictyostelium (Weiner et al., 2007; King et al., 2010; Xiong et al., 2010). However, these imaging modes may obscure molecules whose dynamics differ from the global population. To elucidate mechanisms of SCAR/WAVE complex recruitment to the plasma membrane, convergence with the Arp2/3 complex on a membrane-apposed actin filament, and removal from the membrane, we analyzed the single-molecule dynamics of WAVE2 in Xenopus Tissue Culture (XTC) cells. In addition to its peripheral association with the leading edge, we show that WAVE2 molecules incorporate into the growing lamellipodial actin network. WAVE2 undergoes retrograde flow at similar speeds, sites of initiation, and lifetimes to that of actin and the p40 subunit of the Arp2/3 complex. Using a drug cocktail that stabilizes the existing cytoskeleton while blocking new assembly, we demonstrate that ongoing actin polymerization is not required for WAVE2 association and dissociation with the membrane but is required for WAVE2 removal from the cortex. Finally, we show that p40 and WAVE2 laterally diffuse in the membrane and capture the transition of p40 from lateral diffusion to network incorporation. Based on these data, we propose that the SCAR/WAVE and Arp2/3 complexes locally search the membrane before converging on sites of actin nucleation, and are removed from the actin network through the force of retrograde flow.

RESULTS

Single-molecule imaging shows that WAVE2 undergoes retrograde flow in XTC cells

We used a crippled CMV promoter to express a low concentration of WAVE2-GFP, which is necessary for single-molecule imaging. Because XTC cells have flat protrusions, single molecules can be easily visualized with epifluorescence microscopy. This enables us to image thicker sections than can be achieved with TIRF and with less photodamaging light than needed for confocal imaging. Long camera exposures enabled us to view stabilized fluorescent probes attached the membrane or cytoskeleton while blurring fast diffusing molecules (Watanabe and Mitchison, 2002). Under these imaging conditions, we observed WAVE2-EGFP molecules in the lamellipodium, filopodia, and regions near the lamellipodium interior (**Fig. 1A**, *left*), consistent with the known overall distribution of WAVE2 in non-single-molecule imaging mode (Hahne et al., 2001; Stradal et al., 2001; Lai et al., 2008). WAVE2-EGFP molecules have a unimodal distribution of intensities similar to p40-EGFP and photobleach in a single step (see supplemental material **Fig. S1**), characteristic of single molecules. Surprisingly, we also observed persistent movement of WAVE2 molecules away from the leading edge (**Fig. 1** and **Movie 1**). Kymograph analysis revealed that WAVE2 retrograde motion is smooth and continuous (**Fig. 1A**, *left,* inset). WAVE2 retrograde movement can be visualized easily with a maximum intensity projection over the course of the epifluorescence acquisition (**Fig. 1A,** *middle*). Here, retrograde motion appears as linear streaks, as indicated by the arrows. Retrograde flow of WAVE2 is more difficult to observe with shorter exposures in TIRF microscopy (see supplemental material **Fig. S2A**), because transient recruitment of WAVE2 obfuscates stabilized pools of the WAVE2 on the plasma membrane and/or cytoskeleton. Most of our experiments were performed on polylysine, but we also observed WAVE2 retrograde motion on more physiological substrates such as fibronectin

(see supplemental material **Fig. S2B,C**).

Cells spatially bias actin polymerization to control shape and movement. Both actin and p40 appearance are strongly biased toward the leading edge (Watanabe and Mitchison, 2002; Miyoshi et al., 2006). Similarly, the initial position of appearance for retrograde moving molecules of WAVE2 is biased to 1 μm of the leading edge (**Fig. 1A,** *right* and **Fig.1B**), suggesting that most SCAR/WAVE complex-mediated actin assembly occurs in this region. Molecules of WAVE2 that undergo retrograde flow have a mean speed of 31 nm/s (**Fig. 1C**). The distribution of WAVE2 lifetimes was well fit by a single exponential curve with a mean lifetime (τ) of 14.9±2.1 s (**Fig. 1D** and *inset*). We could not measure speed and lifetime for WAVE2 molecules that stayed on the cell edge because individual molecules were not resolvable. Our lifetime measurements are roughly similar to lifetimes measured with population techniques (**Fig. 4F**, Weiner et al., 2007; Lai et al., 2008). We measured the lifetime of a molecule in relation to the distance from the leading edge it first appeared, but found no correlation (**Fig. 1E**), similar to a lifetime versus position plot for Arp2/3 (Miyoshi et al., 2006).

Actin and p40 retrograde flow are similar to WAVE2 retrograde flow

Because the site of appearance and speed of retrograde flow for WAVE2 molecules are similar to actin retrograde flow, we hypothesized that the SCAR/WAVE complex may be hitchhiking with the Arp2/3 complex on the retrograde-flowing network. To gain greater insight into the relative dynamics of the SCAR/WAVE complex, the Arp2/3 complex, and actin, we compared their rates of retrograde flow and lifetimes in the actin network. Observation of the GFP-tagged p40 subunit of the Arp2/3 complex (**Fig. 2A** and **Movie 2**) demonstrates that p40 has a remarkably similar mean retrograde flow speed of 30 nm/s (**Fig. 2C**) to that of WAVE2 (31 nm/s, **Fig. 1C**). Similarly, the lifetime of p40 during retrograde flow is 15.2±0.5 s (**Fig. 2E,** compared to 14.9±2.1 s for WAVE2, **Fig. 1D**) and

does not depend on where molecules initially appear (see supplemental material **Fig. S2D**). When we observed cells expressing low amounts of actin-EGFP (**Fig. 2B** and **Movie 3**), we also found that actin has a similar mean retrograde speed of 25 nm/s (**Fig. 2D**) and a mean lifetime in the network of 18.4±0.5 s (**Fig. 2F**). This is comparable to previous reported values of actin retrograde flow in XTC cells (Watanabe and Mitchison, 2002), but greater than the mean speed of actin retrograde flow reported in microinjected PtK1 cells using speckle microscopy (Ponti et al., 2004). Like WAVE2, appearance of p40 and actin molecules is heavily biased to within 1 μm of the leading edge (**Fig. 2G,H**). Although p40 distribution is more restricted than either actin or WAVE2, possibly because other Arp2/3 complex activators are restricted to the periphery. These data support a model where SCAR/WAVE and Arp2/3 complexes both incorporate into the actin network, maintain their interaction during retrograde flow, and are dissociated from the network together.

In both p40-EGFP and actin-EGFP expressing cells, all observable molecules undergo retrograde flow. Therefore, a large number of tracks can be collected with few cells. In contrast, WAVE2-EGFP retrograde flow is a comparatively rare event (compare **Fig. 2A,B** middle panels to **Fig. 1A** middle panel and quantified in **Fig. 1F**). We hypothesize that this is because only a subset of SCAR/WAVE complexes participate in Arp2/3 complex recruitment and actin nucleation. This is consistent with the observation that the SCAR/WAVE complex shows a much stronger peripheral association with the lamellipodium than the Arp2/3 complex.

Inhibition of retrograde flow impedes p40 recycling

Previously, actin polymer has been shown to be involved in the recycling of the WAVE complex (Weiner et al., 2007) and other nucleation-promoting factors (Weisswange et al., 2009). Furthermore, actin polymer helps to sculpt the spatial

distribution of the WAVE complex in response to external stimuli (Millius et al., 2009). However, these experiments relied on treating cells with single pharmacological inhibitors of actin assembly such as the actin-sequestering drug latrunculin. Application of these drugs not only inhibit new polymerization, but also result in the disassembly of the existing actin network. These dual effects make it difficult to determine whether basal actin polymer or ongoing actin assembly is more relevant for SCAR/WAVE complex recycling. To address this question, we developed a three-drug cocktail to stabilize the existing network while preventing new actin polymerization. This cocktail involves incubating cells in a mixture of 10 μM Rho Kinase inhibitor Y27632 (Y) for 30 minutes to inhibit myosinII-based actin contraction, then simultaneously adding 20 μM latrunculin (L) to prevent new actin assembly and 20 μM jasplakinolide (J) to stabilize existing actin structures (**Fig. 3A).** Details of this drug cocktail optimization and comparison with other modes of actin stabilization will be described elsewhere (O.D. Weiner, unpublished). We verified that this JLY drug combination blocks actin nucleation (visualized by p40-EGFP retrograde flow) and disassembly of the actin network (visualized by the lifetime of p40-EGFP in the actin network). Untreated cells expressing p40-EGFP have significant retrograde flow (trajectories shown in **Fig. 3B**, *left*), which is apparent by long streaks in a maximum intensity projection (**Fig. 3B**, *middle*) and diagonal lines in the kymograph (**Fig. 3B**, *right*). In contrast, p40-EGFP molecules in cells treated with the JLY cocktail remain stably associated with network; note the lack of long trajectories in drug-treated cells (**Fig. 3C**, *left*) and fixed points in the maximum intensity projection (**Fig. 3C**, *middle*). The lack of retrograde movement is also apparent as vertical instead of diagonal streaks in the kymograph (**Fig. 3C**, *right*). Analysis of trajectories confirms that retrograde speed decreases (**Fig. 3D**) and lifetime increases (**Fig. 3E**) with drug treatment. To test whether our single-molecule measurements reflected the global behavior of the actin network, we examined the morphology and bulk

p40-EGFP fluorescence of a cell before and after JLY drug application (**Fig. 3F** and **Movie 4**). Before JLY drug treatment cell protrusion and retraction leads to a difference of ~8% in the overlapping cell area. In contrast, after drug treatment the overlapping area is nearly identical (only 1% difference) because the cell has ceased to protrude and retract. Fluorescence of p40-EGFP also becomes stabilized after drug addition (**Fig. 3F**, *bottom*). We examined p40-EGFP fluorescence recovery after photobleaching (FRAP) to show that new p40-EGFP incorporation in the actin network does not occur (**Fig. 4E**). Together, these data indicate that the JLY drug cocktail inhibits new actin assembly while stabilizing existing actin structures.

WAVE2 recycles through actin-dependent and actin-independent mechanisms

To examine how actin regulators depend on ongoing actin polymerization and depolymerization, we analyzed the effect of JLY in cells expressing low levels of p40-EGFP or WAVE2-EGFP, imaged with TIRF microscopy. To easily visualize the results of this experiment, we created a kymograph across the whole cell using the "Reslice" function in ImageJ, which shows how molecules change before and after drug treatment. Then we applied a maximum intensity projection ("Z Project" function in ImageJ) across all kymograph slices to visualize every region of the cell in one frame. After JLY drug treatment, Arp2/3 complexes become stabilized (**Fig. 4A**, long vertical streaks; arrow indicates drug addition). Next, we examined WAVE2-EGFP dynamics after acute inhibition of actin polymerization and depolymerization (**Fig. 4B, C**). Before drug treatment, most WAVE2 molecules transiently associate with the cell membrane and/or cytoskeleton (**Fig. 4B**, punctate spots above arrow). After actin dynamics cease, a few WAVE2 molecules remain associated with the membrane and/or cytoskeleton (**Fig. 4B**, long streaks of WAVE2 below arrow in the kymograph; WAVE2 lifetime is quantified in **Fig. 4C**). To test for a general perturbation of plasma membrane interactions, we assayed

the dynamics of Rac2-GFP association with the plasma membrane. Rac2 membrane association is equivalent in the presence and absence of JLY (**Fig. 4D**) and resembles WAVE2 interaction with the membrane before drug treatment (**Fig. 4B,** above arrow). These data suggest that a subset of SCAR/WAVE molecules (likely those associated with the cytoskeleton) require ongoing actin polymerization for recycling, consistent with observed retrograde flow. To test whether this actin dependence is similar for all WAVE2 molecules, we assayed the global pool of WAVE2 for actin-dependent recycling using FRAP. Here, WAVE2-EGFP molecules recovered similarly in both untreated and JLY-treated experiments (**Fig. 4F**) in contrast to p40-EGFP (**Fig. 4E**), which suggests that WAVE2 molecules freely associate and dissociate with the plasma membrane and do not require an actin-nucleation event for membrane dissociation. Together, our data suggest that most WAVE2 molecules interact with the membrane in an actin-independent manner, but once WAVE2 becomes integrated into the actin network (presumably through Arp2/3 activation), actin-dependent retrograde flow is required for WAVE2 turnover.

WAVE2 and p40 undergo lateral diffusion similar to membrane-associated proteins

We next sought to address how SCAR/WAVE and Arp2/3 complexes arrive at sites of actin nucleation. Arp2/3 complex activation involves its association with nucleation-promoting factors (such as the SCAR/WAVE complex) as well as an actin filament (Mullins et al., 1998; Machesky et al., 1999). Furthermore, the SCAR/WAVE complex is recruited and activated at membranes via association with phospholipids and GTP-bound Rac (Lebensohn and Kirschner, 2009; Padrick and Rosen, 2010). How do all of these components converge to one point in space and time for actin nucleation? We envisioned two possibilities – 1) SCAR/WAVE and Arp2/3 complexes are recruited directly from the cytosol to bind a membrane-associated actin filament or 2) SCAR/WAVE and Arp2/3 complexes diffuse in the plane of the membrane in search of an actin filament.

Consistent with the second hypothesis, when we imaged cells expressing low amounts of WAVE2-EGFP in TIRF microscopy at high-temporal resolution, we observed laterally diffusing molecules (see supplemental material **Movie 5**).

We hypothesized that lateral diffusion of WAVE2 reflects its association with membrane-bound components such as Rac-GTP or phosphoinositides. We used mean squared displacement (MSD) versus time lag plots to analyze the diffusion of WAVE2 molecules (a representative plot is shown in **Fig. 5A**). A histogram of lateral diffusion coefficients gives a mean diffusion constant for WAVE2 of 0.41±0.04 $\mu m^2/s$ (**Fig. 5B**). This is similar to previous reported values for Ras-GFP lateral diffusion in the membrane (Murakoshi et al., 2004), and is similar to our own analysis of Rac2-GFP lateral diffusion (see supplemental material **Fig. S3A,B** and **Movie 6**). WAVE2 lateral diffusion was not prevented by the presence of dominant negative RacN17 (see supplemental material **Fig. S3C**). This is consistent with previous data that the SCAR/WAVE complex has multiple modes of binding to the plasma membrane (Miki et al., 1998; Steffen et al., 2004; Oikawa et al., 2004; Lebensohn and Kirschner, 2009; Chen et al., 2010). We could measure a slight, but statistically significant increase in the mean lateral diffusion coefficient of WAVE2 in the presence of RacN17 (0.54±0.02 $\mu m^2/s$, **Fig. S3C** compared to 0.41±0.04 $\mu m^2/s$ in control cells, **Fig. 5B**), which suggests that Rac-GTP may limit the diffusion of the SCAR/WAVE complex through direct binding or through mediating the interaction of the SCAR/WAVE complex with downstream signaling events like association with the actin cytoskeleton. In some cases, we observed WAVE2 transition from lateral diffusion to immobilization (a representative cell is shown in **Fig. 5D**, and **Movie 7**), possibly representing a precursor to retrograde flow. We also observed p40-EGFP diffusion (**Fig. 6** and **Movie 8**) with a mean diffusion constant of 0.63±0.06 $\mu m^2/s$

(**Fig. 6A**). WAVE2 and p40 also have similar residence times on the membrane (τ = 287±43 ms **Fig. 5C** and τ = 325±17 ms **Fig. 6B**, respectively). Our data support a model where the Arp2/3 complex binds the SCAR/WAVE complex and diffuses along the membrane in search of an actin filament for Arp2/3 complex activation.

Are laterally diffusing Arp2/3 complex molecules precursors to actin nucleation? To address this question, we performed extended high-speed imaging of cells that contained both stationary and diffusing p40-EGFP molecules. We observed individual particle diffusion before retrograde flow (an example is shown in **Fig. 6C** and **Movie 9**), although not all retrograde flow events were preceded by detectable lateral diffusion (**Fig. 6D** and **Movie 10**). In this high-intensity rapid imaging mode, molecules photobleached rapidly, which made it difficult to discern retrograde motion from an immobile particle. In order to better capture the transition from lateral diffusion to retrograde flow, we switched imaging frequencies during the acquisition. We first imaged molecules in a high-frequency mode to capture lateral diffusion and then switched to the low-frequency, low-light mode that is more optimal to observe retrograde flow for long periods of time. With this approach, we could capture molecules transitioning from rapid diffusion to an extended period of retrograde movement. In **Fig. 6E** and **Movie 11**, we show a molecule of p40-EGFP, which undergoes 400 ms of lateral diffusion with diffusion coefficient of 0.12 $\mu m^2/s$ (**Fig. 6F,** *right*) before its incorporation into the cytoskeletal network. We then follow the molecule during its retrograde motion in a lower-frequency imaging mode. This method enabled us to easily visualize retrograde flow after particle diffusion (**Fig. 6F,** *left*). We found thirteen p40 molecules that showed clear retrograde flow. Four of these molecules were preceded by at least four frames (400 ms) of lateral diffusion. The other molecules underwent retrograde flow without detectable lateral diffusion, or diffusion was too brief for us to observe. Together, these data show that some Arp2/3

complexes locally search the membrane via 2D diffusion for short periods while other molecules are recruited directly from the cytosol before incorporation into the cytoskeleton.

DISCUSSION

We uncovered new behaviors of SCAR/WAVE and Arp2/3 complexes with single-molecule imaging before, during, and after nucleation in cells. These data are summarized in our model (**Fig. 7**). Our first insight relates to the order of recruitment of SCAR/WAVE and Arp2/3 complexes to the plasma membrane. Actin nucleation is a highly regulated event that requires the convergence of several intracellular signals and cytoskeletal structures. Activation of the Arp2/3 complex requires its interaction with nucleation promoting factors such as the SCAR/WAVE complex as well as actin filaments (Mullins et al., 1998; Machesky et al., 1999). Similarly, SCAR/WAVE complex activation requires the combinatorial input of Rac-GTP, phosphoinositides, and other signals (Oikawa et al., 2004; Lebensohn and Kirschner, 2009; Chen et al., 2010). Two models have been proposed for how the SCAR/WAVE and Arp2/3 complexes first associate with the membrane. In the first model, the SCAR/WAVE complex is recruited and activated via plasma membrane-bound components such as Rac-GTP and phosphoinositides, and then the Arp2/3 complex is recruited from the cytosol to this membrane-bound SCAR/WAVE complex (Lebensohn and Kirschner, 2009; Chen et al., 2010). In the second model, the Arp2/3 complex is pre-associated with the Scar/WAVE complex in the cytosol, and both of these complexes are recruited together to membranes (Stradal et al., 2004). However, WAVE2 and p40 have different distributions on the membrane (**Fig. 1 and 2**), which suggests that not every SCAR/WAVE complex is pre-associated with an Arp2/3 complex.

After the SCAR/WAVE complex initially associates with the plasma membrane by binding to Rac-GTP or phosphoinositides, what happens? The SCAR/WAVE complex likely recruits the Arp2/3 complex to the plasma membrane, as reflected in the similar lifetime of p40 and WAVE2 on the membrane (**Figs. 5C,6B**). Both WAVE2 and p40

laterally diffuse upon recruitment to the plasma membrane, likely because of Rac-GTP or phospholipid binding. Rac2 has a diffusion coefficient of 0.54±0.04 μm2/s (see supplemental material **Fig. S3A,B**); the diffusion coefficient for WAVE2 is 0.41±0.04 μm2/s (**Fig. 5B**); and the diffusion coefficient for p40 is 0.63±0.05 μm2/s (**Fig. 6A**). These values are within the expected range of diffusion coefficients for membrane-associated proteins (Murakoshi et al., 2004; Lommerse et al., 2004; Douglass and Vale, 2005; Matsuoka et al., 2006). Lateral diffusion of SCAR/WAVE and Arp2/3 complexes could help these proteins perform a constrained 2D search for nucleation binding sites, including actin barbed ends or sides of filaments, which are necessary to co-activate the Arp2/3 complex. Limited dimensionality searches have been reported in other biological contexts to decrease search time. For instance, the LacI repressor executes short 1D searches along DNA to find its LacO target 100 times faster than can be accomplished with 3D diffusion in the cytosol (Riggs et al., 1970; von Hippel and Berg, 1989; Wang et al., 2006; Elf et al., 2007). These constrained diffusion events need not be extensive to dramatically decrease search time; the LacI repressor spends 90% of the time diffusing on DNA with a short residence time of 5 milliseconds (Elf et al., 2007). Both WAVE2 and p40 had similar residence times of ~300 ms during lateral diffusion (**Fig. 5C** and **Fig. 6B**), and more rapid imaging as in (Elf et al., 2007) may be needed to capture very short-lived 2D searches.

After SCAR/WAVE and Arp2/3 complexes trigger an actin nucleation event, what happens? We show that the Arp2/3 complex incorporates into the actin network and undergoes retrograde flow, consistent with previous reports (Ponti et al., 2004; Miyoshi et al., 2006; Iwasa and Mullins, 2007). Surprisingly, we also observed retrograde flow of the SCAR/WAVE complex (**Fig. 1**). Because WAVE2 retrograde speed and lifetime matches that of actin and p40 (**Fig. 2**), we hypothesize that WAVE2 incorporates into the

actin meshwork after a nucleation event. Alternatively, WAVE2 may bind the side of an actin filament without first activating Arp2/3 to undergo retrograde motion. In support of the former model, most WAVE2 molecules with retrograde motion first attach to the actin network near the leading edge, where the SCAR/WAVE complex activates the Arp2/3 complex. However, the frequency of WAVE2 retrograde flow is significantly lower than either actin or p40 (**Fig. 1F**). Several possibilities could account for the discrepancy between SCAR/WAVE and Arp2/3 complex localization. The simplest hypothesis is that only a subset of membrane-bound SCAR/WAVE complex is involved in Arp2/3 complex recruitment and actin nucleation. Consistent with this hypothesis, the overall distributions of WAVE2 and p40 differ, with the cell periphery more enriched for the SCAR/WAVE complex (**Fig. 1A**) compared to the Arp2/3 complex (**Fig. 2A**). Alternatively, the SCAR/WAVE complex might activate multiple Arp2/3 molecules before being recycled through retrograde flow. In this scenario most SCAR/WAVE complexes remain associated at the cell periphery after nucleation and only occasionally track with an Arp2/3 complex during retrograde flow. Finally, all SCAR/WAVE complexes that induce actin nucleation may be removed from the membrane by incorporating into the actin network, but some molecules may be removed more rapidly than our imaging conditions can capture. Future studies are needed to distinguish among these possibilities.

Our work sheds new light on the role of actin polymerization in SCAR/WAVE complex recycling. Both SCAR/WAVE complex removal from the plasma membrane or cortex (Weiner et al., 2007; Millius et al., 2009; this study) as well as N-WASP removal from the surface of vaccinia viruses (Weisswange et al., 2009) depend on actin polymer. Similarly, regulators of actin assembly in budding yeast require actin polymer for rapid recycling (Kaksonen et al., 2003). For these experiments, actin drugs such as latrunculin have been used to uncover the role of actin polymer in recycling. However, latrunculin

not only stops new assembly but also results in disassembly of the existing actin network. This makes it difficult to discern whether ongoing actin assembly or recycling proteins associated with the actin network is more relevant for recycling nucleation-promoting factors. There is evidence that both of these mechanisms participate in recycling endocytic components in yeast. For instance, the actin network is known to serve as a scaffold for proteins such as PI(4,5)P2 phosphatases that catabolize signals required for endocytosis (Sun et al., 2007). In contrast, recycling has also been shown to involve the force of actin polymerization to physically dissociate components from the membrane (Kaksonen et al., 2003). To discriminate which of these mechanisms is responsible for SCAR/WAVE complex recycling, we used a combination of actin drugs to stop new actin assembly while also stabilizing the existing actin cytoskeleton. This pharmacological cocktail increases cortical WAVE2 complex lifetime (**Fig. 4B,C**), which suggests that ongoing assembly, and not an actin network-associated effector protein involved in SCAR/WAVE turnover, is more relevant for SCAR/WAVE recycling. However, inhibiting actin dynamics had little effect on the global pool of WAVE2 (assayed by FRAP, **Fig. 4F**). This suggests that SCAR/WAVE molecules exist in two distinct states. In the first state, SCAR/WAVE molecules freely associate and dissociate with the plasma membrane independent of actin polymerization. This likely represents a low affinity interaction of the SCAR/WAVE complex with factors like Rac and phosphoinositides. In the second state, which represents small fraction of the total pool (**Fig 1F**), molecules undergo actin-dependent retrograde flow, and require actin polymerization for recycling. This likely represents SCAR/WAVE molecules that are associated with the actin cytoskeleton. We favor a model where the SCAR/WAVE complex performs multiple diffusive membrane searches until it integrates into the actin meshwork through Arp2/3 activation, and subsequently recycles through actin-based retrograde flow.

MATERIAL AND METHODS

Plasmids and Reagents

Plasmids containing human β-actin or the *Xenopus* p40 subunit of the Arp2/3 complex subcloned into the pEGFP-C1 (CLONTECH Laboratories, Inc.)-derived vector containing a defective cytomegalovirus (delCMV) have been previously published (Watanabe and Mitchison, 2002; Miyoshi et al., 2006). EST clone of *Xenopus* WAVE2 was obtained from the IMAGE consortium and subcloned into this delCMV vector. Human Rac2-GFP (Michaelson et al., 2001) and RacN17 (Srinivasan et al., 2003) have been described previously. Y27632 (Calbiochem) was incubated with cells at final concentration of 10 μM for at least 30 minutes before imaging. Jasplakinolide (Calbiochem) and latrunculin (Calbiochem) were prepared at 2X final concentration (40 μM) and acutely added during imaging. XTC cells were cultured and transfected as described previously (Watanabe and Mitchison, 2002).

Single-molecule microscopy

Single-molecule imaging was performed as previously described (Watanabe and Mitchison, 2002). Images were acquired in Japan and in the United States on a variety of different microscopes (BX52 or IX71; Olympus; or TI-2000, Nikon) with different EM-CCD cameras (MMX 1300-YHS, CoolSNAP HQ, Cascade II:512, or Andor), acquisition software (Metamorph or NIS-Elements), lamps (100W mercury, or 75W Xenon), lasers (20 mW, BCD1 Melles Griot or 100 mW, LMM5 Spectral Research) and objectives (planApo 100x objective; NA 1.40 oil, Olympus or NA 1.49 oil, Nikon). Data from all microscope set-ups were comparable and indicate the robustness of the observed phenomena. XTC cells were plated on polylysine-coated coverglass for 20 minutes in 70% Leibovitz's L-15 medium (Invitrogen) without serum. Time-lapse imaging was performed at 21-23°C up to 3 hours after cells were seeded. Epifluorescence microscopy

imaging of retrograde flow was performed with a 2X lens inserted for cells expressing a low concentration of EGFP-tagged proteins. Neutral density filters were used to reduce illumination intensity so that fluorescence decay caused by photobleaching was minimized. The field diaphragm was closed to restrict illumination to the cell edge and diminish out-of-focus light from the cell body. Diffusing molecules were observed by illuminating for 40 - 100 ms in Total Internal Reflection Fluorescence (TIRF) microscopy for ~100 frames.

Image Analysis

Retrograde motion of WAVE2 molecules were analyzed using the two-dimensional Gaussian fit method over a 5x5 pixel region of interest with GTrack software (G-Angstrom, Sendai, Japan). Retrograde motion of p40 and actin molecules were analyzed using GMimPro software (Mashanov and Molloy, 2007). Lifetime measurements were normalized for photobleaching as described (Watanabe and Mitchison, 2002). Mean lifetime (τ) was determined by taking 1-cumulative frequency (CF) and fitting to the curve $Cexp(-\lambda t)$, where λ is the first-order dissociation rate and C is a constant with Prism 5.0 software (Graphpad, San Diego, CA). For recent examples see (Hansen and Mullins, 2010; Bieling et al., 2007). Particle diffusion was measured in Matlab (Mathworks, Natick, MA) with Utrack (Jaqaman et al., 2008). Error bars for mean diffusion coefficients and mean lifetimes are 95% confidence intervals. Diffusion constants did not vary significantly between the cell periphery and the cell interior (see supplemental material **Fig. S3D,E**). Maximum intensity projections and kymographs were created using ImageJ. We used the image calculator from ImageJ to capture molecules transitioning from diffusion to retrograde flow. We created a maximum intensity projection of the last five frames in the fast imaging mode before switching to the slower imaging mode. This maximum intensity projection highlights stabilized particles that

might subsequently undergo retrograde flow and eliminates diffusing particles. Then we created a maximum intensity projection from five frames earlier in the imaging acquisition. We subtracted these two maximum intensity projections. Most stabilized molecules appear in both maximum intensity projections and thus are eliminated in the subtracted image. However, a few spots remain, which suggests that they were stabilized particles in the maximum intensity projection just prior to switching imaging modes, but not a stabilized particle earlier in the imaging acquisition. These molecules were subsequently analyzed for diffusion and retrograde flow with Utrack in Matlab.

Reducing photodamage on actin retrograde speed

Single-molecule imaging can only be performed at low concentrations of fluorescent protein where the individual fluorophores are well separated. We compared two different strategies for achieving low fluorescent protein concentration. One approach uses high-intensity light to bleach cells expressing moderate/high amounts of fluorescent proteins down to concentrations that are compatible with single-molecule imaging (de Keijzer et al., 2008; van Hemert et al., 2010). When we analyzed XTC cells expressing low levels of the p40 subunit of the Arp2/3 complex under both high- and low-intensity light (see supplemental material **Fig. S4**, 0.11 and 1.8 mW, respectively) we found that, as expected, the higher-intensity light exponentially increased photobleaching (see supplemental material **Fig. S4C**). However, the brighter light also dramatically reduced mean retrograde speed of p40 (see supplemental material **Fig. S4B,D**), suggesting that bleaching cells down to single-molecule levels is unsuitable for analyzing actin dynamics. Instead, we used a crippled CMV promoter to transcriptionally limit expression of fluorescent proteins, thereby achieving low concentrations of fluorescent proteins without the need for photobleaching (Watanabe and Mitchison, 2002). This avoids potential artifacts from overexpression (Riedl et al., 2008) and eliminates the

photodamaging effects of photobleaching on actin dynamics.

ACKNOWLEDGMENTS

We thank members of the Weiner and Watanabe labs for helpful discussions, constructive criticisms, and technical support. Rac2 and RacN17 plasmids were kind gifts from Henry Bourne. A.M. was supported by the JSPS and National Science Foundation EAPSI Fellowship, N.W. was supported by the Funding Program for Next Generation of World-Leading Researchers, and O.D.W. was supported by a National Institutes of Health R01 (GM084040).

REFERENCES

Bear, J.E., J.F. Rawls, and C.L. Saxe. 1998. SCAR, a WASP-related protein, isolated as a suppressor of receptor defects in late Dictyostelium development. *J. Cell Biol.* 142:1325-1335.

Bieling, P., L. Laan, H. Schek, E.L. Munteanu, L. Sandblad, M. Dogterom, D. Brunner, and T. Surrey. 2007. Reconstitution of a microtubule plus-end tracking system in vitro. *Nature*. 450:1100-1105.

Chen, Z., D. Borek, S.B. Padrick, T.S. Gomez, Z. Metlagel, A.M. Ismail, J. Umetani, D.D. Billadeau, Z. Otwinowski, and M.K. Rosen. 2010. Structure and control of the actin regulatory WAVE complex. *Nature*. 468:533-538.

Cramer, L.P., and T.J. Mitchison. 1997. Investigation of the mechanism of retraction of the cell margin and rearward flow of nodules during mitotic cell rounding. *Mol. Biol. Cell*. 8:109-119.

Douglass, A.D., and R.D. Vale. 2005. Single-molecule microscopy reveals plasma membrane microdomains created by protein-protein networks that exclude or trap signaling molecules in T cells. *Cell*. 121:937-950.

Elf, J., G.-W. Li, and X.S. Xie. 2007. Probing transcription factor dynamics at the single-molecule level in a living cell. *Science*. 316:1191-1194.

Hahne, P., A. Sechi, S. Benesch, and J.V. Small. 2001. Scar/WAVE is localised at the tips of protruding lamellipodia in living cells. *FEBS Lett*. 492:215-220.

Hansen, S.D., and R.D. Mullins. 2010. VASP is a processive actin polymerase that requires monomeric actin for barbed end association. *The Journal of Cell Biology*. 191:571 -584.

van Hemert, F., M.D. Lazova, B.E. Snaar-Jagaska, and T. Schmidt. 2010. Mobility of

G proteins is heterogeneous and polarized during chemotaxis. *J. Cell. Sci.* 123:2922-2930.

von Hippel, P.H., and O.G. Berg. 1989. Facilitated target location in biological systems. *Journal of Biological Chemistry*. 264:675 -678.

Ibarra, N., S.L. Blagg, F. Vazquez, and R.H. Insall. 2006. Nap1 regulates Dictyostelium cell motility and adhesion through SCAR-dependent and -independent pathways. *Curr. Biol*. 16:717-722.

Iwasa, J.H., and R.D. Mullins. 2007. Spatial and temporal relationships between actin-filament nucleation, capping, and disassembly. *Curr. Biol*. 17:395-406.

Jaqaman, K., D. Loerke, M. Mettlen, H. Kuwata, S. Grinstein, S.L. Schmid, and G. Danuser. 2008. Robust single-particle tracking in live-cell time-lapse sequences. *Nat. Methods*. 5:695-702.

Kaksonen, M., Y. Sun, and D.G. Drubin. 2003. A pathway for association of receptors, adaptors, and actin during endocytic internalization. *Cell*. 115:475-487.

de Keijzer, S., A. Serge, F. van Hemert, P.H.M. Lommerse, G.E.M. Lamers, H.P. Spaink, T. Schmidt, and B.E. Snaar-Jagalska. 2008. A spatially restricted increase in receptor mobility is involved in directional sensing during Dictyostelium discoideum chemotaxis. *J Cell Sci*. 121:1750-1757.

King, J.S., D.M. Veltman, M. Georgiou, B. Baum, and R.H. Insall. 2010. SCAR/WAVE is activated at mitosis and drives myosin-independent cytokinesis. *J. Cell. Sci*. 123:2246-2255.

Lai, F.P., M. Szczodrak, J. Block, J. Faix, D. Breitsprecher, H.G. Mannherz, T.E. Stradal, G.A. Dunn, J.V. Small, and K. Rottner. 2008. Arp2/3 complex interactions and actin network turnover in lamellipodia. *EMBO J*. 27:982-992.

Lebensohn, A.M., and M.W. Kirschner. 2009. Activation of the WAVE complex by coincident signals controls actin assembly. *Mol. Cell*. 36:512-524.

Lin, C.H., and P. Forscher. 1995. Growth cone advance is inversely proportional to retrograde F-actin flow. *Neuron*. 14:763-771.

Lommerse, P.H.M., G.A. Blab, L. Cognet, G.S. Harms, B.E. Snaar-Jagalska, H.P. Spaink, and T. Schmidt. 2004. Single-molecule imaging of the H-ras membrane-anchor reveals domains in the cytoplasmic leaflet of the cell membrane. *Biophys. J*. 86:609-616.

Machesky, L.M., R.D. Mullins, H.N. Higgs, D.A. Kaiser, L. Blanchoin, R.C. May, M.E. Hall, and T.D. Pollard. 1999. Scar, a WASp-related protein, activates nucleation of actin filaments by the Arp2/3 complex. *Proc. Natl. Acad. Sci. U.S.A*. 96:3739-3744.

Machesky, L.M., and R.H. Insall. 1998. Scar1 and the related Wiskott-Aldrich syndrome protein, WASP, regulate the actin cytoskeleton through the Arp2/3 complex. *Curr. Biol*. 8:1347-1356.

Mashanov, G.I., and J.E. Molloy. 2007. Automatic detection of single fluorophores in live cells. *Biophys. J*. 92:2199-2211.

Matsuoka, S., M. Iijima, T.M. Watanabe, H. Kuwayama, T. Yanagida, P.N. Devreotes, and M. Ueda. 2006. Single-molecule analysis of chemoattractant-stimulated membrane recruitment of a PH-domain-containing protein. *J Cell Sci*. 119:1071-1079.

Michaelson, D., J. Silletti, G. Murphy, P. D'Eustachio, M. Rush, and M.R. Philips. 2001. Differential Localization of Rho Gtpases in Live Cells. *The Journal of Cell Biology*. 152:111 -126.

Miki, H., S. Suetsugu, and T. Takenawa. 1998. WAVE, a novel WASP-family protein involved in actin reorganization induced by Rac. *EMBO J*. 17:6932-6941.

Millius, A., S.N. Dandekar, A.R. Houk, and O.D. Weiner. 2009. Neutrophils establish

rapid and robust WAVE complex polarity in an actin-dependent fashion. *Curr Biol*. 19:253-9.

Miyoshi, T., T. Tsuji, C. Higashida, M. Hertzog, A. Fujita, S. Narumiya, G. Scita, and N. Watanabe. 2006. Actin turnover–dependent fast dissociation of capping protein in the dendritic nucleation actin network: evidence of frequent filament severing. *The Journal of Cell Biology*. 175:947 -955.

Mullins, R.D., J.A. Heuser, and T.D. Pollard. 1998. The interaction of Arp2/3 complex with actin: nucleation, high affinity pointed end capping, and formation of branching networks of filaments. *Proc. Natl. Acad. Sci. U.S.A.* 95:6181-6186.

Murakoshi, H., R. Iino, T. Kobayashi, T. Fujiwara, C. Ohshima, A. Yoshimura, and A. Kusumi. 2004. Single-molecule imaging analysis of Ras activation in living cells. *Proc. Natl. Acad. Sci. U.S.A.* 101:7317-7322.

Oikawa, T., H. Yamaguchi, T. Itoh, M. Kato, T. Ijuin, D. Yamazaki, S. Suetsugu, and T. Takenawa. 2004. PtdIns(3,4,5)P3 binding is necessary for WAVE2-induced formation of lamellipodia. *Nat. Cell Biol*. 6:420-426.

Padrick, S.B., and M.K. Rosen. 2010. Physical mechanisms of signal integration by WASP family proteins. *Annu. Rev. Biochem*. 79:707-735.

Patel, F.B., Y.Y. Bernadskaya, E. Chen, A. Jobanputra, Z. Pooladi, K.L. Freeman, C. Gally, W.A. Mohler, and M.C. Soto. 2008. The WAVE/SCAR complex promotes polarized cell movements and actin enrichment in epithelia during C. elegans embryogenesis. *Dev. Biol*. 324:297-309.

Ponti, A., M. Machacek, S.L. Gupton, C.M. Waterman-Storer, and G. Danuser. 2004. Two distinct actin networks drive the protrusion of migrating cells. *Science*. 305:1782-1786.

Ponti, A., A. Matov, M. Adams, S. Gupton, C.M. Waterman-Storer, and G. Danuser. 2005. Periodic patterns of actin turnover in lamellipodia and lamellae of migrating epithelial cells analyzed by quantitative Fluorescent Speckle Microscopy. *Biophys. J.* 89:3456-3469.

Riedl, J., A.H. Crevenna, K. Kessenbrock, J.H. Yu, D. Neukirchen, M. Bista, F. Bradke, D. Jenne, T.A. Holak, Z. Werb, M. Sixt, and R. Wedlich-Soldner. 2008. Lifeact: a versatile marker to visualize F-actin. *Nat. Methods*. 5:605-607.

Riggs, A.D., S. Bourgeois, and M. Cohn. 1970. The lac repressor-operator interaction. 3. Kinetic studies. *J. Mol. Biol*. 53:401-417.

Rogers, S.L., U. Wiedemann, N. Stuurman, and R.D. Vale. 2003. Molecular requirements for actin-based lamella formation in Drosophila S2 cells. *J. Cell Biol*. 162:1079-1088.

Rohatgi, R., L. Ma, H. Miki, M. Lopez, T. Kirchhausen, T. Takenawa, and M.W. Kirschner. 1999. The interaction between N-WASP and the Arp2/3 complex links Cdc42-dependent signals to actin assembly. *Cell*. 97:221-231.

Srinivasan, S., F. Wang, S. Glavas, A. Ott, F. Hofmann, K. Aktories, D. Kalman, and H.R. Bourne. 2003. Rac and Cdc42 play distinct roles in regulating PI(3,4,5)P3 and polarity during neutrophil chemotaxis. *The Journal of Cell Biology*. 160:375 -385.

Steffen, A., K. Rottner, J. Ehinger, M. Innocenti, G. Scita, J. Wehland, and T.E.B. Stradal. 2004. Sra-1 and Nap1 link Rac to actin assembly driving lamellipodia formation. *EMBO J*. 23:749-759.

Stradal, T., K.D. Courtney, K. Rottner, P. Hahne, J.V. Small, and A.M. Pendergast. 2001. The Abl interactor proteins localize to sites of actin polymerization at the tips of lamellipodia and filopodia. *Curr. Biol*. 11:891-895.

Stradal, T.E.B., K. Rottner, A. Disanza, S. Confalonieri, M. Innocenti, and G. Scita. 2004. Regulation of actin dynamics by WASP and WAVE family proteins. *Trends Cell Biol*. 14:303-311.

Sun, Y., S. Carroll, M. Kaksonen, J.Y. Toshima, and D.G. Drubin. 2007. PtdIns(4,5)P2 turnover is required for multiple stages during clathrin- and actin-dependent endocytic internalization. *J. Cell Biol*. 177:355-367.

Theriot, J.A., and T.J. Mitchison. 1991. Actin microfilament dynamics in locomoting cells. *Nature*. 352:126-131.

Theriot, J.A., and T.J. Mitchison. 1992. Comparison of actin and cell surface dynamics in motile fibroblasts. *J. Cell Biol*. 119:367-377.

Wang, Y.L. 1985. Exchange of actin subunits at the leading edge of living fibroblasts: possible role of treadmilling. *J. Cell Biol*. 101:597-602.

Wang, Y.M., R.H. Austin, and E.C. Cox. 2006. Single molecule measurements of repressor protein 1D diffusion on DNA. *Phys. Rev. Lett*. 97:048302.

Watanabe, N., and T.J. Mitchison. 2002. Single-molecule speckle analysis of actin filament turnover in lamellipodia. *Science*. 295:1083-6.

Weiner, O.D., W.A. Marganski, L.F. Wu, S.J. Altschuler, and M.W. Kirschner. 2007. An actin-based wave generator organizes cell motility. *PLoS Biol*. 5:e221.

Weiner, O.D., M.C. Rentel, A. Ott, G.E. Brown, M. Jedrychowski, M.B. Yaffe, S.P. Gygi, L.C. Cantley, H.R. Bourne, and M.W. Kirschner. 2006. Hem-1 complexes are essential for Rac activation, actin polymerization, and myosin regulation during neutrophil chemotaxis. *PLoS Biol*. 4:e38.

Weisswange, I., T.P. Newsome, S. Schleich, and M. Way. 2009. The rate of N-WASP exchange limits the extent of ARP2/3-complex-dependent actin-based motility. *Nature*.

458:87-91.

Xiong, Y., C.-H. Huang, P.A. Iglesias, and P.N. Devreotes. 2010. Cells navigate with a local-excitation, global-inhibition-biased excitable network. *Proc. Natl. Acad. Sci. U.S.A.* 107:17079-17086.

Yan, C., N. Martinez-Quiles, S. Eden, T. Shibata, F. Takeshima, R. Shinkura, Y. Fujiwara, R. Bronson, S.B. Snapper, M.W. Kirschner, R. Geha, F.S. Rosen, and F.W. Alt. 2003. WAVE2 deficiency reveals distinct roles in embryogenesis and Rac-mediated actin-based motility. *EMBO J.* 22:3602-3612.

Zallen, J.A., Y. Cohen, A.M. Hudson, L. Cooley, E. Wieschaus, and E.D. Schejter. 2002. SCAR is a primary regulator of Arp2/3-dependent morphological events in Drosophila. *J. Cell Biol.* 156:689-70

Figure 1

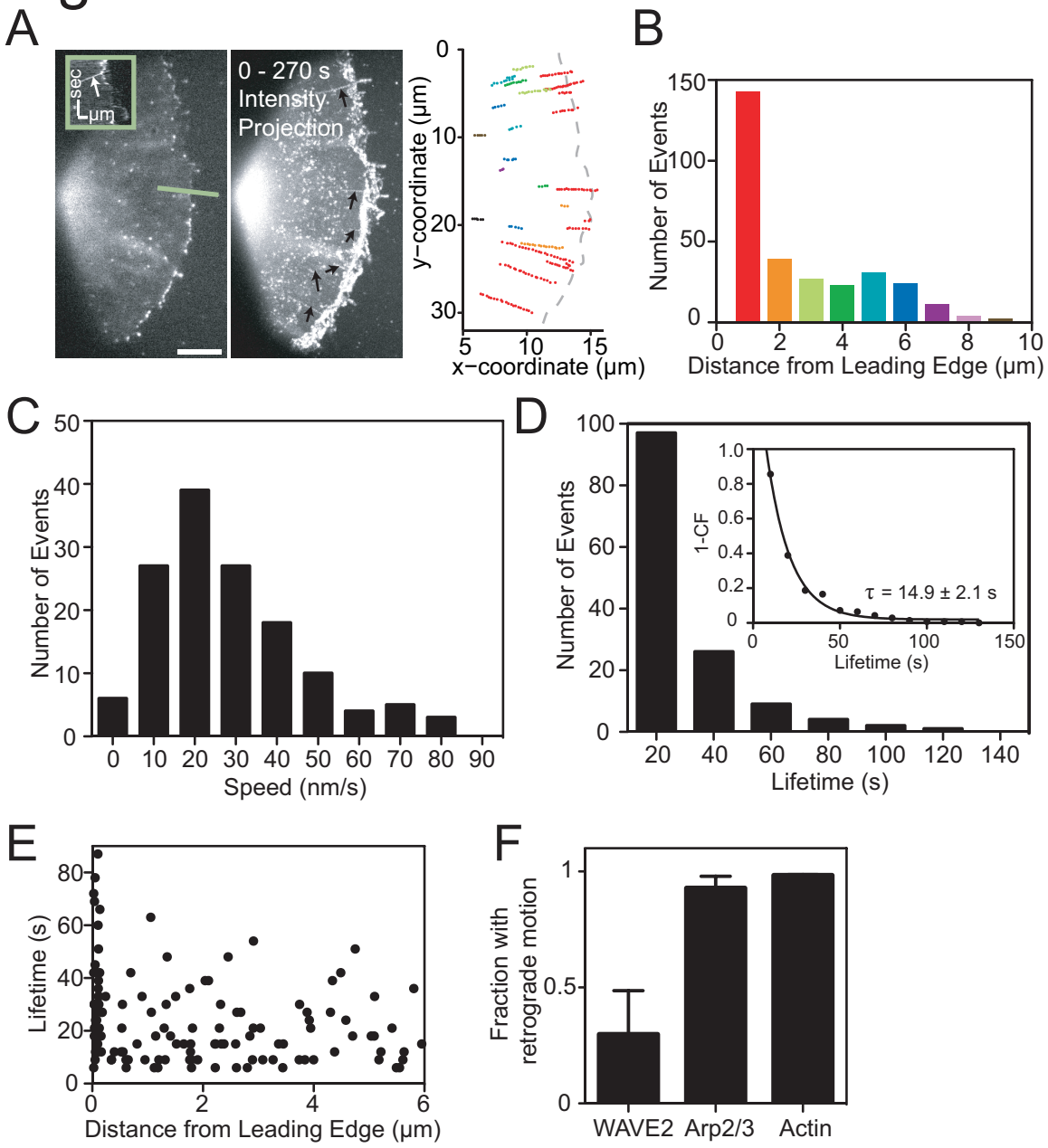
A
5 sec
5 µm
0 - 270 s
Intensity
Projection
y−coordinate (µm)
x−coordinate (µm)
B
Number of Events
Distance from Leading Edge (µm)
C
Number of Events
Speed (nm/s)
D
Number of Events
1-CF
τ = 14.9 ± 2.1 s
Lifetime (s)
Lifetime (s)
E
Lifetime (s)
Distance from Leading Edge (µm)
F
Fraction with retrograde motion
WAVE2
Arp2/3
Actin

Fig. 1. Single-molecule epifluorescence imaging demonstrates retrograde flow of WAVE2 in XTC cells. **(A)** Fluorescence image (*left*) of an XTC cell expressing a low concentration of WAVE2-EGFP. Some molecules undergo smooth and continuous retrograde flow (*inset kymograph, bars: horizontal, 1 μm; vertical, 1 min; time flows top to bottom*). Middle panel shows maximum intensity projection (90 frames, 4.5 min) of this cell. Arrows indicate retrograde flow events. Corresponds to **Movie 1**. Trajectories of retrograde flowing molecules (*right*). Color corresponds to histogram in (B) and indicates the distance to the leading edge when the molecule first appears. Bar, 5 μm. **(B)** Initial positions of appearance for retrograde moving WAVE2 molecules as a function of distance from the leading edge (n=304, nine cells). **(C)** Distribution of WAVE2 retrograde velocities with a mean speed of 31±18 nm/s (n=345, nine cells). **(D)** Lifetime distribution of WAVE2 molecules (n=345, nine cells) that appear over the course of a 90 s time window. Single exponential fit of 1-cumulative frequency (CF) of WAVE2 lifetimes gives a mean lifetime (τ) of 14.9±2.1 s (*inset*). **(E)** Lifetime versus position plot for WAVE2 molecules. Dots represent the lifetime and emerging position of individual WAVE2 molecules (n=143, six cells). **(F)** Fraction of fluorescent WAVE2 (19%, n=1810, nine cells), p40 (93%, n=3068, three cells), and actin (98%, n=4503, three cells) molecules undergoing retrograde flow. Error bars are s.d.

Figure 2

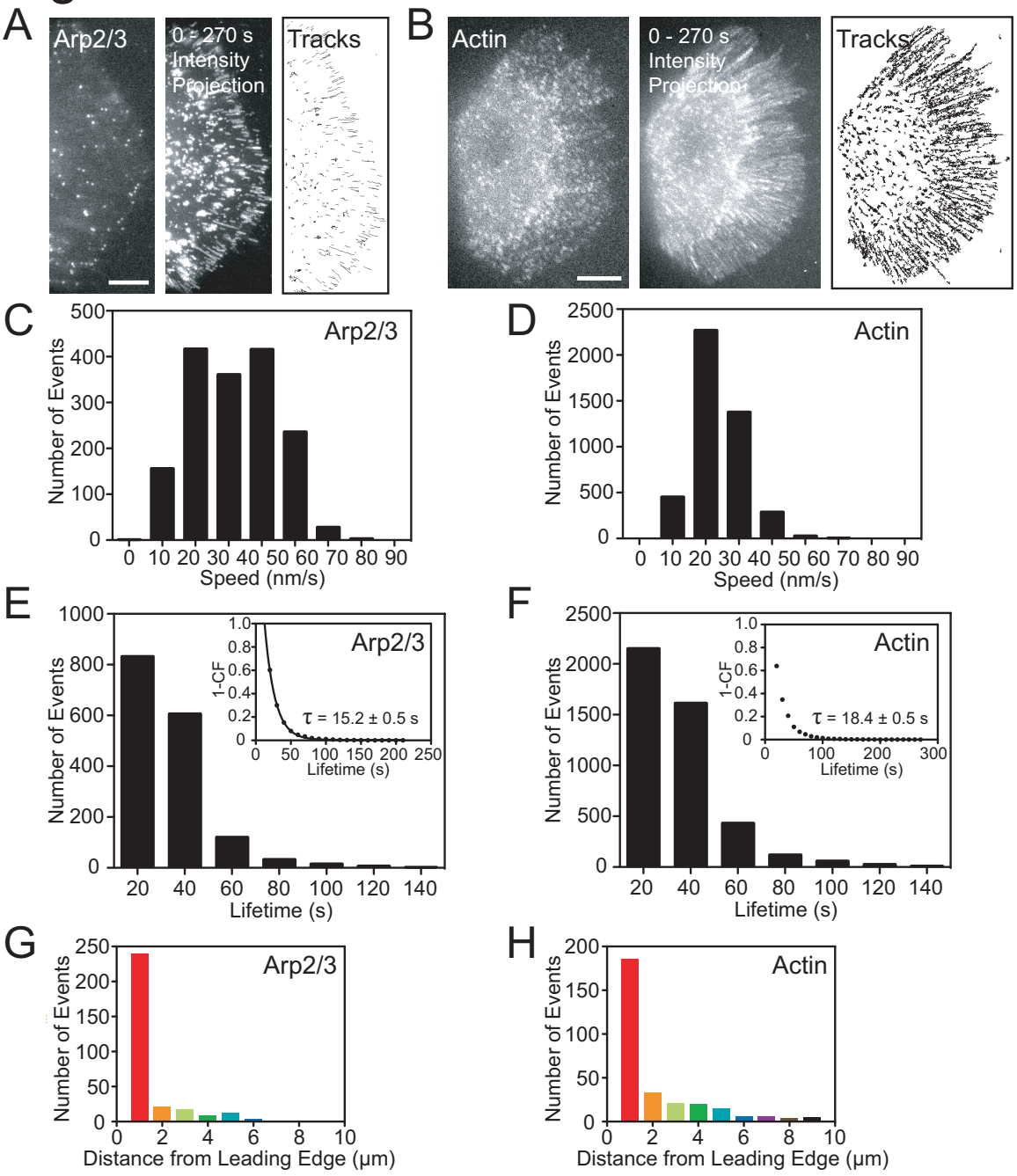
A
Arp2/3
0 - 270 s Intensity Projection
Tracks
B
Actin
0 - 270 s Intensity Projection
Tracks
C
Arp2/3
Number of Events
Speed (nm/s)
D
Actin
Number of Events
Speed (nm/s)
E
Arp2/3
Number of Events
Lifetime (s)
1-CF
τ = 15.2 ± 0.5 s
F
Actin
Number of Events
Lifetime (s)
1-CF
τ = 18.4 ± 0.5 s
G
Arp2/3
Number of Events
Distance from Leading Edge (μm)
H
Actin
Number of Events
Distance from Leading Edge (μm)

Fig. 2. Actin and p40 retrograde flow are similar to WAVE2 retrograde flow. **(A)** Left panel shows epifluorescence image of an XTC cell expressing a low concentration of EGFP-tagged p40 subunit of the Arp2/3 complex (corresponds to **Movie 2**). Bar, 5 μm. Middle panel shows maximum intensity projection (90 frames, 4.5 min) of this cell, and right panel shows the trajectories of retrograde flowing molecules. **(B)** Left panel shows fluorescence image of an XTC cell expressing a low concentration of actin-EGFP (corresponds to **Movie 3**). Bar, 5 μm. Middle panel shows maximum intensity projection (90 frames, 4.5 min) of this cell, and right panel shows trajectories of retrograde flowing molecules. **(C)** Distribution of p40 retrograde velocities with a mean speed of 30±13 nm/s (n=1696, three cells). **(D)** Distribution of actin retrograde velocities with a mean speed of 24±8 nm/s (n=4503, three cells). **(E)** Lifetime distribution of p40 molecules (n=1696, three cells) that appear over the course of a 90 s time window. Four speckles had lifetimes longer than 140 s; the longest speckle lifetime was 200s. Single exponential fit of 1-CF of p40 lifetimes (τ=15.2±0.5 s, *inset*). **(F)** Lifetime distribution of actin molecules (n=4503, three cells) that appear over the course of a 90 s time window. Fourteen speckles had lifetimes longer than 140 s; the longest speckle lifetime was 280s. Single exponential fit of 1-CF of actin lifetimes (τ=18.4±0.5 s, *inset*). **(G** and **H)** Initial positions of appearance for retrograde moving p40 (G, n=304, three cells) and actin (H, n=304, three cells) molecules as a function of distance from the leading edge.

Figure 3

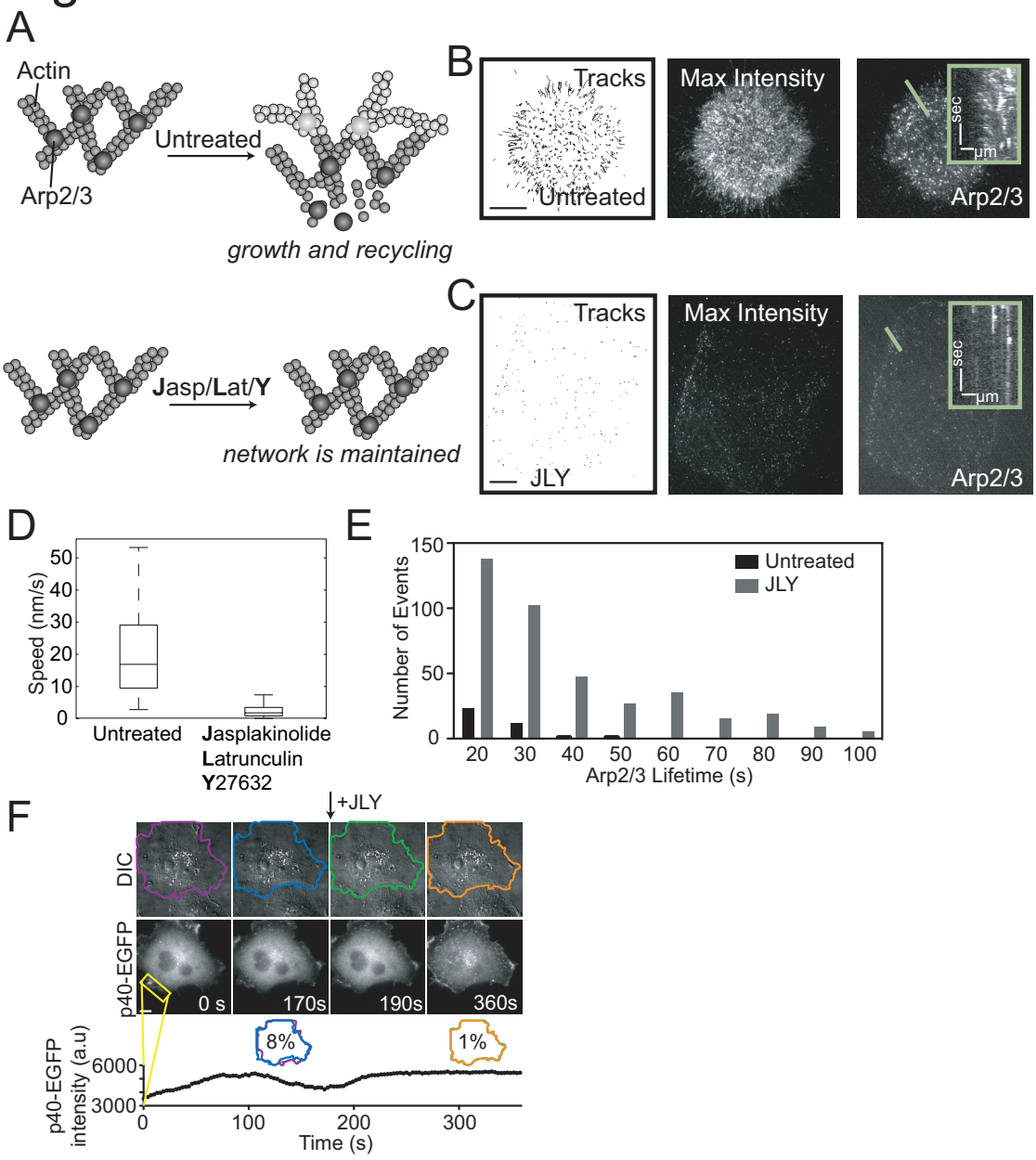
A
Actin
Arp2/3
Untreated
growth and recycling
B
Tracks
Untreated
Max Intensity
sec
µm
Arp2/3
C
Jasp/Lat/Y
network is maintained
Tracks
JLY
Max Intensity
sec
µm
Arp2/3
D
Speed (nm/s)
50
40
30
20
10
0
Untreated
Jasplakinolide
Latrunculin
Y27632
E
Number of Events
150
100
50
0
Untreated
JLY
20
30
40
50
60
70
80
90
100
Arp2/3 Lifetime (s)
F
+JLY
DIC
p40-EGFP
0 s
170s
190s
360s
8%
1%
p40-EGFP intensity (a.u)
6000
3000
0
100
200
300
Time (s)

Fig. 3. p40 recycling depends on actin dynamics. **(A)** XTC cells were treated with a drug cocktail that inhibits both actin polymerization and network turnover: cells were pretreated for 30 min with 10 μM Y27632 (Y) and then acutely treated with 20 μM jasplakinolide (J) and 20 μM latrunculinB (L). Small circles represent actin and large circles represent the Arp2/3 complex. Dark grey shows the existing network, and new network growth is shown in light grey. **(B)** Left panel shows trajectories of retrograde flowing molecules from an XTC cell expressing a low concentration of p40-EGFP. Middle panel shows maximum intensity projection (90 frames, 4.5 min) of this cell, and right panel shows a single TIRF image of the cell. Diagonal streaks in the inset kymograph show most molecules undergo smooth and continuous retrograde flow (*inset bars: horizontal, 2 μm; vertical, 1 min; time flows top to bottom*). Bar, 10 μm. **(C)** Left panel shows trajectories of retrograde flowing molecules from a p40-EGFP expressing cell treated with JLY cocktail described in (A). Middle panel shows maximum intensity projection (90 frames, 4.5 min) of this cell, and right panel shows a single TIRF image of the cell. Vertical streaks in inset kymograph indicate that freezing actin dynamics causes p40 to cease retrograde flow (*inset bars: horizontal, 2 μm; vertical, 1 min; time flows top to bottom*). Bar, 10 μm. **(D)** p40 retrograde flow speed is reduced in JLY-treated cells (mean=3 nm/s) compared to untreated cells (mean=18 nm/s), indicating a drug-dependent block of retrograde flow. **(E)** p40 lifetime increases after drug addition, indicating stabilization of the existing actin network (before, n=37; after, n=397). **(F)** An XTC cell expressing p40-EGFP imaged in DIC (*top*) and GFP (*middle*) was treated at 180 s with JLY cocktail. A section of lamellipodium (yellow box) was measured for protrusion and retraction over time and the cell's boundary was measured at each frame for area of overlap with previous frames (*bottom*). Percentages inside colored cell traces indicate the difference in overlap between indicated frames. Corresponds to **Movie 4**. Bar, 5 μm.

Figure 4

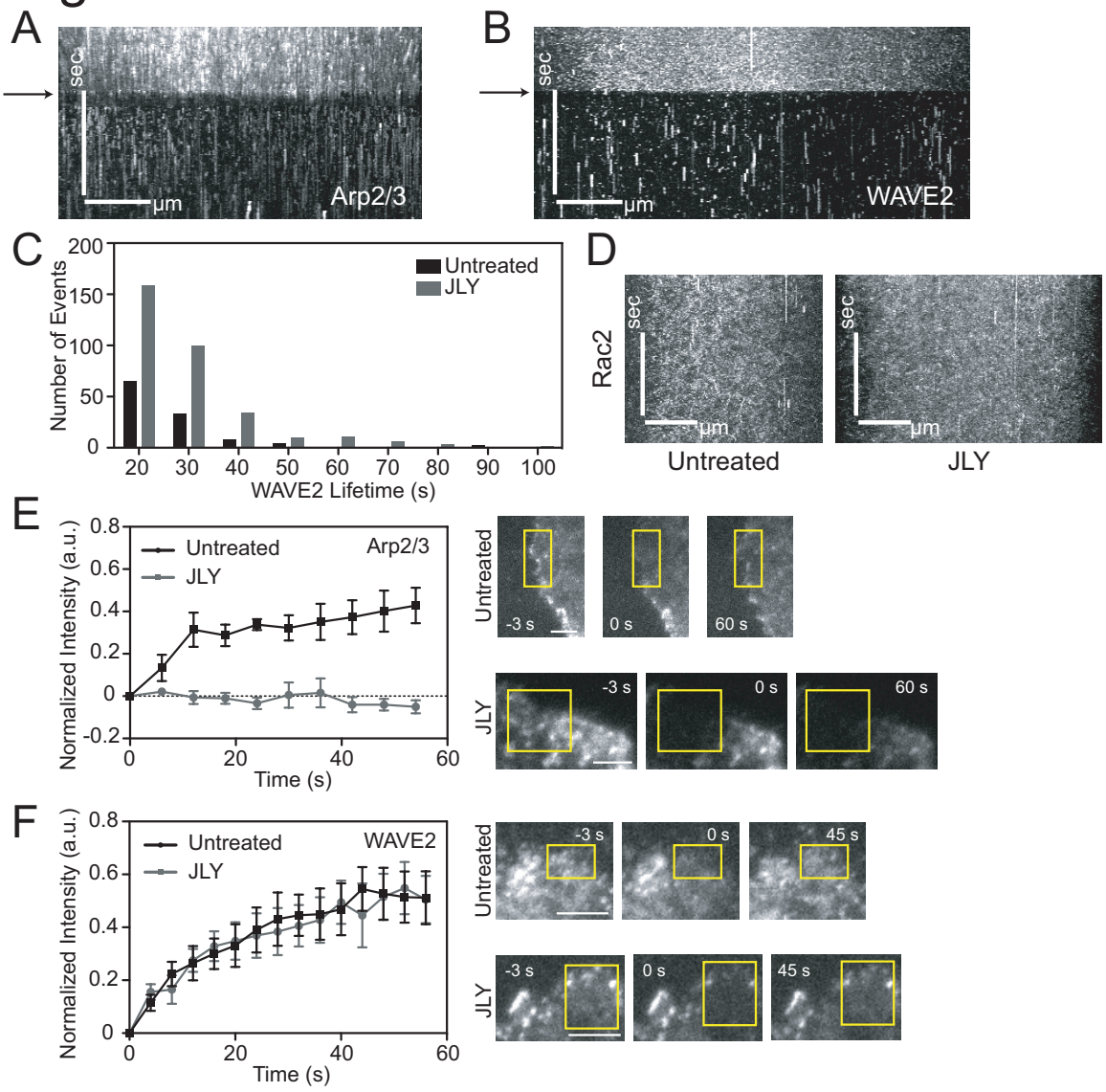
A
sec
μm
Arp2/3
B
sec
μm
WAVE2
C
Number of Events
200
150
100
50
0
20
30
40
50
60
70
80
90
100
WAVE2 Lifetime (s)
Untreated
JLY
D
Rac2
sec
μm
Untreated
sec
μm
JLY
E
Normalized Intensity (a.u.)
0.8
0.6
0.4
0.2
0
-0.2
0
20
40
60
Time (s)
Untreated
JLY
Arp2/3
Untreated
-3 s
0 s
60 s
JLY
-3 s
0 s
60 s
F
Normalized Intensity (a.u.)
0.8
0.6
0.4
0.2
0
0
20
40
60
Time (s)
Untreated
JLY
WAVE2
Untreated
-3 s
0 s
45 s
JLY
-3 s
0 s
45 s

Fig. 4. (A and **B)** Max intensity projection (180 frames, 9 min) of a kymograph across an XTC cell expressing p40-EGFP (A) or WAVE2-EGFP (B) before and after treatment with JLY drug cocktail. Arrow indicates drug addition. Bars: horizontal 1 μm, vertical 5 min. Time flows top to bottom. Drug treatment stabilizes both p40 and WAVE2 molecules on the membrane, as indicated by vertical streaks at time points below arrow in the kymograph. **(C)** Lifetime of stabilized WAVE2 molecules increases after drug treatment (before, n=113; after, n=324). **(D)** Max intensity kymograph projections of XTC cells expressing Rac2-EGFP in the absence or presence of the JLY drug cocktail. Compare to portion of kymograph in Fig. 4B above the black arrow. Bars: horizontal 1 μm, vertical 5 min. Time flows top to bottom. **(E** and **F)** We used FRAP to ascertain how bulk populations of Arp2/3 (E) and WAVE2 (F) behave after actin network stabilization with JLY. Cells were pretreated for 30 min with JLY (gray lines) or buffer (black lines). (**E**) p40-EGFP recovers ~40% of its pre-bleached fluorescence (n=7), whereas cells treated with JLY do not show any recovery (n=6). (**F**) WAVE2-EGFP recovers similarly in both drug-treated (n=7) and untreated (n=8) cells. Representative images shown (*right*). Yellow rectangles indicate photobleached region. Bars, 2.5 μm.

Figure 5

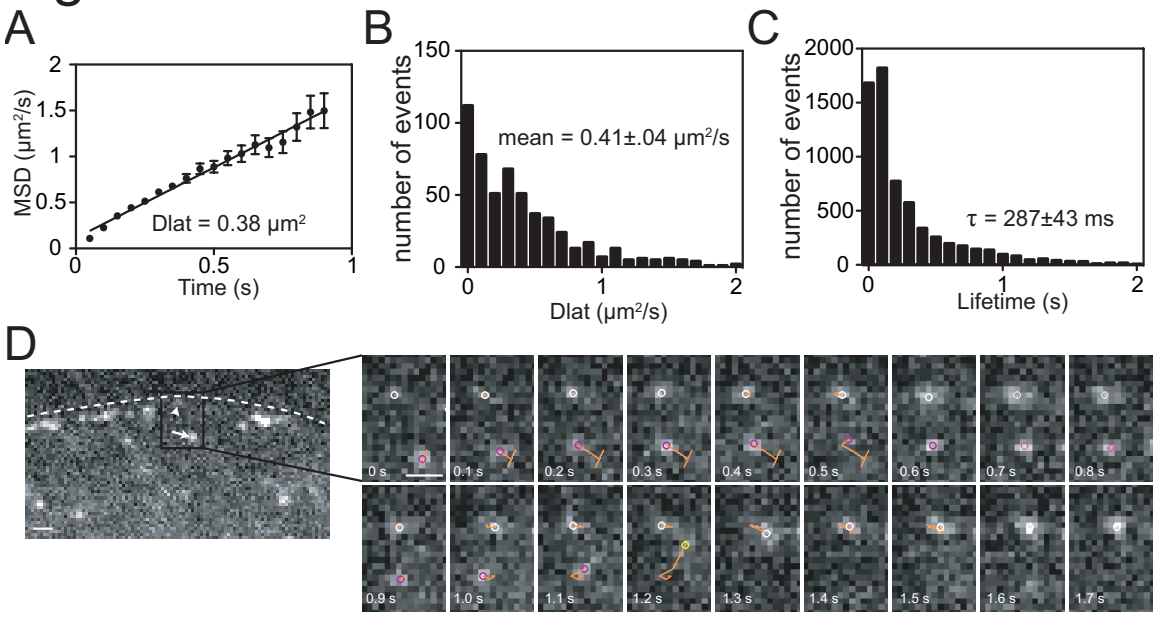
A
MSD (μm²/s)
Dlat = 0.38 μm²
Time (s)
B
number of events
mean = 0.41±.04 μm²/s
Dlat (μm²/s)
C
number of events
τ = 287±43 ms
Lifetime (s)
D
0 s
0.1 s
0.2 s
0.3 s
0.4 s
0.5 s
0.6 s
0.7 s
0.8 s
0.9 s
1.0 s
1.1 s
1.2 s
1.3 s
1.4 s
1.5 s
1.6 s
1.7 s

Fig. 5. WAVE2-EGFP molecules diffuse at rates consistent with membrane diffusion. **(A)** An example of a MSD versus time lag plot for all diffusing particles in a cell expressing WAVE2-EGFP gives a mean lateral diffusion coefficient of 0.38 $\mu m^2/s$ (corresponds to **Movie 5**). Error bars are s.e.m. **(B)** Histogram of WAVE2 lateral diffusion coefficients for particles that diffuse at least 20 frames (n=543, five cells) with mean diffusion coefficient of 0.41±0.04 $\mu m^2/s$. **(C)** Lifetime distribution of diffusing WAVE2 molecules (n=6647, five cells). Single exponential fit of 1-CF (not shown) gives a mean lifetime of 287±43 ms. **(D)** Representative time-lapse image sequence of a WAVE2-EGFP molecule (arrow) diffusing and then stabilizing at the leading edge (arrowhead indicates stabilization point; corresponds to **Movie 7**). Dashed line indicates cell edge.

Figure 6

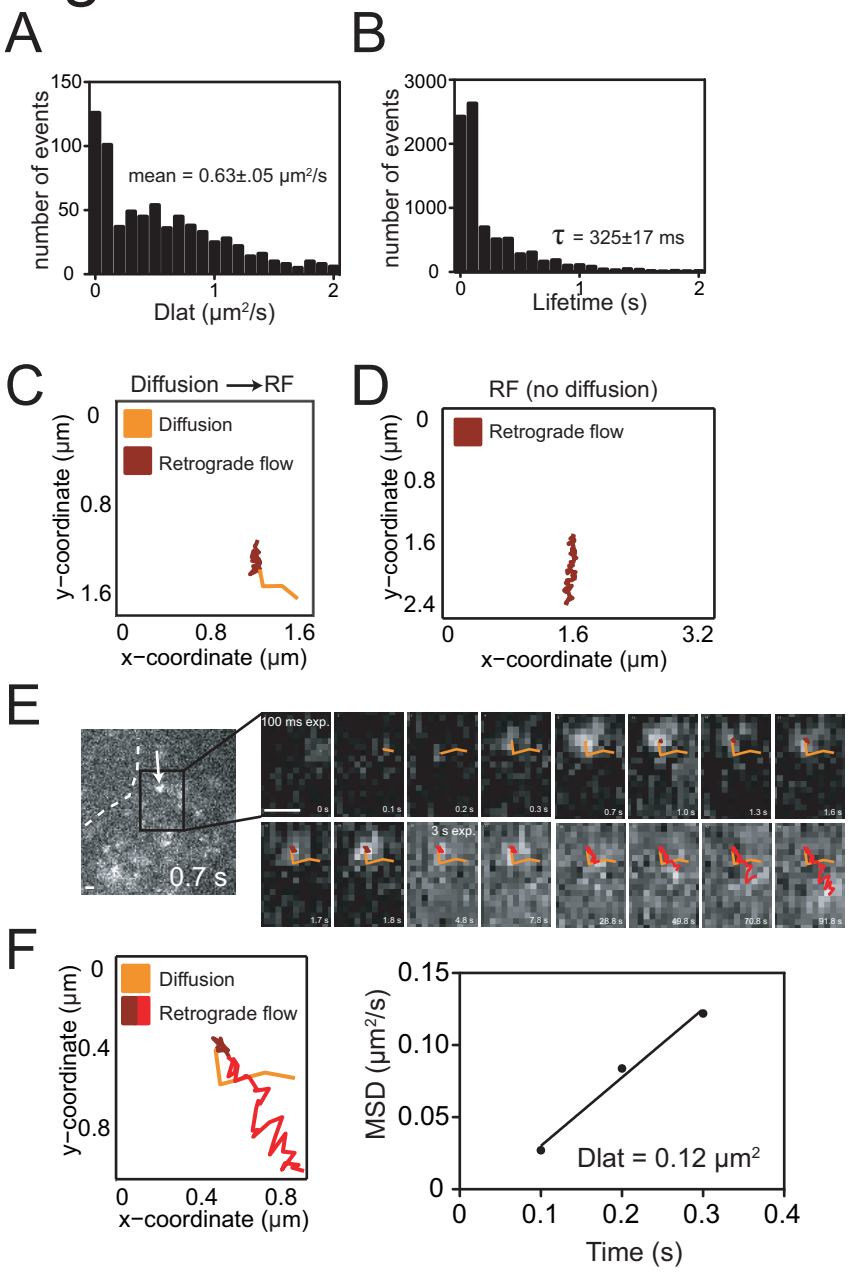
A
number of events
150
100
50
0
mean = 0.63±.05 μm²/s
0
1
2
Dlat (μm²/s)
B
number of events
3000
2000
1000
0
τ = 325±17 ms
0
1
2
Lifetime (s)
C
Diffusion ⟶RF
Diffusion
Retrograde flow
y−coordinate (μm)
0
0.8
1.6
0
0.8
1.6
x−coordinate (μm)
D
RF (no diffusion)
Retrograde flow
y−coordinate (μm)
0
0.8
1.6
2.4
0
1.6
3.2
x−coordinate (μm)
E
0.7 s
100 ms exp.
3 s exp.
F
Diffusion
Retrograde flow
y−coordinate (μm)
0
0.4
0.8
0
0.4
0.8
x−coordinate (μm)
MSD (μm²/s)
0.15
0.10
0.05
0
Dlat = 0.12 μm²
0
0.1
0.2
0.3
0.4
Time (s)

Fig. 6. The Arp2/3 complex transitions from lateral diffusion to retrograde flow. **(A)** Histogram of p40 lateral diffusion coefficients for particles that diffuse at least 20 frames (n=716, three cells) with mean diffusion coefficient of 0.63±0.05 $\mu m^2/s$. An example is shown in **Movie 8**. **(B)** Lifetime distribution of diffusing p40 molecules (n=8325, three cells). Single exponential fit of 1-CF (not shown) gives a mean lifetime of 325±17 ms. **(C)** Trajectory of a p40-EGFP molecule that laterally diffuses before transitioning to retrograde flow (corresponds to **Movie 9**). Orange section of the track indicates diffusion, and maroon section indicates retrograde flow. Camera exposures occur at fast 10 fps imaging conditions. **(D)** Trajectory of a p40-EGFP molecule that undergoes retrograde motion without any prior diffusion (corresponds to **Movie 10**). Exposures are 10 fps. **(E)** Selected images from **Movie 11**, which shows diffusion of a p40-EGFP molecule (first five frames, *orange tracks*, 10 fps imaging conditions), then retrograde motion (next five frames, *maroon tracks*, 10 fps imaging conditions), and then retrograde motion with 0.33 fps imaging conditions (final six frames, *red tracks*). The slower imaging mode is better able to capture retrograde motion. Dashed line indicates cell edge. Bars, 500 nm. **(F)** Trajectory of the p40-EGFP molecule in (E). Orange section of the track shows diffusion at 10 fps, maroon section indicates retrograde flow at 10 fps, and red section shows retrograde flow at 0.33 fps imaging frequency (*left*). MSD versus time plot shows that this particle has a lateral diffusion coefficient of 0.12 $\mu m^2/s$ (*right*).

Figure 7

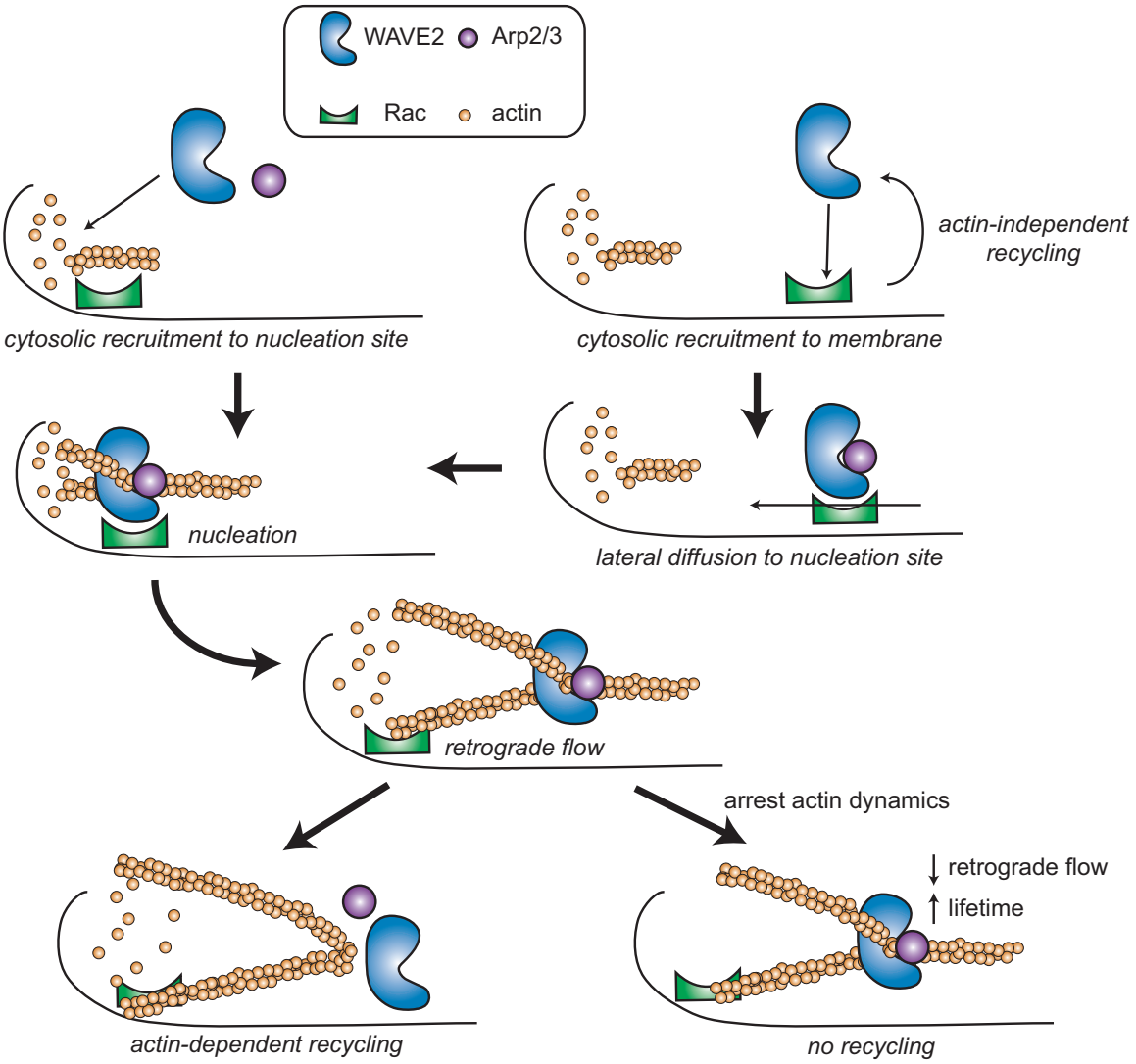
WAVE2
Arp2/3
Rac
actin
cytosolic recruitment to nucleation site
cytosolic recruitment to membrane
actin-independent recycling
nucleation
lateral diffusion to nucleation site
retrograde flow
arrest actin dynamics
retrograde flow
lifetime
actin-dependent recycling
no recycling

Fig. 7. Model for SCAR/WAVE complex-mediated actin nucleation in cells. SCAR/WAVE and Arp2/3 complexes have two modes of recruitment to nucleation sites – through cytosol recruitment or through membrane-bound lateral diffusion. SCAR/WAVE complex diffusing molecules can release from the membrane independent of actin nucleation. Once a SCAR/WAVE complex integrates into the actin meshwork after nucleation, recycling occurs through actin-based retrograde flow.

Supplemental Figure 1

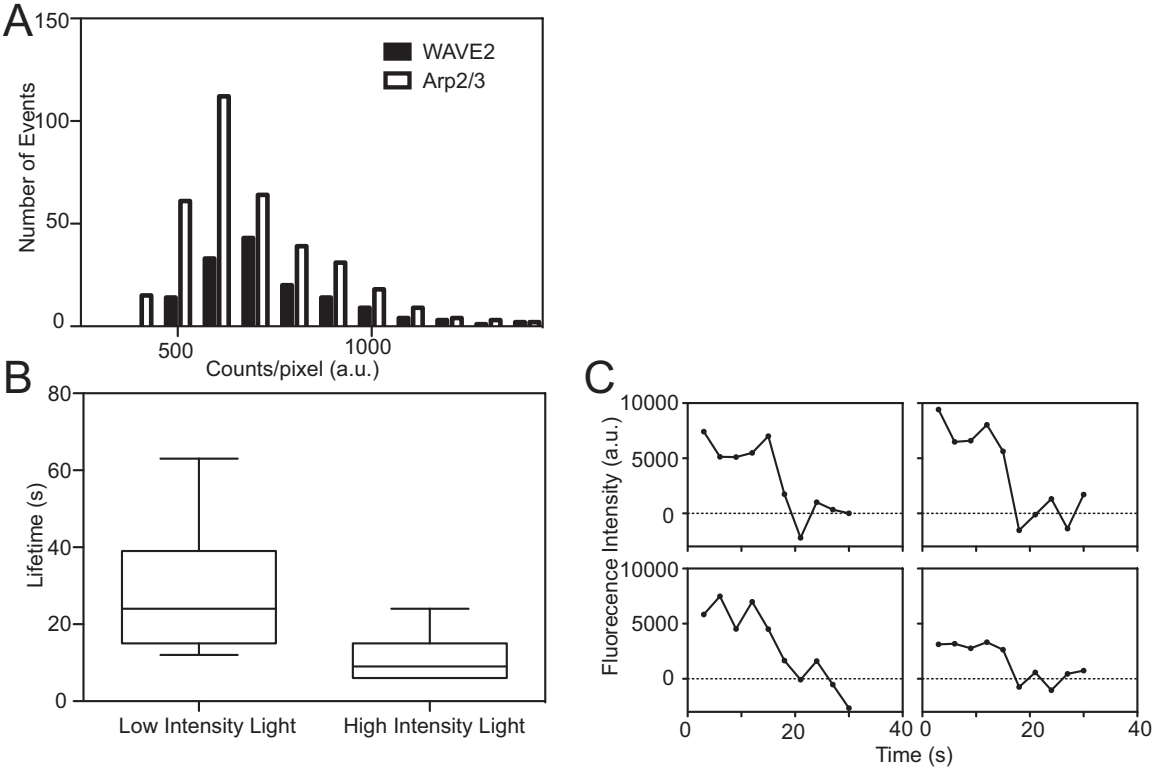

Fig. S1. WAVE2-EGFP foci are single molecules. **(A)** Fluorescence intensities of WAVE2-EGFP foci have a unimodal distribution similar to p40-EGFP molecules, which have previously been shown to be single molecules (Miyoshi et al., 2006). **(B)** High-intensity light reduces the lifetime of WAVE-EGFP molecules. In this mode, photobleaching, not dissociation from the cytoskeleton, dominates. **(C)** Four examples of WAVE2-EGFP molecules photobleaching in a single step in the high-intensity light mode. Three pieces of data argue that single molecules are being imaged: (1) Unimodal intensities (A) similar to p40-EGFP single molecules, (2) single step photobleaching (B), and (3) single exponential lifetime kinetics (**Fig. 1D**).

Supplemental Figure 2

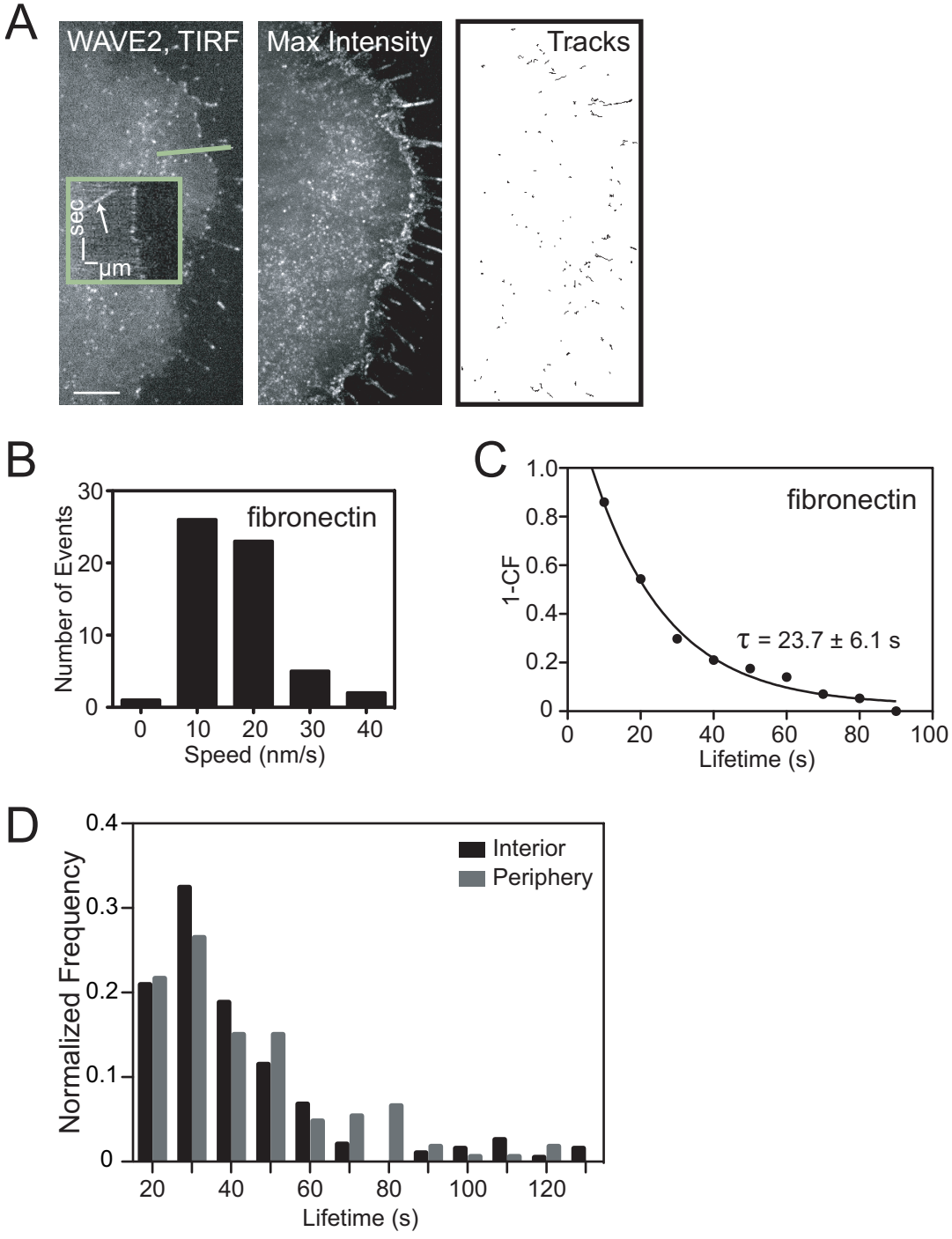

Fig. S2. (A) Left panel shows a TIRF image of an XTC cell expressing a low concentration of WAVE2-EGFP with some molecules undergoing retrograde flow (*inset kymograph, bars: horizontal, 2 μm; vertical, 1 min; time flows top to bottom*). Bar, 10 μm. Middle panel shows maximum intensity projection (90 frames, 4.5 min) of this cell, and right panel shows trajectories of retrograde flowing molecules. **(B)** Distribution of WAVE2-EGFP retrograde velocities for cells plated on 200 μg/ml fibronectin. Mean speed is 16±8 nm/s (n=57, four cells). **(C)** Single exponential fit of 1-CF of WAVE2-EGFP lifetimes for cells plated on 200 μg/ml fibronectin gives mean lifetime of 14.3±5.4 s (n=57, four cells). **(D)** Distribution of WAVE2-EGFP retrograde lifetimes for molecules appearing near the cell periphery versus in the cell interior.

Supplemental Figure 3

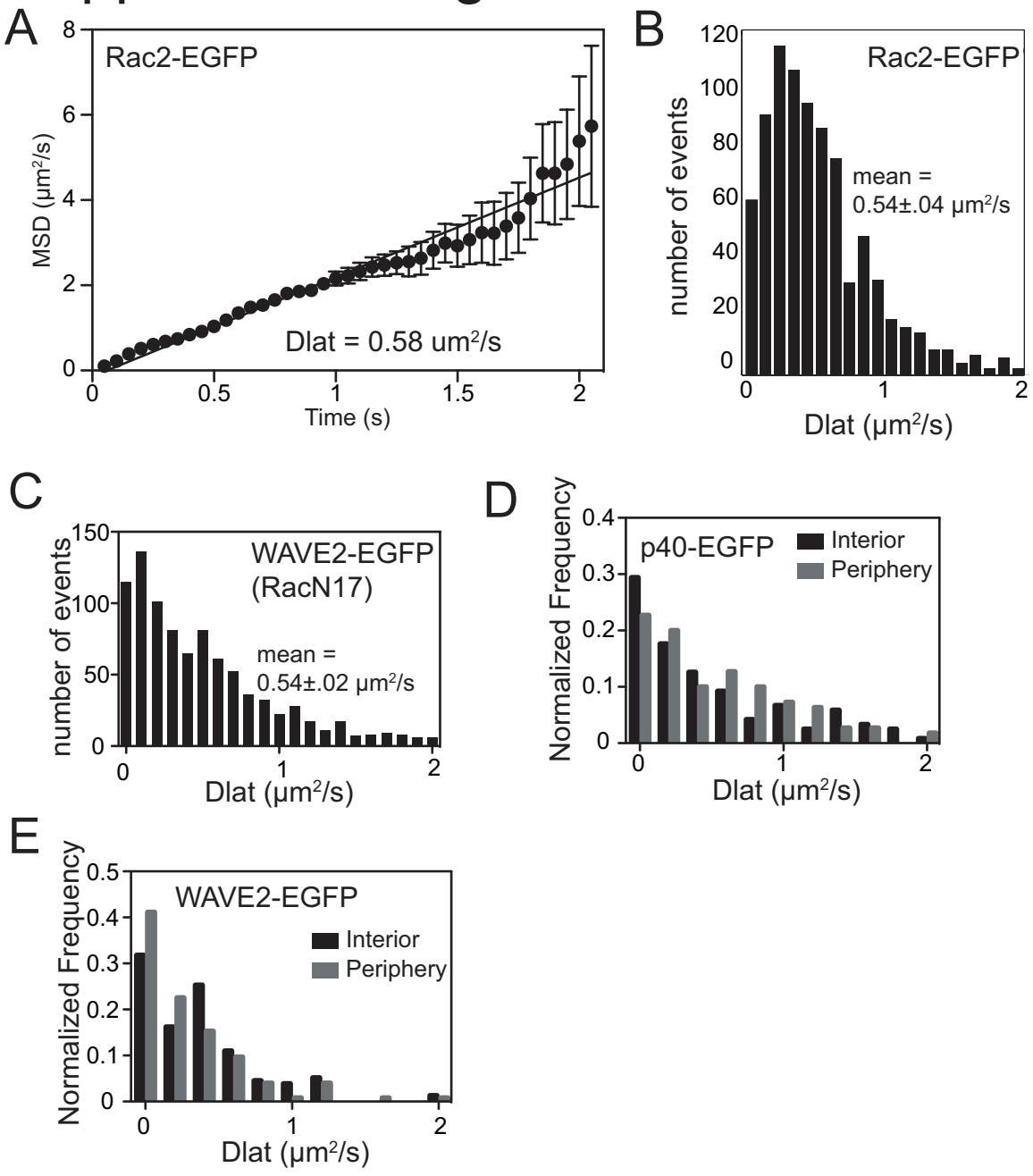

Fig. S3. (A) An example of a MSD versus time lag plot for diffusing particles in a cell expressing Rac2-EGFP with lateral diffusion coefficient of 0.58 $\mu m^2/s$ (corresponds to **Movie 6**). Error bars are s.e.m. **(B)** Histogram of Rac2 lateral diffusion coefficients for particles that diffuse at least 20 frames with mean of 0.54±0.04 $\mu m^2/s$ (n=870, three cells). **(C)** Histogram of WAVE2 lateral diffusion coefficients for particles that diffuse at least 20 frames with mean of 0.54±0.02 $\mu m^2/s$ (n=918, six cells) in cells expressing RacN17. **(D)** Histogram p40-EGFP lateral diffusion coefficients for molecules that diffuse at least 20 frames appearing near the cell periphery (mean=0.62±0.07 $\mu m^2/s$, n=119, three cells) versus in the cell interior (mean=0.63±0.07 $\mu m^2/s$, n=110, two cells). **(E)** Histogram WAVE2-EGFP lateral diffusion coefficients for molecules that diffuse at least 20 frames appearing near the cell periphery (mean=0.31±0.07 $\mu m^2/s$, n=124, two cells) versus in the cell interior (mean=0.39±0.07 $\mu m^2/s$, n=154, four cells).

Supplemental Figure 4

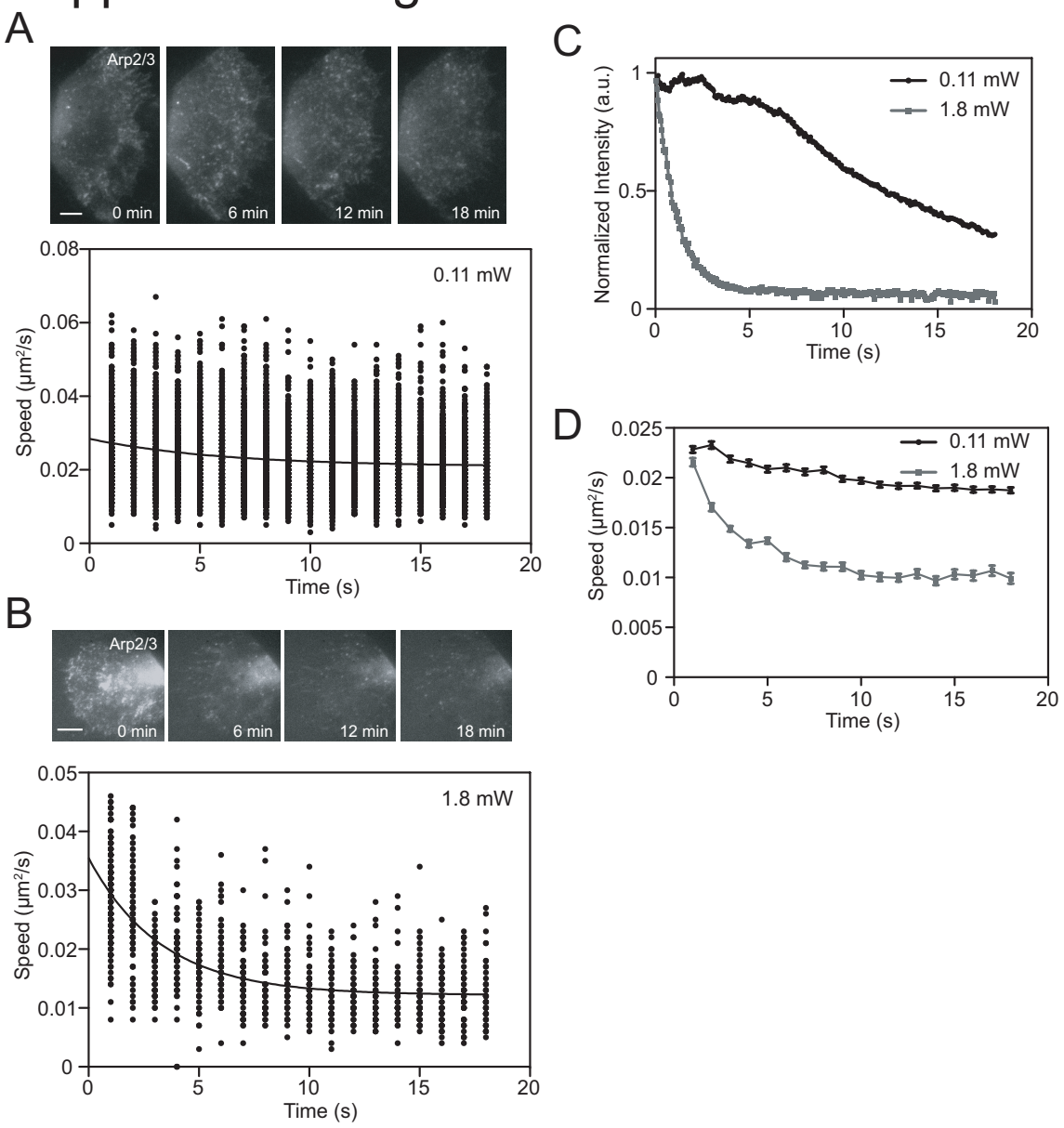

Fig. S4. Arp2/3 complex retrograde flow is highly photosensitive. **(A)** Top panel shows selected images of an XTC cell expressing a low concentration of p40-EGFP illuminated with attenuated 0.11 mW epifluorescence light. Bar, 5 μm. p40 retrograde flow velocity minimally decreases over time (*bottom panel*). **(B)** Top panels show selected images of an XTC cell expressing a low concentration of p40-EGFP illuminated with high-intensity 1.8 mW laser light. Bar, 5 μm. p40 retrograde flow velocity significantly decreases over time (*bottom panel*). **(C)** Background-subtracted fluorescence intensities of XTC cells expressing p40-GFP illuminated with low (0.11 mW) and high (1.8 mW) intensity light. Cells are rapidly photobleached in the high intensity imaging mode **(D)** Mean retrograde flow is significantly reduced after 1.8 mW illumination (n=3744, two cells) compared to 0.11 mW illumination (n=14957, three cells). Error bars are s.e.m.

SUPPLEMENTAL MOVIE LEGENDS

Movie 1. WAVE2-EGFP molecules undergo retrograde flow in XTC cells. Images were collected in epifluorescence every 3 seconds and are displayed at a rate of 20 frames per second. Corresponds to Fig. 1A.

Movie 2. p40-EGFP molecules undergo retrograde flow in XTC cells. Images were collected in epifluorescence every 3 seconds and are displayed at a rate of 20 frames per second. Corresponds to Fig. 2A.

Movie 3. Actin-EGFP molecules undergo retrograde flow in XTC cells. Images were collected in epifluorescence every 3 seconds and are displayed at a rate of 20 frames per second. Corresponds to Fig. 2B.

Movie 4. Acute addition of JLY drug cocktail perturbs protrusion and retraction in XTC cells. Images were collected in DIC (*left*) and epifluorescence of p40-EGFP (*right*) every 3 seconds and are displayed at a rate of 20 frames per second. Corresponds to Fig. 3F.

Movie 5. WAVE2-EGFP molecules laterally diffuse in XTC cells. Images were collected in TIRF every 50 milliseconds and are displayed at a rate of 20 frames per second.

Movie 6. Rac2-EGFP molecules laterally diffuse in XTC cells. Images were collected in TIRF every 50 milliseconds and are displayed at a rate of 20 frames per second.

Movie 7. An example of a WAVE2-EGFP molecule laterally diffusing and then becoming immobilized at the cell periphery (*left*) and tracked in Matlab (*right*). Images were collected in TIRF every 100 milliseconds and are displayed at a rate of 20 frames per second. Corresponds to Fig. 5D.

Movie 8. An example of p40-EGFP molecules laterally diffusing in XTC cells. Images were collected in TIRF every 40 milliseconds and are displayed at a rate of 20 frames per second.

Movie 9. An example of a p40-EGFP molecule diffusing and then undergoing retrograde flow. Images were collected in TIRF every 100 milliseconds and are displayed at a rate of 10 frames per second. Corresponds to Fig. 6C.

Movie 10. An example of a cell expressing a p40-EGFP molecule that undergoes retrograde flow without any prior lateral diffusion. Images were collected in TIRF every 100 milliseconds and are displayed at a rate of 10 frames per second. Corresponds to Fig. 6D.

Movie 11. An example of a cell expressing p40-EGFP first imaged in a high frequency mode, where a p40-EGFP molecule was observed to laterally diffuse. We switched to a low frequency mode, where retrograde flow of the same p40-EGFP molecule could be observed more clearly. Images were first collected in TIRF every 100 milliseconds for 19 frames and then collected in epifluorescence every 3 s for 29 frames. Both sequences are displayed at a rate of 10 frames per second. Corresponds to Fig. 6E.

CHAPTER SIX

Summary

There's always another pathway

-Keith Mostov's 1st law

We uncovered several new aspects of WAVE-mediated actin assembly:

1. *Mechanisms of polarity establishment*.

Theoretical models for how cells interpret external gradients during chemotaxis have been around for more than two decades – for review see (Devreotes and Zigmond, 1988), but it is only recently that they have received significant experimental support. Two recent publications have analyzed how cells reorient existing polarity in response to external gradients. One of these studies found that spatially biased generation (Arrieumerlou and Meyer, 2005) may account for reorientation of polarity during chemotaxis. The other study found that selection of randomly produced pseudopodia (Andrew and Insall, 2007) may account for the ability of cells to reorient existing polarity. Several aspects of these studies contradict one another, and it is not obvious

whether these contradictions arise from differences in model cells used or differences in analyses. A limitation of these studies is that they were based on the analysis of cell morphology during chemotaxis. However, morphology is an indirect readout of the specific activities that actually control the cytoskeleton. Therefore, we analyzed underlying signals such as the WAVE complex during polarization and directional migration. We found that neutrophils use both spatially controlled wave generation and selection to establish WAVE-complex polarity. By extensively correlating the chemoattractant input with semi-automated quantitation of wave dynamics, we were able to determine the stimulation conditions under which each mechanism dominates. Both (Arrieumerlou and Meyer, 2005) and (Andrew and Insall, 2007) rely on existing polarity for spatial control of protrusion, but we found that even unpolarized cells can spatially control wave selection and generation. These data suggest that polarity does not act alone, but rather acts in conjunction with gradient amplification to spatially pattern protrusions. Furthermore, we found that the basic unit of selection and generation is not the pseudopod as in (Andrew and Insall, 2007), but rather many individual protrusive elements controlled by waves. Our discovery of spatially biased wave generation and selection provides the basis for mechanistic studies aimed at dissecting how cells establish and guide polarity during chemotaxis.

2. *Relationship between polarity and gradient sensing*.

Current chemotaxis models postulate that cells *internally* restrict the regions of their surface that are capable of protruding in response to chemoattractant increases (Arrieumerlou and Meyer, 2005; Iglesias and Devreotes, 2008)—we refer to this cell's ability to limit the distribution of its own signals as morphological polarity. Alternatively, internal cell signals can be restricted by *external* gradients – we refer to the cell's ability to be restricted in by external gradients as gradient sensing. In agonist gradients, both

morphological polarity and gradient sensing can influence the establishment and maintenance of WAVE-complex activity. We took advantage of the ability of neutrophils to polarize in response to uniform chemoattractant to analyze the role of morphological polarity independent of gradient sensing (i.e. no external gradient was present). In response to small changes in agonist receptor occupancy, morphological polarity suffices to maintain an asymmetric wave distribution, whereas a gradient sensing mechanism is required to maintain an asymmetric wave distribution in response to larger changes in receptor occupancy. Our work provides novel insights into the relative roles of morphological polarity and gradient sensing in signaling to the cytoskeleton during chemotaxis. In contrast to (Devreotes and Zigmond, 1988) and (Arrieumerlou and Meyer, 2005), gradient sensing appears to play a larger role than a cell's internal polarization machinery for restricting the spatial control of protrusions.

3. *Relationship between polarity and cytoskeletal rearrangements*.

Gradient sensing, polarity, and morphological rearrangements are often considered to be linear, separable steps. A common approach for studying upstream signaling independent of morphological rearrangements is to treat cells with latrunculin, thereby blocking actin polymerization and cell movement (Parent et al., 1998; Servant et al., 2000; Janetopoulos et al., 2004; Xu et al., 2007). Some cues such as PIP3 can polarize in the absence of actin rearrangements. In contrast, we find that actin polymer, which is generated downstream of the WAVE complex (Stradal and Scita, 2006), is required for establishing and focusing WAVE complex polarity in neutrophils. Under these conditions, the WAVE complex can still be uniformly recruited to and released from the membrane in a chemoattractant-dependent fashion. Our data represent the first example of a perturbation that converts a spatially polarized signal into a spatially uniform one

while maintaining the signal's ability to respond to stimulus changes. Thus, actin polymer is a unique regulator of gradient amplification during polarization. Our data demonstrate that signaling and the cytoskeleton collaborate to pattern intracellular molecules during polarization, and that gradient sensing, polarity, and cytoskeletal rearrangements are not strictly linear, separable steps.

4. *Nucleation factors diffuse to nucleation sites.*

The Arp2/3 complex initiates actin nucleation upon binding to actin filaments and nucleation-promoting factors such as the WAVE complex. We show that before incorporating into the cytoskeleton, the Arp2/3 complex undergoes lateral diffusion in the plasma membrane. This 2D search along the membrane may facilitate Arp2/3 and WAVE complex binding to the membrane-apposed filaments that are essential to trigger nucleation. Reduced dimensionality searches are well-known in other biological contexts. For example, LacI repressor finds its transcription factor binding site through a series of short 1D searches along DNA, which accelerates binding to its target 100 fold over 3D cytosolic diffusion (Riggs et al., 1970; von Hippel and Berg, 1989; Wang et al., 2006; Elf et al., 2007). These constrained diffusion events need not be extensive to dramatically decrease search time; the LacI repressor spends 90% of the time diffusing on DNA with a short residence time of 5 milliseconds (Elf et al., 2007). Both WAVE and Arp2/3 complexes had short residence times of ~300 ms during lateral diffusion, and more rapid imaging as in (Elf et al., 2007) may be needed to capture very short-lived 2D searches.

5. *Actin-dependent retrograde flow facilitates WAVE-complex recycling.*

Once nucleation occurs, how are these proteins recycled for the next round of actin assembly? Unlike the Arp2/3 complex, the majority of the WAVE complex is not broadly

distributed throughout the actin network, but is instead observed only at the edge of the lamellipodium. By performing single-molecule imaging of WAVE2, we uncovered a previously unknown pool of the WAVE complex that incorporates into the actin network and undergoes retrograde flow. We used a new pharmacological cocktail to determined that the force of ongoing actin assembly (and not the organization of the existing actin network) helps remove the WAVE complex from the membrane. Additionally, we used FRAP to show that the global pool of the WAVE-complex can still freely associate and dissociate with the plasma membrane independent of actin polymerization.

The advent of single-molecule imaging, TIRF microscopy and micropipette techniques coupled to real-time activity readouts in cells has led to a torrent of quantitative data uncovering new principles in directed cell migration. Collectively, our studies argue for a model where nucleation factors like the WAVE complex locally search the membrane through diffusion until converging at a nucleation site (i.e. RacGTP, anionic phospholipids, or actin filaments). This process occurs continuously and stochastically, but can be biased by external stimuli. In response to stimulation, WAVE-mediated actin assembly propagates in a positive feedback loop at the cell's leading edge even as individual Arp2/3 and WAVE complex molecules are recycled from the leading edge through actin-based retrograde flow. Many questions remain. First, what is the stoichiometry of the WAVE complex to upstream activators and downstream effectors? We observed WAVE-complex retrograde flow with less frequency than the Arp2/3 complex, which could indicate that only a subset of WAVE molecules activate or Arp2/3 ones or could suggest that the WAVE complex can activate Arp2/3 molecules before being recycling through retrograde flow. Intriguingly, there is evidence that multiple WAVE molecules may be the more appropriate unit of nucleation (Padrick et al., 2008). Second, how does actin assembly affect WAVE complex activity? We show that actin

helps sculpt the spatial distribution of the WAVE complex and is necessary for WAVE-complex retrograde recycling after nucleation, but it is not clear if the WAVE complex together with Arp2/3 binds an actin filament or if binding is more sequential. Third, what is the minimal unit of actin filament nucleation in cells? From purified components, phosphorylated WAVE complex is activated by RacGTP and anionic phospholipids (Lebensohn and Kirschner, 2009). In cells it's unknown which GEF brings RacGTP and the WAVE complex together, nor if Rac remains attached to the WAVE complex during nucleation. We provide a bit of evidence that the GEF β-pix is involved, but much work still remains. Oh, and remember:

There's always a pathway that can be disproved

-Keith Mostov's 3rd law

REFERENCES

Andrew, N. and Insall, R. H. (2007). Chemotaxis in shallow gradients is mediated independently of PtdIns 3-kinase by biased choices between random protrusions. *Nat Cell Biol*, **9**, 193-200.

Arrieumerlou, C. and Meyer, T. (2005). A local coupling model and compass parameter for eukaryotic chemotaxis. *Dev Cell*, **8**, 215-27.

Devreotes, P.N. and Zigmond, S. H. (1988). Chemotaxis in eukaryotic cells: a focus on leukocytes and Dictyostelium. *Annu Rev Cell Biol*, **4**, 649-86.

Elf, J., Li, G.-W., and Xie, X. S. (2007). Probing transcription factor dynamics at the single-molecule level in a living cell. *Science*, **316**, 1191-1194.

von Hippel, P. H. and Berg, O. G. (1989). Facilitated target location in biological systems. *Journal of Biological Chemistry*, **264**, 675 -678.

Iglesias, Pablo A and Devreotes, Peter N (2008). Navigating through models of chemotaxis. *Current Opinion in Cell Biology*, **20**, 35-40.

Janetopoulos, C., Ma, L., Devreotes, P.N., and Iglesias, P.A. (2004). Chemoattractant-induced phosphatidylinositol 3,4,5-trisphosphate accumulation is spatially amplified and adapts, independent of the actin cytoskeleton. *Proc Natl Acad Sci U S A*, **101**, 8951-6.

Lebensohn, A. M. and Kirschner, M. W. (2009). Activation of the WAVE complex by coincident signals controls actin assembly. *Mol. Cell*, **36**, 512-524.

Padrick, S. B., Cheng, H. C., Ismail, A. M., Panchal, S. C., Doolittle, L. K., Kim, S., Skehan, B. M., Umetani, J., Brautigam, C. A., Leong, J. M., et al. (2008). Hierarchical regulation of WASP/WAVE proteins. *Molecular cell*, **32**, 426-38.

Parent, C. A., Blacklock, B. J., Froehlich, W. M., Murphy, D. B., and Devreotes, P.N. (1998). G protein signaling events are activated at the leading edge of chemotactic cells. *Cell*, **95**, 81-91.

Riggs, A. D., Bourgeois, S., and Cohn, M. (1970). The lac repressor-operator interaction. 3. Kinetic studies. *J. Mol. Biol*, **53**, 401-417.

Servant, G., Weiner, O. D., Herzmark, P., Balla, T., Sedat, J. W., and Bourne, H. R. (2000). Polarization of chemoattractant receptor signaling during chemotaxis. *Science*, **287**, 1037-40.

Stradal, T. E. and Scita, G. (2006). Protein complexes regulating Arp2/3-mediated actin assembly. *Curr Opin Cell Biol*, **18**, 4-10.

Wang, Y. M., Austin, R. H., and Cox, E. C. (2006). Single molecule measurements of repressor protein 1D diffusion on DNA. *Phys. Rev. Lett*, **97**, 048302.

Xu, X., Meier-Schellersheim, M., Yan, J., and Jin, T. (2007). Locally controlled inhibitory mechanisms are involved in eukaryotic GPCR-mediated chemosensing. *J. Cell Biol*, **178**, 141-153.

PUBLISHING AGREEMENT

It is the policy of the University to encourage the distribution of all theses, dissertations, and manuscripts. Copies of all UCSF theses, dissertations, and manuscripts will be routed to the library via the Graduate Division. The library will make all theses, dissertations, and manuscripts accessible to the public and will preserve these to the best of their abilities, in perpetuity.

I hereby grant permission to the Graduate Division of the University of California, San Francisco to release copies of my thesis, dissertation, or manuscript to the Campus Library to provide access and preservation, in whole or in part, in perpetuity.

Arthur Millen — 8/31/11

Author Signature — Date